# Studies of Light-Matter Interactions in Atomic Ensembles for Creation of Entangled States and Quantum Interfaces

by

Tanvi P. Gujarati

A dissertation submitted in partial fulfillment
of the requirements for the degree of
Doctor of Philosophy
(Physics)
in The University of Michigan
2019

Doctoral Committee:

Professor Luming Duan, Co-Chair
Professor Alex Kuzmich, Co-Chair
Associate Professor Hui Deng
Professor Georg Raithel
Professor John Schotland


Bob, I really want to understand this universe.
Alice, know first if you are entangled with it...

Tanvi Gujarati
tanvipg@umich.edu
ORCID ID: 0000-0002-8463-3037

To my family

# ACKNOWLEDGEMENTS

Time is a mysterious thing, it knows how to fly fast but has never learned to stand still. All I hope is that it slows down for only a few moments so that I can deeply thank everyone who helped me reach here.

It was the time to apply to universities for PhD positions, and I remember discussing this with one of my undergrad teachers, Prof. Anil Shaji. He had asked me if there was a particular field that I felt strongly about for pursuing research and I had told him that I wasn't sure, but I found light fascinating and wanted to learn more about light-matter interactions. Fast forward, I was fortunate to be a part of Prof. Luming Duan's research group where I could shine light upon, well, light.

I am immensely thankful to Prof. Luming for his guidance throughout the years of my PhD program. It has been a great learning experience to have worked with him. I hope and wish that consciously or unconsciously I have been able to imbibe some of his many virtuous qualities like his calm demeanor, humility and sharp intellect. Thank you for giving me an opportunity to learn from you and also for the chance to travel to China! My PhD experience wouldn't have been the same if it wasn't for my fellow lab mates. I am grateful to Zhen Zhang, Dong-Ling Deng, Sheng-Tao Wang, Zhengyu Zhang, Yukai Wu and Ceren Dag for helping me learn and understand many different concepts and topics, not only about science, but also about cultures, languages and food! It has been an honour to have known such hard working and amazing people. I would also like to thank Prof. Paul Berman, Prof. Alex Kuzmich, Prof. Georg Raithel, Prof. Kai Sun, Prof. Emanuel Gull and Prof. Wolfgang Lorenzon for their

valuable support and guidance. I am also grateful to Prof. John Schotland and Prof. Hui Deng for being a part of my thesis committee. I will be forever grateful to Prof. Anil Shaji, Prof. Shaijumon, Prof. Sreedhar Dutta, Prof. S. Shankarnaryanan, Prof. Archana Pai, Prof. Hema Somanathan, Prof. E.D. Jemmis, Prof. Gopinanthan and all my teachers at IISER-TVM for shaping my curiosity and encouraging me always. A special thanks to my friends Jamie McLennan and Uttam Paudel for the wonderful and eye opening discussions.

When someone asks if moving to a new country, away from your family and friends is very difficult, it makes me wonder how has it affected me? It would have been very difficult had it not been for all the fabulous people I got to meet and share my happiness and PhD pains with. Transition to Ann Arbor couldn't have been smoother all because of Surojit, Vimal, Dhruv and Kelly. Every experience that we have had, will always be cherished. A heartfelt thank you to Neha, Mohit N., Subhashis, Animesh, Siva, Manu, Mantha, Naincy, Prachi, Adithya and all the wonderful friends for all the memorable times we have spent together! Neha and Mohit N., chai-pe-charcha always woke me up! They say friends that you make in your college years are for life, and that couldn't be more true. Thank you dearest Saranya, Manogna, Pranav, Varma, Gaurav, Gopu, Pooja, Preeti and the whole IISER-TVM gang for being my rock solid support. Thank you Atmaram and Kashi for bringing more love and wisdom in my life. You are all a part of my family now.

And finally, family. I am the luckiest person in the world to have a family like ours and even this is an understatement. Thank you so much Dadi, Dada, Pappa and Mummy, Pappa and Mummy again, Madhavi, Saurabh, Prateek, Pooja, Bharati Masi and Masaji and most of all Ved! I have no words to describe how much your love and support means to me and getting here wouldn't have been possible without you all. There are so many more people that I want to thank and remember, I hope my gratitude reaches you, thank you all! And finally, my dearest husband and partner

in all my dreams for a great future, thank you from the bottom of my heart. Thank you, Mohit J., thank you for being there for me since kindergarten!

# TABLE OF CONTENTS

# LIST OF FIGURES

# LIST OF APPENDICES

**Appendix**

# LIST OF ABBREVIATIONS

**DLCZ** Duan-Lukin-Cirac-Zoller

**EIT** Electromagnetically Induced Transparency

**EPR** Einstein-Podolsky-Rosen

**GHZ** Greenberger-Horne-Zeilinger

**IRE** Intrinsic Retrieval Efficiency

**OD** Optical Depth

**RWA** Rotating Wave Approximation

**STIRAP** Stimulated Raman Adiabatic Passage

**WR** Width Ratio

# ABSTRACT

The field of quantum computation and communication has prospered over the last few decades because of multiple advances in our understanding of trapping and controlling physical quantum systems like neutral atoms, superconducting qubits, trapped ions, quantum dots etc. using light. A lot of research has gone into development of techniques which facilitate trapping and manipulation of ensembles of neutral atoms by studying how the atomic properties of the system respond to properties of light used to control them. In this dissertation we shall explore some applications of light-matter interactions in ensembles of lambda three level neutral atoms for the purpose of entanglement generation and distribution.

The first part of this dissertation focuses on the study of a protocol that can be used to generate multi-particle entangled quantum states called the Greenberger-Horne-Zeilinger (GHZ) states in an ensemble of N neutral atoms. Schemes for creation of N particle entangled Greenberger-Horne-Zeilinger (GHZ) states are important for understanding multi-particle non-classical correlations. A theoretical protocol for creation of a multi-particle GHZ state implemented on a target ensemble of N, three-level Rydberg atoms and a single Rydberg atom as a control using Stimulated Raman Adiabatic Passage (STIRAP) is presented. We work in the Rydberg blockade regime for the ensemble atoms induced due to excitation of the control atom to a high lying Rydberg level. It is shown that using STIRAP, atoms from one ground state of the ensemble can be adiabatically transferred with high fidelity to the other multi-particle ground state, depending on the state of the control atom. Measurement of the control atom in a specific basis after this conditional transfer facilitates one-step creation of

a N particle GHZ state. A thorough analysis of adiabatic conditions associated with STIRAP for this scheme and the influence of radiative decay from the excited Rydberg levels is presented. The most important and novel feature of this scheme is that it is immune to the decay rate of the excited level in ensemble atoms and provides a robust way of creating GHZ states.

In the second part of this dissertation, we study atomic ensemble based quantum interfaces used in quantum repeater protocols for entanglement distribution. Quantum interfaces provide a platform where in the flying photonic qubits used for information and entanglement transfer can interact with a physical system which stores, processes and releases this information back as photons. The Duan-Lukin-Cirac-Zoller (DLCZ) quantum repeater protocol, which was proposed to realize long distance quantum communication, requires usage of quantum memories or quantum interfaces. Atomic ensembles interacting with optical beams based on off-resonant Raman scattering serve as convenient on-demand quantum memories. Here a complete, free space, three-dimensional theory of the associated read and write process for this quantum memory is worked out with the aim of understanding intrinsic retrieval efficiency. We develop a formalism to calculate the transverse mode structure for the signal and the idler photons and use the formalism to study the intrinsic retrieval efficiency under various configurations. The effects of atomic density fluctuations and atomic motion are incorporated by numerically simulating this system for a range of realistic experimental parameters. Results describe the variation in the intrinsic retrieval efficiency as a function of the memory storage time for skewed beam configuration at a finite temperature, which provides valuable information for optimization of the retrieval efficiency in experiments.

# CHAPTER I

# Introduction

## 1.1 Motivation

"The changing of Bodies into Light, and Light into Bodies, is very conformable to the Course of Nature, which seems delighted with Transmutations. "

-Sir Isaac Newton

Opticks, 2nd edition (1718), Book 3, Query 30, 349.

What we see and what we don't, is a matter of how light interacts with matter. Whether it's the light being emitted from the sun, or that which bounces off the surface of water or even that which is absorbed by the rods in the retina (quantum or not [1]) are all instances of light interacting with matter. Quantum mechanical theories have succeeded immensely in describing the structure of matter [2–5]. The natural question then arises, whether light can also be described quantum mechanically and when is it that such a description is necessary? The field of quantum optics with it's rich history provides answers to these questions with the perspective of how light interacts with matter.

Towards the end of the $19^{th}$ century - beginning of $20^{th}$, new understanding regarding the nature of radiation started unfolding when Max Planck modelled the black body radiations using discrete quanta of light [6] soon to be followed by Einstein's

description of the photo-electric effect [7]. What started out as spectroscopic studies of atomic level structure [5, 8] paved way for lasers [9–11], complex descriptions of non-classical states of light on interaction with matter [12–14], trapping and cooling matter to study exotic phenomena like BECs [15–17] and Rydberg molecules [18]. In the past few decades, with the amalgamation of the two fields of quantum optics and computer science, a lot of path breaking research and innovation in the field of quantum information has been achieved. The understanding that quantum entanglement can be looked upon as a resource has led to development of many quantum communication protocols like quantum teleportation [19–21] and quantum cryptography [22, 23] to name a few. The fact that we now have functional quantum computers based on varied platforms ranging from atomic scale systems like ions and neutral atoms to macroscopic systems with superconducting qubits has been made possible due to theoretical and experimental progress in the understanding of light-matter interactions.

In this dissertation we are going to explore two different phenomenon that arise due to light-matter interactions in atomic ensembles using tools from quantum optics. We will study a protocol to generate highly entangled quantum states called the Greenberger-Horne-Zeilinger (GHZ) states using atomic ensembles in the first half. Then, using similar atomic ensembles but a different flavour of light-matter interactions, we will study the efficiency of atomic interfaces used for quantum communication protocols. Before we start delving into the details of these two systems, let us review the concepts that will be relevant for the forthcoming discussions.

## 1.2 Background

In this section, we will briefly discuss the Hamiltonians used for treating light-matter interactions using an example of a two-level atom. We will then focus on the differences between systems with multiple atoms in ensembles interacting with

light as opposed to single atom systems followed by a short discussion on quantum communication and quantum networks.

### 1.2.1 Light-matter interactions

Let us start by describing the method that is used in this dissertation to model light-matter interactions in quantum atomic systems. There are two major approaches that are used to describe matter interacting with light, the semi-classical approach and the quantum optics approach. In the semi-classical approach, matter is modelled quantum mechanically and light is described classically, whereas in the quantum approach both light and matter are described quantum mechanically. The choice of using one method or the other depends on the phenomenon that one wishes to describe. A general rule of thumb is to use a quantized description of electric field when the average number of photons in the system under consideration is of the order or less compared to the number of atoms in the system [24]. Let us first look at the Hamiltonian that describes light-matter interactions semi-classically followed by the quantum optical treatment.

Consider a mono-chromatic classical electric field given in Eq. (1.2) with frequency $\omega$, wave-vector $\mathbf{k}$ and unit polarization vector $\boldsymbol{\varepsilon}$ at a point $\mathbf{r}$. Such a mono-chromatic field is typically used to describe electric field generated from lasers which are generally used for manipulating atoms.

$$\begin{aligned} \mathbf{E}(\mathbf{r},t) &= E_0\boldsymbol{\varepsilon}\cos(\omega t - \mathbf{k}\cdot\mathbf{r}) && (1.1)\\ &= \frac{E_0\boldsymbol{\varepsilon}}{2}(e^{-i(\omega t-\mathbf{k}\cdot\mathbf{r})} + e^{i(\omega t-\mathbf{k}\cdot\mathbf{r})}) && (1.2)\\ &\equiv \mathbf{E}^+(\mathbf{r},t) + \mathbf{E}^-(\mathbf{r},t) && (1.3) \end{aligned}$$

For the kind of interactions that we will be interested in, the wavelength of the light used is much longer than the size of atom, which means that the electric field is

constant over the extent of the atom and it is given by the value of the field evaluated at the nucleus of the atom. This is called the dipole approximation or the long-wavelength approximation [25]. Consider a two-level atom with a ground state level $|g\rangle$ and an exited level $|e\rangle$ stationary at position $\mathbf{r}$. Here we are approximating an atom that has an infinite set of bound levels by two levels under the assumption that the light interacting with this atom does not excite any other atomic levels. Let the energy of the state $|g\rangle$ be given by $E_g$ and that of the excited state be $E_e$. We can set the ground state energy to be 0 so that the energy of the excited state on the relative scale is now given by $E = \hbar\omega_0 = E_e - E_g$. The Hamiltonian for this system, $H$, is the sum of the Hamiltonian for free atom, $H_A$, and the atom-field interaction Hamiltonian in the dipole approximation, $H_{AF}$.

$$\hat{H} = \hat{H}_A + \hat{H}_{AF} \tag{1.4}$$

$$\hat{H}_A = \hbar\omega_0 |e\rangle\langle e| \tag{1.5}$$

$$\hat{H}_{AF} = -\hat{\boldsymbol{\mu}} \cdot \mathbf{E}(\mathbf{r}, t) \tag{1.6}$$

In the above Eq. (1.6), $\hat{\boldsymbol{\mu}} = -e\hat{\mathbf{r}}_e$ is the dipole moment of the atom with $\hat{\mathbf{r}}_e$ being the position operator of the electron in the atom relative to the nucleus and $e = 1.6 * 10^{-19}$ C is the electron charge. Since the atomic operator $\hat{\mathbf{r}}_e$ has an odd parity and the atom has an inversion symmetry, the diagonal elements corresponding to the dipole moment operator vanish [24, 25]. Thus, we can expand the dipole moment operator as in Eq. (1.7):

$$\hat{\boldsymbol{\mu}} = \langle g|\hat{\boldsymbol{\mu}}|e\rangle|g\rangle\langle e| + \langle e|\hat{\boldsymbol{\mu}}|g\rangle|e\rangle\langle g| \tag{1.7}$$

$$\equiv \hat{\boldsymbol{\mu}}^+ + \hat{\boldsymbol{\mu}}^- \tag{1.8}$$

The component of the dipole moment operator $|g\rangle\langle e| \propto e^{-i\omega_0 t}$ since the expectation

value of $|g\rangle\langle e|$ for any state under free atom Hamiltonian evolution goes as $e^{-i\omega_0 t}$. Thus, $\hat{\boldsymbol{\mu}}^{\pm} \propto e^{\mp i\omega_0 t}$. On expanding the interaction part of the Hamiltonian using Eqs. (1.3),(1.6) and (1.8) we get:

$$\hat{H}_{AF} \;=\; -(\hat{\boldsymbol{\mu}}^{+} + \hat{\boldsymbol{\mu}}^{-}) \cdot (\mathbf{E}^{+}(\mathbf{r},t) + \mathbf{E}^{-}(\mathbf{r},t)) \tag{1.9}$$

The terms in Eq. (1.9), $\hat{\boldsymbol{\mu}}^{\pm} \cdot \mathbf{E}^{\pm}(\mathbf{r},t) \propto e^{\mp i(\omega_0+\omega)t}$ and the other two terms go as, $\hat{\boldsymbol{\mu}}^{\pm} \cdot \mathbf{E}^{\mp}(\mathbf{r},t) \propto e^{\mp i(\omega_0-\omega)t}$. Let us define the detuning as $\delta = \omega_0 - \omega$. Assuming that $\omega_0 + \omega \gg |\delta|$ we keep only the terms with slow dynamics corresponding to the frequency $\delta$. The terms oscillating with the frequency $|\omega_0 + \omega|$ will be averaged over and washed out on the time scales of $\delta^{-1}$. This is called the Rotating Wave Approximation (RWA) [5, 24, 25]. Let us also define:

$$\Omega_0 = \frac{\langle g|\hat{\boldsymbol{\mu}} \cdot \boldsymbol{\varepsilon}|e\rangle E_0}{\hbar} \tag{1.10}$$

as the Rabi frequency of the light-matter interaction. Rabi frequency is a measure of how strongly given light and matter interact with each other. We can now rewrite the full Hamiltonian of the system as:

$$\hat{H} \;=\; \hbar\omega_0 |e\rangle\langle e| + \hbar\big[\frac{\Omega_0}{2} e^{-i\delta t}|g\rangle\langle e| + \frac{\Omega_0^*}{2} e^{i\delta t}|e\rangle\langle g|\big] \tag{1.11}$$

Eq. (1.11) is a thoroughly studied form of the Hamiltonian for light-matter interactions that gives rise to many phenomena like Rabi flopping, Ramsey Fringes, Spin echoes, Mollow Triplet spectrum to name a few [5, 24–26]. Modifications to this Hamiltonian can be introduced by adding more atomic levels as well as electric fields with more than one frequency components. Let us now extend this analysis to the case when electric field is treated quantum mechanically.

Quantization of electromagnetic fields is useful for studying phenomena involving

only a few photons like spontaneous emissions, fields in a cavity etc. We shall not elaborate on the methods used for quantization of electric fields here, more information on that can be found in [27, 28]. The general way of quantization is to assign annihilation and creation operators to classical spatial field modes associated with a set of given boundary conditions.

Consider a cubic volume $V$ of free space with the dimension of each side given by $L$. The classical field modes with these boundary conditions are given by plane wave eigen-modes $e^{i\mathbf{k}\cdot\mathbf{r}}$, where:

$$\mathbf{k} = k_x\mathbf{x} + k_y\mathbf{y} + k_z\mathbf{z} \tag{1.12}$$

$$k_x = \frac{2\pi n_x}{L}, \quad k_y = \frac{2\pi n_y}{L} \text{ and } k_z = \frac{2\pi n_z}{L} \tag{1.13}$$

$n_x$, $n_y$ and $n_z$ are integers. The expression for quantized electric field in free space of volume $V$ is given in Eq. (1.14) [24]

$$\hat{\mathbf{E}}(\mathbf{r}) = i\sum_j E_j[\hat{a}_j\boldsymbol{\varepsilon}_j e^{i\mathbf{k}_j\cdot\mathbf{r}} - \hat{a}_j^\dagger\boldsymbol{\varepsilon}_j^* e^{-i\mathbf{k}_j\cdot\mathbf{r}}] \tag{1.14}$$

$$\equiv \hat{\mathbf{E}}^+(\mathbf{r}) + \hat{\mathbf{E}}^-(\mathbf{r}) \tag{1.15}$$

In the above equation, $\mathbf{k}$ represents the wave-vector and $\boldsymbol{\varepsilon}$ the polarization unit vector. For electric fields in free space, $\mathbf{k}_j \cdot \boldsymbol{\varepsilon}_j = 0$. The sum is taken over all field modes which include two independent polarization directions for a given frequency mode. Operators $\hat{a}_j$ and $\hat{a}_j^\dagger$ are the annihilation and creation operators for each mode $j$ respectively. They satisfy the commutation relations given in Eq. (1.16)-(1.17)

$$[\hat{a}_i, \hat{a}_j] = [\hat{a}_i^\dagger, \hat{a}_j^\dagger] = 0 \tag{1.16}$$

$$[\hat{a}_i, \hat{a}_j^\dagger] = \delta_{ij} \tag{1.17}$$

In Eq. (1.14), $E_j$ is the real electric field co-efficient and by choosing it to be:

$$E_j = \sqrt{\frac{\hbar|\mathbf{k}_j|c}{2\epsilon_0 V}} \tag{1.18}$$

we can write the free field Hamiltonian as given in Eq. (1.19)

$$\hat{H}_F \;=\; \sum_j \hbar\omega_j(\hat{a}_j^\dagger \hat{a}_j + \frac{1}{2}) \tag{1.19}$$

where $\omega_j = |\mathbf{k}_j|c$ is the angular frequency of the electric field mode $j$ and $c$ is the speed of light in vacuum. Also, in Eq. (1.18) $\epsilon_0$ is the permittivity of free space. From the Hamiltonian in Eq. (1.19), we notice that quantized electric field in free space is analogous to a sum of harmonic oscillators each operating at a different frequency which can be determined by the eigen-modes of plane waves in a cubic volume $V$. The constant factor of $\frac{1}{2}\sum_j \hbar\omega_j$ leads to divergences when calculating the energy density of vacuum field. This can be taken care of by renormalization techniques [29]. For our purpose we shall ignore the contributions from this zero-point energy.

The choice of the quantization volume $V$ is arbitrary, one can choose volumes of different shapes and sizes but the real measurable physical quantities should remain independent of them. The final step in quantization is to take the limit $L \to \infty$ such that $V$ would include all space. When taking the limit to infinity, following the rules laid out below in Eqs. (1.20) and (1.21) will make calculations easier and help in accounting for extra factors of $V$.

$$\sum_{\mathbf{k}} \;\to\; \frac{V}{(2\pi)^3} \int_{-\infty}^{\infty} dk_x \int_{-\infty}^{\infty} dk_y \int_{-\infty}^{\infty} dk_z \tag{1.20}$$

We should also change any state amplitudes $c_j$ describing the quantum state of pho-

tons as described in [24]:

$$c_j(t) \to \sqrt{\frac{(2\pi)^3}{V}} c(\mathbf{k}, t) \tag{1.21}$$

Now using the expressions for quantized electric field given in Eq. (1.14) and Hamiltonian of the free field in Eq. (1.19) we can proceed to analyze the system of a single stationary two level atom at position $\mathbf{r}$, interacting with the quantized electric field. The complete derivation of atom interacting with quantized electro-magnetic fields is rather lengthy and complicated with a few subtleties regarding gauge-choice involved. For a complete derivation, please refer to the material listed within these references [24, 25]. We shall skip the steps involved in this derivation and jump directly to the result. The Hamiltonian for this system will now have three parts, the free atomic Hamiltonian $H_A$, the free field Hamiltonian $H_F$ and the atom-field interaction Hamiltonian $H_{AF}$ as given in Eq. (1.23)

$$\begin{aligned} \hat{H} &= \hat{H}_A + \hat{H}_F + \hat{H}_{AF} && (1.22) \\ &= \hbar\omega_0 |e\rangle\langle e| + \sum_{\mathbf{k},\tau} \hbar\omega_{\mathbf{k}} \hat{a}^\dagger_{\mathbf{k},\tau} \hat{a}_{\mathbf{k},\tau} - \hat{\boldsymbol{\mu}} \cdot \hat{\mathbf{E}}(\mathbf{r}) && (1.23) \\ \hat{\boldsymbol{\mu}} \cdot \hat{\mathbf{E}}(\mathbf{r}) &= -(\hat{\boldsymbol{\mu}}^+ + \hat{\boldsymbol{\mu}}^-) \cdot (\hat{\mathbf{E}}^+(\mathbf{r}) + \hat{\mathbf{E}}^-(\mathbf{r})) && (1.24) \end{aligned}$$

In Eq. (1.23), we have explicitly taken sum over all the wave-vector modes, $\mathbf{k}$ and the two polarization modes associated to every wave-vector mode denoted by $\tau$. We also work in the dipole approximation regime and hence consider only the dipole interactions here. As was done earlier, we can drop off the energy non-conserving

terms using the RWA from $\hat{H}_{AF}$ and we would get:

$$\hat{H}_{AF} = \sum_{\mathbf{k},\tau} i\sqrt{\frac{\hbar\omega_{\mathbf{k}}}{2\epsilon_0 V}}\left[\langle g|\hat{\boldsymbol{\mu}}|e\rangle\cdot\boldsymbol{\varepsilon}_\tau^*|g\rangle\langle e|\hat{a}_{\mathbf{k},\tau}^\dagger e^{-i\mathbf{k}\cdot\mathbf{r}} - \langle e|\hat{\boldsymbol{\mu}}|g\rangle\cdot\boldsymbol{\varepsilon}_\tau|e\rangle\langle g|\hat{a}_{\mathbf{k},\tau}e^{i\mathbf{k}\cdot\mathbf{r}}\right] \tag{1.25}$$

$$= \hbar\sum_{\mathbf{k},\tau}\left[g_{\mathbf{k},\tau}^*|g\rangle\langle e|\hat{a}_{\mathbf{k},\tau}^\dagger e^{-i\mathbf{k}\cdot\mathbf{r}} + g_{\mathbf{k},\tau}|e\rangle\langle g|\hat{a}_{\mathbf{k},\tau}e^{i\mathbf{k}\cdot\mathbf{r}}\right] \tag{1.26}$$

where we have defined:

$$g_{\mathbf{k},\tau} = -i\sqrt{\frac{\omega_{\mathbf{k}}}{2\hbar\epsilon_0 V}}\langle e|\hat{\boldsymbol{\mu}}|g\rangle\cdot\boldsymbol{\varepsilon}_\tau \tag{1.27}$$

In Eq. (1.27), $g_{\mathbf{k},\tau}$ defines the single photon Rabi frequency at wavelength $\omega_{\mathbf{k}}$ for polarization given by $\boldsymbol{\varepsilon}_\tau$. It signifies the strength of the dipolar interaction between the atom and the component of the electric field with angular frequency $\omega_{\mathbf{k}}$ and polarization $\boldsymbol{\varepsilon}_\tau$. The Hamiltonion in Eq. (1.23) is the starting point for many quantum optical calculations including the studies of spontaneous emissions [30]. We shall revisit this formalism in the context of ensemble of three level atoms in Chapter III.

### 1.2.2 Single atoms vs Ensembles

One of the most important reasons for studying light-atom interactions and ways of manipulating light via atoms and vice-versa is to be able to use these systems for varied applications like single-photon emitters[31, 32], quantum gates [33–35], generation of quantum memories that can store quantum information [34, 36, 37], for studies of metrology [38, 39] etc. The natural question then arises, is there any advantage in using a single atom interacting with optical fields vs an ensemble of identical atoms? And what are the differences between these systems in terms of modelling them as well as performing experiments with them? In this section we will discuss these questions.

The resonant absorption cross section for a single atom is proportional to the transition wavelength squared, which means that it is generally very small (of the order of about $10^{-9}\text{cm}^2$) [40, 41]. For atomic ensembles with non-interacting atoms, this cross section increases by a factor of the number of atoms in the ensemble assuming the intensity of light is uniform across the ensemble.

Another interesting avenue for observing and applying multi-atom effects is the case of non-linear interactions between Rydberg atoms via dipole-dipole Rydberg blockade interactions [41–43]. The phenomenon of Rydberg blockade is such that when one Rydberg atom in an ensemble is excited to a Rydberg level, it prohibits excitation of another Rydberg atom in its vicinity to the same Rydberg level. This effectively creates a super-atom. When Rabi flopping [44–46] for such a system is measured, the effective Rabi frequency is observed to vary with the number of atoms under the influence of Rydberg blockade. The effective Rabi frequency is:

$$\Omega_{eff} = \sqrt{N}\Omega_0 \tag{1.28}$$

In the above equation, the number atoms in the super atom are denoted by $N$ and $\Omega_0$ stands for single atom Rabi frequency between ground and excited Rydberg state [44]. Further discussion on Rydberg blockade will be presented in Chapter II.

In some cases, for example two-photon Raman transitions in atomic ensembles, collective enhancement in emitted signal mode can be observed [47]. In such systems, emission of a Stoke's photon corresponds to a single atom being transferred from one atomic state to another. Since, it is not possible to identify which atom emitted the photon, such processes are described by multi-atom collective quantum states or spin-wave states. Because of multi-atom interference effects, the Stokes photons are emitted in a particular directional light mode that is correlated with the atomic spin-wave mode instead of being emitted in a random direction. This collectively enhanced

coupling provides immense improvement in the signal to noise ratio of the emitted signal which is a huge advantage over a single atom system [36, 47]. More discussion and mathematical derivation of this phenomenon will be presented in Chapter III.

Apart from the enhancement in atom-light coupling in an atomic ensemble compared to single atoms, it is also easier to trap, store and manipulate an atomic ensemble rather than a single atom. Single atoms are usually trapped using single beam dipole traps [48–50], lattice optical micro-traps [51, 52], nano-photonic waveguides [53] or in optical cavities [54, 55]. They are susceptible to being lost due to atomic motion and fluctuations in trapping potentials. It is also harder to detect signal emitted from single atoms since single photon losses are hard to account for. Ensuring that the traps are singly occupied is also challenging. On the other hand, atomic ensembles are trapped using optical lattices [56, 57] or magneto-optic traps [58, 59]. The whole atomic ensemble can be manipulated by using a few broad waist beams which makes experimental setups for atomic ensembles easier to handle.

### 1.2.3 Quantum networks and quantum communication

The ability to store, process and transfer quantum information which consists of quantum states and entanglement across long distances is one of the most lucrative applications that quantum sciences have to offer [60, 61]. The concept of quantum networks to facilitate this was introduced around two decades ago and since then a lot of progress has been made both theoretically and experimentally [62]. A quantum network comprises of individual quantum nodes that can generate, process and store quantum information which can then be communicated via quantum channels across multiple nodes as depicted by the schematic in Fig. 1.1. These quantum nodes play the role of quantum interfaces which interact with information carrying quantum channels. Most quantum communication protocols involve photonic qubits as information carries in optical channels. Though photons are ideal for transport-

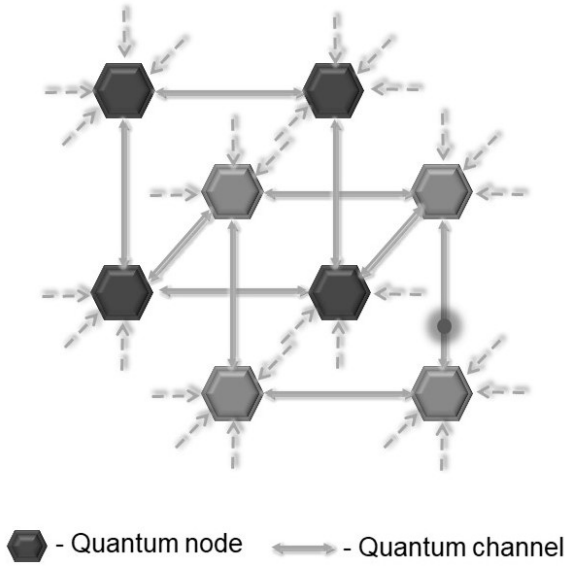


Figure 1.1: Schematic of a Quantum Network: This is a cartoon representation of a quantum network where different quantum information carrying channels are interconnected with quantum interfaces made of physical systems that are capable of storing, processing and releasing quantum information carried in the quantum channels.

ing information, it is extremely difficult to store and manipulate them. Therefore, the need of quantum nodes made of physical systems that can interact with photons and convert them into stationary material qubits that can be stored and efficiently converted back to carrier photons. Many systems are being investigated as potential quantum interfaces such as room temperature or cold atomic ensembles [63], trapped ion systems [64], solid state ensembles [65], quantum dots [66] and NV centers [67]. Of all these systems, atomic ensembles have been most well studied for applications as quantum interfaces. Atomic ensembles are easier to trap and manipulate using simple linear optics and interact efficiently with information carrying photons. Quantum atomic ensembles provide a way to coherently convert a photonic qubit to an atomic qubit and vice-versa using schemes involving Raman transitions and Electromagnetically Induced Transparency (EIT) [41]. For a good review of different protocols used for storing and retrieving photons coherently from atomic ensembles refer the article by Hammerer *et. al.* [63]. Apart from efficient quantum interfaces, another impor-

tant requirement for quantum communication is the ability to improve state transfer across multiple quantum nodes. Quantum repeater protocols have been formulated to achieve this long distance states transfer using atomic ensembles and light-matter interactions [36]. More discussion on quantum repeaters and a brief explanation of the Duan-Lukin-Cirac-Zoller protocol is provided in Chapter III.

## 1.3 Outline of the Dissertation

Having laid out the basic concepts that will be important for the discussions in the following Chapters, let us now look at the organization of this dissertation. In Chapter II, we will be looking at a protocol to create multi-atom entangled Greenberger-Horne-Zeilinger (GHZ) states using Stimulated Raman Adiabatic Passage (STIRAP) and Rydberg blockade. The concepts of STIRAP and Rydberg blockade will be discussed before delving into the details of the protocol. In Chapter III we will study intrinsic retrieval efficiency of quantum interfaces formed from atomic ensembles that play an important role in quantum repeater protocols. A brief introduction to Duan-Lukin-Cirac-Zoller (DLCZ) quantum repeater protocol will also be provided in this Chapter. In Chapter IV, we will conclude with a discussion of the impacts of studying these two avenues exploring light-matter interactions in neutral cold-atom ensembles. Future outlook and improvements that can be made in these approaches will also be discussed.

# CHAPTER II

# Generating GHZ States in Atomic Ensembles using STIRAP and Rydberg Blockade

## 2.1 Introduction

In this chapter, we will propose a protocol for the creation of multi-particle Greenberger-Horne-Zeilinger (GHZ) states in an atomic ensemble of three level $\Lambda$ atoms using Stimulated Raman Adiabatic Passage (STIRAP) and Rydberg blockade. The effects of spontaneous emissions from excited atomic levels are also studied along with numerical results on the performance of this protocol.

We start this chapter by providing a brief introduction to GHZ states, the process of STIRAP and Rydberg blockade. It is then followed by the description of the main protocol and we conclude with discussion of the numerical results obtained for this method.

### 2.1.1 Greenberger-Horne-Zeilinger (GHZ) States

At the heart of quantum mechanics lies the phenomenon of quantum entanglement. Bell states, which are maximally entangled two qubit states show 'measurement correlations stronger than could ever exist between classical systems' in the words of Neilson and Chuang [61]. These non-classical correlations are the essence of Bell's

inequalities that were formulated by John Bell in 1964 [68] addressing the paradox raised by Einstein-Podolsky-Rosen (EPR) in their famous paper on nature of physical reality described by quantum mechanics[69]. Bell states play a central role in many quantum communication protocols like quantum teleportation, quantum key distribution etc. [20, 21, 61, 70–73]. Let us look at one of the four Bell states given below in Eq. (2.1).

$$|\Phi\rangle = \frac{|00\rangle + |11\rangle}{\sqrt{2}} \tag{2.1}$$

Bell states show perfect correlation between the measurement results of the first qubit and the second qubit in any given basis irrespective of the physical separation between the two qubits. For example, in Eq. (2.1) whatever be the outcome of the measurement on the first qubit in a given basis, the outcome of the measurement of the second qubit is instantaneously determined. This perfect correlation in measurements violates the notion of local realism [68] and is the peculiar phenomenon at the heart of the EPR paradox.

Generalizations of these two qubit Bell states are the multi-particle entangled quantum states called the Greenberger-Horne-Zeilinger (GHZ) states given in Eq. (2.2) [74, 75].

$$|\mathrm{GHZ}\rangle_m = \frac{|0\rangle^{\otimes m} \pm |1\rangle^{\otimes m}}{\sqrt{2}}, \qquad m > 2 \tag{2.2}$$

They exhibit entanglement based effects which are much more rich compared to Bell states [74–77]. Consider for example a three qubit GHZ state given in Eq. (2.3).

$$|\mathrm{GHZ}\rangle_3 = \frac{|000\rangle + |111\rangle}{\sqrt{2}} \tag{2.3}$$

On measuring any one of the three qubits in Eq. (2.3) in the standard basis, half the

times we get the unentangled pure state $|00\rangle$ and the pure state $|11\rangle$ rest of the time. On the other hand, taking a trace over one of the qubits leads to an unentangled mixed state whose density matrix is given in Eq. (2.4)

$$\mathrm{Tr}_1(|\mathrm{GHZ}\rangle_{33}\langle\mathrm{GHZ}|) = \frac{|00\rangle\langle 00| + |11\rangle\langle 11|}{2} \tag{2.4}$$

If instead of measuring one of the qubits of the three qubit GHZ state in the standard basis, one measures it in superposition basis $|\pm\rangle$ where:

$$|+\rangle = \frac{|0\rangle + |1\rangle}{\sqrt{2}} \tag{2.5}$$

$$|-\rangle = \frac{|0\rangle - |1\rangle}{\sqrt{2}} \tag{2.6}$$

we would get maximally entangled two qubit Bell states $\frac{|00\rangle \pm |11\rangle}{\sqrt{2}}$ with a probability of one half each.

These highly entangled GHZ states violate Bell-like inequalities more strongly than their two qubit counter parts [76, 77]. The multi-particle entangled GHZ state shows unique non-local correlations which are essential for understanding the fundamental principles of quantum entanglement [74, 78]. Exploration of unique non-local properties shown by GHZ states is a topic of ongoing research and will hopefully help define multi-particle quantum entanglement more concretely [79–81].

Like Bell states, GHZ states are important for various applications of quantum communication, cryptography and precision measurements [82–88]. With this short introduction to GHZ states, their important properties and applications, let us now briefly look at the concept of STIRAP.

### 2.1.2 Stimulated Raman Adiabatic Passage (STIRAP)

The method of STIRAP introduced in the 1980s is a well known technique that allows a robust method of population transfer between two specific levels of a (generally, three level) atomic system [89–91]. Consider a three level $\Lambda$ atomic system shown in Fig. 2.1 such that the two levels $|g\rangle$ and $|s\rangle$ are stable or meta-stable states and $|e\rangle$ is an excited state. The transitions between states $|g\rangle - |e\rangle$ are driven by a classical probe field and the transitions between the $|s\rangle - |e\rangle$ states by a similar pump field. The strength of both the pump and probe fields change as a function of time. Let $\delta_{g/s}$ be the detuning between the transition frequency and the carrier frequency of the applied optical fields for the $|g\rangle - |e\rangle$ and $|s\rangle - |e\rangle$ transitions respectively. Under the two photon resonance condition which implies that $\delta \equiv \delta_g - \delta_s = 0$ as illustrated in Fig. 2.1, the Hamiltonian of the system in the Rotating Wave Approximation (RWA) for a basis set $\{|g\rangle, |e\rangle, |s\rangle\}$ is given in Eq. (2.7)

$$\mathrm{H} = \frac{\hbar}{2} \begin{bmatrix} 0 & \Omega_g(t) & 0 \\ \Omega_g(t) & 2\delta & \Omega_s(t) \\ 0 & \Omega_s(t) & 0 \end{bmatrix}. \tag{2.7}$$

Where $\Omega_g(t)$ is the time dependent Rabi frequency corresponding to the $|g\rangle - |e\rangle$ transition and similarly $\Omega_s(t)$ is the Rabi frequency for the $|s\rangle - |e\rangle$ transition. We have chosen the Rabi frequencies to be real for the sake of simplicity. One of the eigenergies of the above Hamiltonian in Eq. (2.7) is 0. The corresponding eigenstate of the Hamiltonian which has been traditionally called the Dark state, $|D\rangle$ given in Eq. (2.8) is at the center of this population transfer protocol.

$$|D(t)\rangle = \frac{\Omega_s(t)}{\sqrt{\Omega_g^2(t) + \Omega_s^2(t)}}|g\rangle - \frac{\Omega_g(t)}{\sqrt{\Omega_g^2(t) + \Omega_s^2(t)}}|s\rangle \tag{2.8}$$

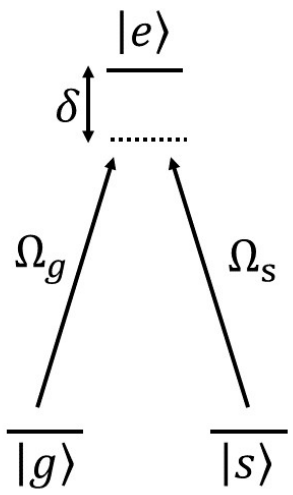


Figure 2.1: $\Lambda$ atomic level structure: The states $|g\rangle$ and $|s\rangle$ are two stable ground states that interact with the excited state $|e\rangle$ through Rabi frequencies $\Omega_g$ and $\Omega_s$ respectively. Under the two photon resonance condition, the detuning for transitions $|g\rangle - |e\rangle$ and $|s\rangle - |e\rangle$ is equal given by $\delta$

We can simplify the analysis by considering the substitution $\tan\theta(t) = \dfrac{\Omega_g(t)}{\Omega_s(t)}$. The dark state can now be re-written as given below:

$$|D(t)\rangle = \cos\theta(t)|g\rangle - \sin\theta(t)|s\rangle \tag{2.9}$$

Notice that state $|D\rangle$ has no contributions from the excited state $|e\rangle$. If we start out with the atomic population in the state $|g\rangle$, we can transfer it to state $|s\rangle$ by adiabatically changing the co-efficients of the dark state from $\cos\theta(0) = 1$ to $\sin\theta(T) = 1$ over a duration of time period $T$ in Eq. (2.9), with negligible occupation of the excited state. To enable this, optical fields controlling the $|s\rangle - |e\rangle$ transitions are turned on first, followed by the field for $|g\rangle - |e\rangle$ transition. It is important that these fields are turned on and off adiabatically with sufficient temporal overlap between them to facilitate complete population transfer[89]. Since, the fields corresponding to Rabi frequency $\Omega_s(t)$ is turned on first even though the atomic population is occupying the state $|g\rangle$, this pulse sequence is referred to as counter intuitive STIRAP pulse scheme

[90, 92]. Unlike schemes of atomic population transfer where in precise control of the pulse shapes and intensities are required for high fidelity transfer, STIRAP is immune to minor fluctuations in these experimental conditions [89]. Thus, STIRAP is a robust method of population transfer from one state to another with extremely small loses due to spontaneous emission from the excited levels. Population transfer efficiency of more than 95% has been reported in numerous experiments using STIRAP [93–95]. Since, it is an adiabatic process, a discussion about the conditions required to maintain adiabaticity is important and they will be discussed in detail in the forthcoming Sec. 2.2.3. For a comprehensive review on STIRAP please refer to Vitanov *et. al.* [89]. Let us now briefly discuss the second important piece of our proposed GHZ state generation protocol, namely Rydberg blockade.

### 2.1.3 Rydberg Blockade

Rydberg atoms allow atomic excitation of the electrons to atomic levels with large principal quantum numbers, $n \gg 1$. Since the size of the atom scales as $n^2$, atoms excited to high lying states have a large size and therefore a large dipole moment. These large dipole moments provide a controllable means of generating strong dipole-dipole interactions between Rydberg atoms [41, 42, 96]. The strong resonant dipole-dipole interactions scale as $\frac{1}{R^3}$ at short distances, $R$, and scale as $\frac{1}{R^6}$ corresponding to Van der Waals interactions at long distances [96]. This novel feature of Rydberg atoms where the interactions can be turned on and off based on whether the atoms are excited to Rydberg levels or not plays an important role in many quantum information protocols to entangle atoms [41, 43, 97, 98].

In an ensemble of neutral atoms, when two atoms are excited to Rydberg energy levels, because of the strong resonant dipolar interactions between them, the energy of doubly occupied Rydberg levels shifts. This energy shift is a function of the atomic dipole moment as well as the separation between the atoms. As a result, Rydberg

atoms in the vicinity of an excited Rydberg atom cannot be excited to the same Rydberg state because of these energy level shifts [96, 99]. It is explained pictorially in Fig. 2.2; because of the dipolar interaction between the two Rydberg atoms with a Rabi frequency $\Omega$, the energy level with both the atoms excited to Rydberg level $|R, R\rangle$ undergoes an energy shift given by $\Delta$ as a function of their inter-atomic distance $d$. Notice that there is no effect on the energy levels when only one atom is excited to the Rydberg level and the other is in the ground state $|0, R\rangle$. This phenomenon of 'dipole blockade' provides an atomic control that acts on multiple atoms at the same time, which is necessary for generating entanglement between the atoms of the ensemble within the blockade radius. A blockade radius can be thought of as the radius of the sphere around an excited Rydberg atom within which no other atom can be excited to the Rydberg level with optical transitions. Thus, in essence only one Rydberg excitation is allowed within this sphere giving rise to a super-atom with multiple atoms. We will be using this phenomenon of Rydberg blockade as a controllable means of generating one step entanglement on a mesoscopic scale.

Let us now get into the details of the scheme for GHZ state generation using STIRAP and Rydberg blockade.

## 2.2 Proposal for GHZ state generation

Many ingenious schemes for creation of GHZ states in atomic systems have been previously proposed using a multi-step or a single-step process [96, 100, 101]. We present here a single-step scheme for GHZ state creation employing Rydberg dipole blockade and STIRAP [89, 102] using a single control atom and an ensemble of target atoms. Approaches to create a multi-particle GHZ state by using Electromagnetically Induced Transparency (EIT) and adiabatic passage along with Rydberg blockade have been previously studied [97, 98, 100]. Fidelity of the GHZ states obtained at the end of these protocols is an important parameter to consider. Because of radiative decay

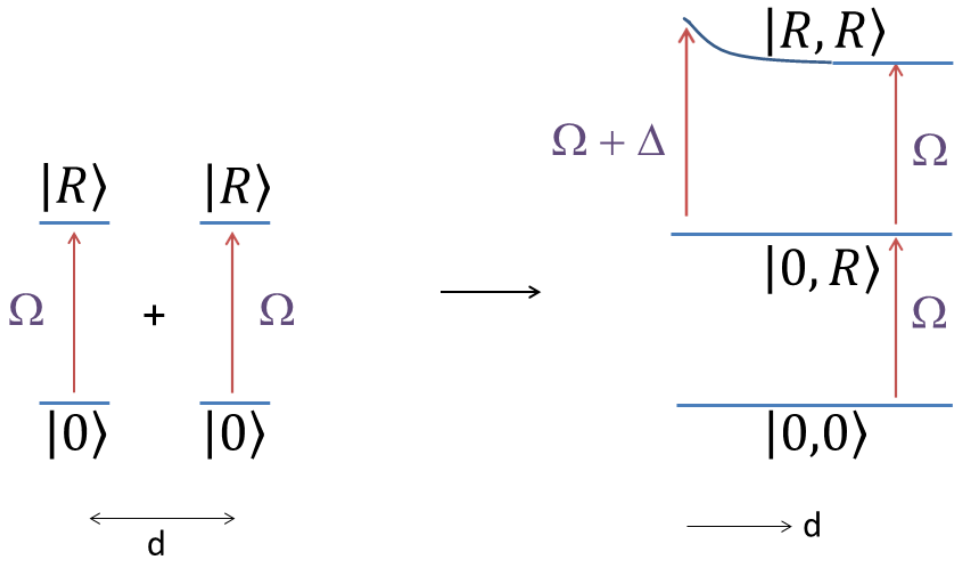


Figure 2.2: Schematic of Rydberg blockade: When two Rydberg atoms with ground state $|0\rangle$ and excited Rydberg level $|R\rangle$ are brought in close proximity, the energy level corresponding to the doubly excited $|R, R\rangle$ state undergoes a distance dependent shift given by $\Delta$. For values of inter-atomic separation, $d$, smaller than the blockade radius, excitation of two Rydberg atoms to the excited state is prohibited for a Rabi frequency $\Omega$ corresponding to the $|0\rangle - |R\rangle$ transition.

from the excited Rydberg states of the ensemble atoms, the fidelity of the GHZ states obtained in these schemes is adversely affected [96].

Here we propose a different theoretical scheme to realize the creation of a multi-particle GHZ state in an ensemble of $\Lambda$ three-level Rydberg atoms which is robust to radiation decay from the excited Rydberg levels of the ensemble atoms. In this setup, the control atom and the ensemble of the target atoms are assumed to be independently addressable. This can be achieved by storing them in two separate trapping potentials in close proximity or in a lattice where the control atom can be efficiently addressed. This setup is similar to what has been discussed in the proposal by Muller et. al. [100].

The control atom has a three level structure as is shown in Fig. 2.3a. The two meta-stable levels $|0\rangle$ and $|1\rangle$ determine the state of the control atom. Level $|0\rangle$ is connected to the excited Rydberg level $|R\rangle$ via a control pulse with Rabi frequency

given by $\Omega_c(t)$.

Level $|1\rangle$ is chosen such that dipolar transitions between $|1\rangle$ and $|0\rangle$ as well as $|R\rangle$ are forbidden. An ensemble having N target Rydberg atoms is considered to be within the blockade radius of the excited control atom. The level structure of the ensemble atoms and the corresponding pulse sequence acting on them is shown in Fig. 2.3. Every ensemble atom has two metastable ground states, namely, $|g\rangle$ and $|s\rangle$ and one Rydberg excited level $|r\rangle$. All the ensemble atoms are initiated in the $|g\rangle$ state. This GHZ state creation protocol begins with a control $\pi$ pulse having Rabi frequency $\Omega_c(t)$ which is used to excite the control atom. If the control atom is in state $|1\rangle$, the control pulse has no effect. On the other hand, if it is in state $|0\rangle$, with the action of the control $\pi$ pulse, the atom is excited to the Rydberg level $|R\rangle$. Due to the long range dipole-dipole interactions between the excited Rydberg level $|R\rangle$ and Rydberg levels $|r\rangle$, the target ensemble Rydberg levels undergo energy level shift given by a frequency $\Delta$ (refer to Sec. 2.1.3). In the absence of this energy shift, the condition for adiabatic population transfer of the ensemble atoms from the ground state $|g^N\rangle = \otimes_{j=1}^{N}|g\rangle_j$ to $|s^N\rangle = \otimes_{j=1}^{N}|s\rangle_j$ via the counter-intuitive STIRAP pulse sequence $\Omega_s(t)$ and $\Omega_g(t)$ [Fig. 2.3] is satisfied (refer to Sec. 2.1.2). The parameters of the system are set up in such a way that when the control atom is excited to $|R\rangle$, the induced energy shift $\Delta$ in the ensemble atoms disrupts the STIRAP condition for population transfer from $|g^N\rangle$ to $|s^N\rangle$. Due to the added detuning the population remains in the state $|g^N\rangle$ after the application of the STIRAP pulses. Finally, another control $\pi$ pulse is used to bring the control atom back to the original state. When the control atom is prepared in the $\frac{1}{\sqrt{2}}(|0\rangle + |1\rangle)$ superposition state at the beginning of the protocol and finally measured in the superposition basis, the ensemble atoms get projected to a N particle GHZ state.

If the conditions for STIRAP are met, the instantaneous eigenstate occupied by the ensemble atoms has no contribution from the level $|r\rangle$ at all times. Hence, this

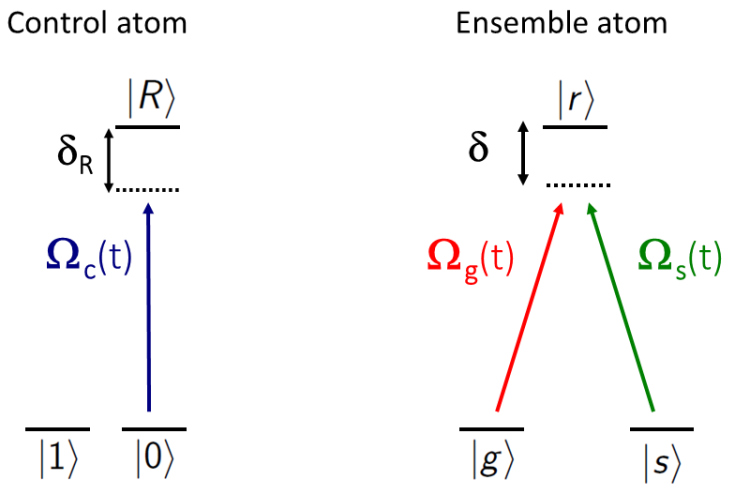


(a) Atomic level structure

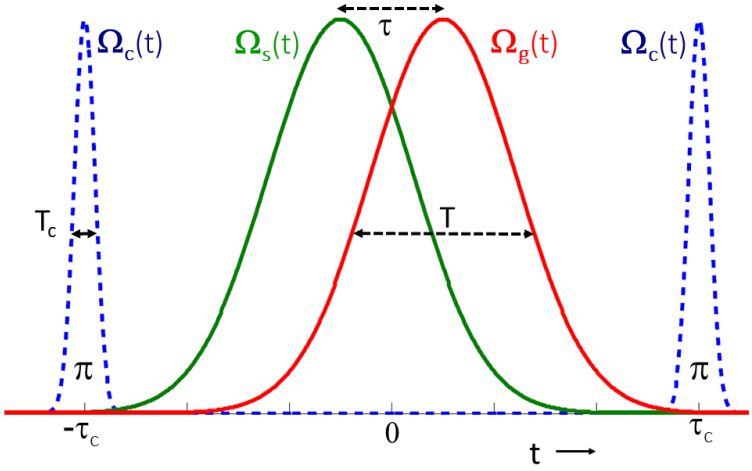


(b) Pulse Scheme

Figure 2.3: Atomic level structure and pulse scheme for GHZ state generation: (a) This figure describes the atomic level structure of the control atom and the target ensemble atoms. The control atom has two metastable states $|0\rangle$ and $|1\rangle$. The level $|0\rangle$ interacts with the excited Rydberg level $|R\rangle$ via Rabi frequency $\Omega_c(t)$. $\delta_R$ is the detuning between the carrier frequency of the light pulse and the frequency of transition between the levels $|0\rangle$ and $|R\rangle$. The level $|1\rangle$ is isolated from the other levels. Each target atom has a $\Lambda$ type level structure with two metastable states, $|g\rangle$ and $|s\rangle$. They interact with the excited Rydberg level $|r\rangle$ via Gaussian pulses having Rabi frequencies $\Omega_g(t)$ and $\Omega_s(t)$ respectively. The detuning for both the pulses is given by $\delta$. (b) This figure describes the pulse sequences for the GHZ state generation protocol. The protocol begins with a Gaussian $[\Omega_c(t)]$ $\pi$ pulse having a standard deviation given by $T_c$ to take the control atom from $|0\rangle$ to $|R\rangle$. It is then followed by counter-intuitive STIRAP pulse sequence with Gaussian profiles, each having $T(\gg T_c)$ standard deviation. $\tau$ is the time interval between the peaks of these two STIRAP pulses. Finally, another control $\pi$ pulse is used to bring the control atom back to state $|0\rangle$.

protocol is insensitive to the radiative decay losses from the excited Rydberg level of the ensemble atoms.

Let us now analyze this scheme in detail and study the dependence of the STIRAP transfer conditions on the parameters of the system. In Sec. 2.2.1 we discuss the dynamics of the control atom. This is followed by the discussion of the transfer mechanism in the target atoms and the adiabaticity conditions required for efficient transfer in Sec. 2.2.2. Numerical simulations of this protocol for realistic parameters are then presented in Sec. 2.3 . In Sec. 2.5 we conclude the discussion.

### 2.2.1 The control atom

Hamiltonian for the control atom interacting with the classical control field in the field interaction representation with the Rotating Wave Approximation (RWA) is given below:

$$\frac{H_C(t)}{\hbar} = \delta_R|R\rangle\langle R| + \frac{\Omega_c^*(t)}{2}|0\rangle\langle R| + \frac{\Omega_c(t)}{2}|R\rangle\langle 0| \tag{2.10}$$

The energy levels are measured relative to the ground state energy $\hbar\omega_0 = 0$. In Eq. (2.10), $\delta_R \equiv \omega_R - \omega_c$ is the detuning between the frequency of transition from $|0\rangle$ to $|R\rangle$ (denoted by $\omega_R$) and the optical frequency of the control pulse, $\omega_c$. As noted previously, $\Omega_c(t)$ is the Rabi frequency of the control pulse with a Gaussian temporal profile given below.

$$\Omega_c(t) = \Omega_{c0} \exp\big[-\frac{(t-\tau_c)^2}{2T_c^2}\big] \tag{2.11}$$

We will assume the peak Rabi frequency, $\Omega_{c0}$, to be real in all the calculations here after. As already noted, level $|1\rangle$ is isolated from the levels $|0\rangle$ and $|R\rangle$ and hence is not included in the Hamiltonian. For $\delta_R = 0$, on solving the Schrodinger's equation

for a general wave-function, $|\Psi(t)\rangle = c_0(t)|0\rangle + c_R(t)|R\rangle$, with $|c_0(-\infty)| = 1$, we get:

$$|c_0(\infty)|^2 = \cos^2\Theta \tag{2.12}$$

$$|c_R(\infty)|^2 = \sin^2\Theta \tag{2.13}$$

$$\Theta \equiv \int_{-\infty}^{\infty} \frac{\Omega_c(t')}{2} dt' = \Omega_{c0} T_c \sqrt{\frac{\pi}{2}} \tag{2.14}$$

For complete transfer of population from $|0\rangle$ to $|R\rangle$ state, $\Theta$ should be an odd multiple of $\frac{\pi}{2}$. Thus, we need:

$$\Omega_{c0} T_c = (2p+1)\sqrt{\frac{\pi}{2}},\ p \in \mathbb{Z} \tag{2.15}$$

To check for the robustness of this transfer against variations in the Rabi frequency, we look at the derivative of $|c_R(\infty)|$ with respect to $\Omega_{c0}$.

$$\frac{\partial |c_R(\infty)|}{\partial \Omega_{c0}} = -T_c \sqrt{\frac{\pi}{2}} \cos(\Omega_{c0} T_c \sqrt{\frac{\pi}{2}}) \tag{2.16}$$

Eq. (2.16) implies that smaller values of $T_c$ provide more robustness against variation in $\Omega_{c0}$. For $\delta_R \neq 0$, analytic solution for Gaussian form of the Rabi frequency is difficult to derive. Hence, we will look at the dependence of $|c_R(\infty)|^2$ on different values of $\Omega_{c0}$, $\delta_R$ and $T_c$ numerically in Fig. 2.4. For the value of $T_c = 0.1T$, where $T$ is the standard deviation of the Gaussian STIRAP pulses, we see from Fig. 2.4a that the population gets completely transferred to the $|R\rangle$ state when $\frac{\Omega_{c0} T}{2} = 6.2$ and $\delta_R T = 0$. From Fig. 2.4b, we see that there are multiple periodic values of $\Omega_{c0} T$ for which complete population transfer to the excited level can be achieved via a $\pi$ pulse as expected from Eq. (2.15) for $T_c = 1T$. As $\delta_R T$ becomes larger, the fraction of population in the excited state decreases and eventually becomes zero. The effect of larger values of $\delta_R T$ is more prominent for larger values of $T_c$. As derived in Eq.

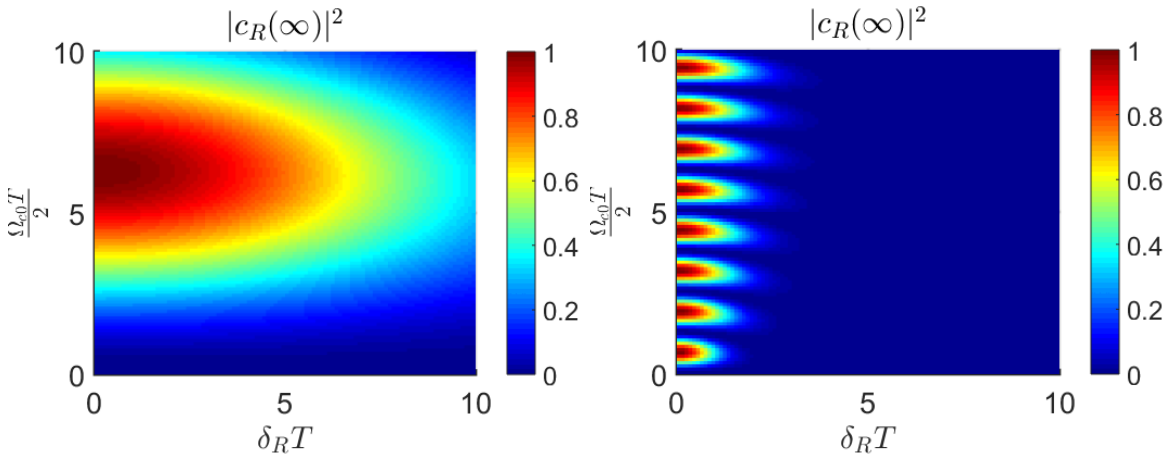


(a) $T_c = 0.1T$ (b) $T_c = 1T$

Figure 2.4: Population distribution of the control atoms for different values of detuning and Rabi frequencies: (a) The coefficient of population in state $|R\rangle$ transferred from $|0\rangle$, $|c_R(\infty)|^2$, due to the control $\pi$ pulse is plotted as a function of scaled detuning $\delta_R T$ and scaled peak control Rabi frequency $\Omega_{c0}T$ for a value of $T_c = 0.1T$. (b) Same as plot (a) but for value of $T_c = 1T$. We see that smaller values of $T_c$ are more robust to variations in detuning and peak Rabi frequency.

(2.16), we see that smaller values of $T_c$ provide more robust transfer against variations in $\Omega_{c0}$ and $\delta_R$.

### 2.2.2 The target ensemble

In this section, we will derive the conditions that are necessary to maintain adiabatic transfer of the ensemble atoms from $|g^N\rangle$ to $|s^N\rangle$ when the control atom is in state $|1\rangle$ and to remain in the state $|g^N\rangle$ when the control atom is in the $|0\rangle$ state. The Hamiltonian for ensemble atoms interacting with the counter-intuitive STIRAP pulse sequence in the RWA is given below:

$$\begin{aligned}\frac{H_T(t)}{\hbar} &= \sum_{j=1}^{N}\left[(\omega_r^0-\delta_g)|g\rangle_j\langle g| + (\omega_r^0-\delta_s)|s\rangle_j\langle s|\right] \\ &+ \sum_{j=1}^{N}\left[\frac{\Omega_g^*(t)}{2}e^{-i\omega_r^0 t}|g\rangle_j\langle r| + \frac{\Omega_s^*(t)}{2}e^{-i\omega_r^0 t}|s\rangle_j\langle r| + \text{h.c.}\right]\end{aligned} \tag{2.17}$$

In Eq. (2.17), $\hbar\omega_r^0$ is the energy of the excited level $|r\rangle$. For the energy of states $|g\rangle$ and $|s\rangle$ denoted by $\hbar\omega_g^0$ and $\hbar\omega_s^0$ respectively, $\delta_{g(s)} = \omega_r^0 - \omega_{g(s)}^0 - \omega_{g(s)}$ are the detunings of these levels with respect to the optical frequencies $\omega_g$ and $\omega_s$ of the STIRAP pulses shown in Fig. 2.3b. The corresponding Rabi frequencies $\Omega_g(t)$ and $\Omega_s(t)$ are defined as follows:

$$\Omega_g(t) = \Omega \exp\big[-\frac{(t-\frac{\tau}{2})^2}{2T^2}\big] \tag{2.18}$$

$$\Omega_s(t) = \Omega \exp\big[-\frac{(t+\frac{\tau}{2})^2}{2T^2}\big] \tag{2.19}$$

In Eqs. (2.18)-(2.19), $\Omega$ is the peak Rabi frequency of the Gaussian STIRAP pulses, $\tau$ is the time separation between the peaks of the two pulses and $T$ is the standard deviation. We can simplify the Hamiltonian in Eq. (2.17) by setting $\omega_r^0 = 0$ and assuming two photon resonance condition for the system i.e. $\delta_g = \delta_s = \delta$ [102]. Boosting the energy of all the levels by $\delta$, we get the modified Hamiltonian for the target ensemble as:

$$\frac{H_T(t)}{\hbar} = \sum_{j=1}^{N}\big[\delta|r\rangle_j\langle r| + \big(\frac{\Omega_g^*(t)}{2}|g\rangle_j\langle r| + \frac{\Omega_s^*(t)}{2}|s\rangle_j\langle r| + \text{h.c.}\big)\big] \tag{2.20}$$

We will restrict the set of basis states for the analysis of this system to a set containing only one Rydberg level excitation by assuming that all the atoms are within the Rydberg blockade radius of each other. We can rewrite the Hamiltonian in Eq. (2.20) in the symmetric Fock state basis set defined by [103]:

$$\Sigma_{\mu,\nu} = \sum_j |\mu\rangle_j\langle\nu| = a_\mu^\dagger a_\nu; \tag{2.21}$$

$$|g^{N-n}; s^n; r^0\rangle = \sqrt{\frac{(N-n)!}{N!n!}}\Sigma_{s,g}^n|g^N\rangle \tag{2.22}$$

$$|g^{N-n-1}; s^n; r^1\rangle = \sqrt{\frac{(N-n-1)!}{N!n!}}\Sigma_{s,g}^n\Sigma_{r,g}|g^N\rangle \tag{2.23}$$

In the above equation, $a_\mu^\dagger$ is an operator for creation of atomic excitation in the state $\mu$ and similarly, $a_\nu$ is the destruction operator. There are in all (2N+1) states in this basis set, namely,

$$\begin{aligned}\left\{|g;s;r\rangle_N\right\} &= \left\{|g^N;s^0;r^0\rangle,..,|g^{N-n};s^n;r^0\rangle,..|g^0;s^N;r^0\rangle,\right. \\ &\quad \left.|g^{N-1};s^0;r^1\rangle,..,|g^{N-n-1};s^n;r^1\rangle,..|g^0;s^{N-1};r^1\rangle\right\} \qquad (2.24)\end{aligned}$$

As a short hand notation, we use $|g^N\rangle \equiv |g^N;s^0;r^0\rangle$ and $|s^N\rangle \equiv |g^0;s^N;r^0\rangle$. The corresponding Hamiltonian in the Fock number basis is then:

$$\frac{H_T(t)}{\hbar} = \delta\sigma_r^+\sigma_r^- + \left[\frac{\Omega_g^*(t)}{2}a_g^\dagger\sigma_r^- + \frac{\Omega_s^*(t)}{2}a_s^\dagger\sigma_r^- + \text{h.c.}\right] \qquad (2.25)$$

Where:

$$\sigma_r^+|r^0\rangle = |r^1\rangle,\ \sigma_r^-|r^0\rangle = 0 \qquad (2.26)$$

$$\sigma_r^-|r^1\rangle = |r^0\rangle,\ \sigma_r^+|r^1\rangle = 0 \qquad (2.27)$$

Using the properties of block [104] and tri-diagonal matrices [105] it can be shown that the Hamiltonian in Eq. (2.25) when expressed as a matrix in the basis set defined by Eq. (2.24) always has one eigenvalue as 0. The characteristic equation for this Hamiltonian is invariant when $\delta \to -\delta$ and the eigenvalue $\lambda \to -\lambda$. The details of finding the eigenvalues of the Hamiltonian given in Eq. (2.25) in the basis set defined in Eq. (2.24) is provided in Appendix A. With the following new definitions given in Eqs. (2.28)-(2.29), let us explore the eigen-structure of this system.

$$\Omega_0(t) \equiv \sqrt{\Omega_g^2(t) + \Omega_s^2(t)} \qquad (2.28)$$

$$\tan\theta(t) \equiv \frac{\Omega_g(t)}{\Omega_s(t)}; \qquad \tan\varphi(t) \equiv \frac{\Omega_0(t)}{\delta} \qquad (2.29)$$

On solving for the eigenvalues of this system, we find that the non-zero eigen-energies are (refer to Appendix A for details):

$$E^N_{\pm n} = \frac{\hbar\Omega_0(t)}{2}[\cot\varphi(t) \pm \sqrt{n + \cot^2\varphi(t)}],\ n = 1, .., N \tag{2.30}$$

The corresponding eigen-states are denoted by $|\lambda^N_{\pm n}\rangle$. The eigenstate with eigenenergy 0 is given as:

$$|O(t)\rangle = \sum_{n=0}^{N}(-1)^{N-n}\alpha^N_n(t)|g^{N-n}; s^n; r^0\rangle \tag{2.31}$$

$$\alpha^N_n(t) = \sqrt{\frac{N!}{n!(N-n)!}}\cos^{N-n}(\theta(t))\sin^n(\theta(t)) \tag{2.32}$$

State $|O(t)\rangle$ is the N particle STIRAP state. As $t \to -\infty$, $|O(-\infty)\rangle = |g^N\rangle$ and $t \to \infty$, $|O(\infty)\rangle = |s^N\rangle$. If this system evolves adiabatically, then the population of the target ensemble can be coherently transferred from $|g^N\rangle$ to $|s^N\rangle$. This eigenstate with eigenvalue 0 has no contribution from the excited level $|r\rangle$ for any number of ensemble atoms at all times. It is also independent of the detuning $\delta$. In the STIRAP process our aim is to keep the target ensemble in the instantaneous eigenstate $|O(t)\rangle$ at all times. Adiabatic population transfer along this eigenstate implies that this protocol is insensitive to the spontaneous emissions from the excited level $|r\rangle$. This is a key feature of this scheme which provides us with a robust mechanism of population transfer even in the presence of decay. Numerical studies in the presence of decay are described in Sec. 2.3.

### 2.2.3 Adiabaticity conditions

Let us now look at the adiabaticity conditions required for the desired population transfer. The condition for maintaining adiabatic transfer along the $|O(t)\rangle$ state is

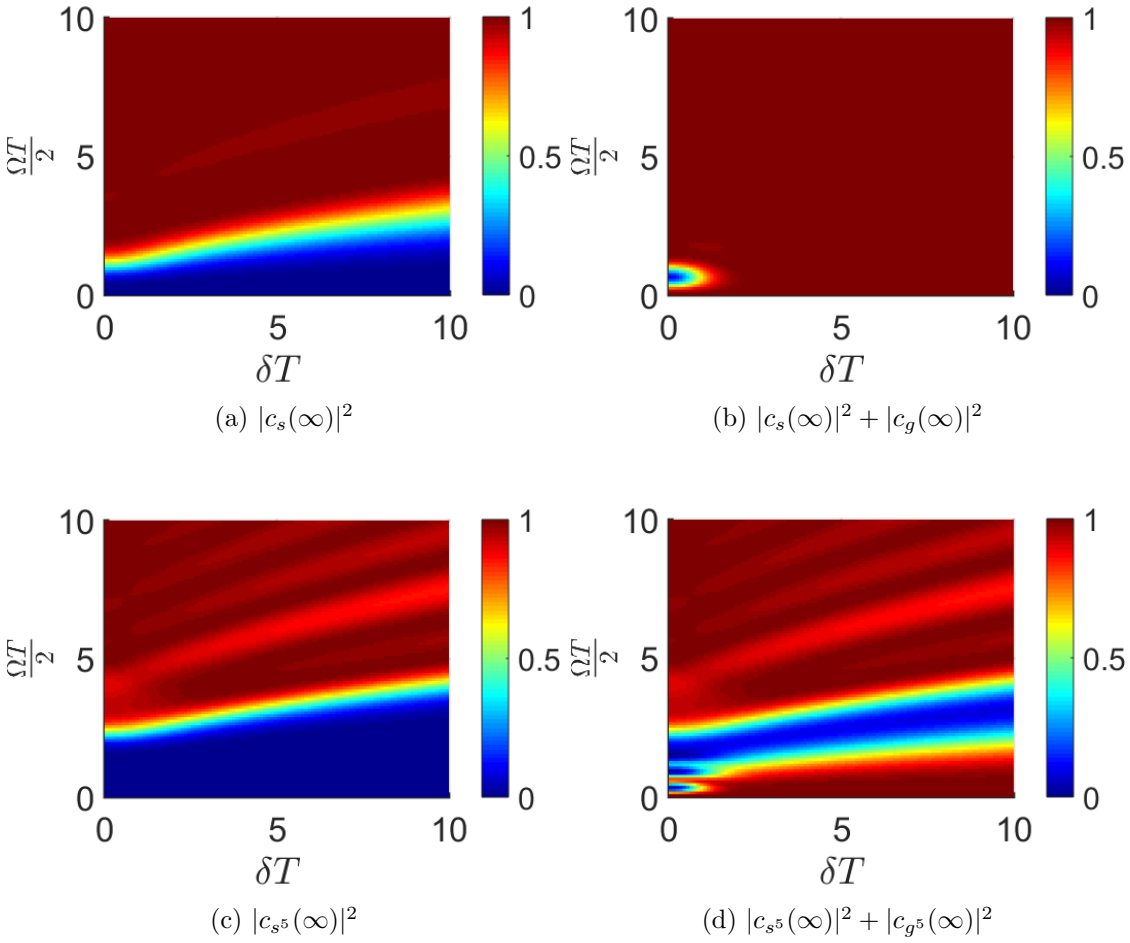


(a) $|c_s(\infty)|^2$ (b) $|c_s(\infty)|^2 + |c_g(\infty)|^2$

(c) $|c_{s^5}(\infty)|^2$ (d) $|c_{s^5}(\infty)|^2 + |c_{g^5}(\infty)|^2$

Figure 2.5: Population distribution of ensemble atoms in the multi-particle ground states $|g^N\rangle$ and $|s^N\rangle$: (a) Co-efficient of population in state $|s\rangle$ for a target ensemble with 1 atom after the application of STIRAP pulses as a function of the scaled peak Rabi frequency $\Omega T$ and scaled detuning $\delta T$ for $\tau = 1.4T$.(b)Total population in the state $|s\rangle$ and $|g\rangle$ after the STIRAP pulses for a single target atom as a function of $\Omega T$ and $\delta T$. (c) Same as plot (a) but for a target ensemble of 5 atoms. (d) Same as plot (b) for N = 5 atoms. We see that as the number of target atoms goes up, the parameter space for adiabatic transfer from $|g^N\rangle$ to $|s^N\rangle$ or no transfer gets modified as per the conditions derived in Eqs. (2.43)-(2.45)

summarized by the adiabaticity criterion discussed in [106] given as:

$$\sum_{m\neq 0} \left| \frac{\hbar\langle m|\dot{O}(t)\rangle}{E_0 - E_m} \right| \ll 1 \tag{2.33}$$

In the above Eq. (2.33), $E_0$ is the eigenenergy of the eigenstate $|O(t)\rangle$ and the sum is taken over all the other eigenstates $|m\rangle$ with eigenenergies $E_m$.

From here onwards, we will assume $\Omega$ to be real. On analyzing the eigenstates $|\lambda^N_{\pm 1}\rangle$ corresponding to eigenenergies $E^N_{\pm 1}$, we find that the projection of state $|\lambda^N_{\pm 1}\rangle$ onto the $|r^0\rangle$ subspace is co-linear with $|\dot{O}(t)\rangle$:

$$\langle \lambda^N_{+1}(t)|\dot{O}(t)\rangle = \dot{\theta}(t)\sqrt{N}\sin(\frac{\varphi(t)}{2}) \tag{2.34}$$

$$\langle \lambda^N_{-1}(t)|\dot{O}(t)\rangle = \dot{\theta}(t)\sqrt{N}\cos(\frac{\varphi(t)}{2}) \tag{2.35}$$

The eigen-structure is such that for any value of N, all the eigenstates except the zeroth eigenstate have non-zero projections in the $|r^1\rangle$ subspace. From the orthonormality properties of the eigenvectors we can deduce that:

$$\langle \lambda^N_{\pm n}|P_{r^0}P^\dagger_{r^0}|\lambda^N_{\pm m}\rangle = \langle \lambda^N_{\pm n}|P_{r^1}P^\dagger_{r^1}|\lambda^N_{\pm m}\rangle = 0 \;\forall\; n \neq m \tag{2.36}$$

Here, $P^\dagger_{r^0}$ and $P^\dagger_{r^1}$ are projection operators for the $|r^0\rangle$ and $|r^1\rangle$ subspace respectively. From the above deduction we can conclude that only the $|\lambda^N_{\pm 1}\rangle$ eigenstates contribute to the sum in Eq. (2.33). On simplifying the adiabatic condition we get:

$$\dot{\theta}(t) \ll \frac{\Omega_0(t)}{2\sqrt{N}} f(\varphi(t)) \tag{2.37}$$

$$f(\varphi(t)) = \frac{\sin\frac{\varphi(t)}{2}\cos\frac{\varphi(t)}{2}}{\sin^3\frac{\varphi(t)}{2} + \cos^3\frac{\varphi(t)}{2}} \tag{2.38}$$

Substituting the expressions for $\Omega_0(t)$ and $\dot{\theta}(t)$ in Eq. (2.37), the adiabaticity condi-

tion is rewritten in Eq. (2.39). Here, we have scaled all the variables with $T$, thus, $\tilde{\Omega} \equiv \Omega T$, $\tilde{\tau} \equiv \frac{\tau}{T}$ and similarly $\tilde{\delta}$ and $\tilde{t}$.

$$1 \ll \sqrt{\frac{2}{N}} \frac{\tilde{\Omega}}{\tilde{\tau}} \exp\left(-\frac{(\tilde{t}^2 + \frac{\tilde{\tau}^2}{4})}{2}\right) \cosh^{3/2}(\tilde{t}\tilde{\tau}) f(\varphi(\tilde{t})) \tag{2.39}$$

Since, the Rabi frequencies and detuning are positive, $0 \leq \varphi(t) < \frac{\pi}{2}$. The function $f(\varphi(t))$ is a monotonically increasing function of $\varphi(t)$ in this range. For the strictest adiabaticity condition, we should choose the limit when $\varphi(t) \to 0$. In this limit, $f(\varphi(t)) = \frac{\Omega_0(t)}{2\delta}$, given $\delta \gg \Omega_0(t)$. On the other hand, when $\varphi(t) \to \frac{\pi}{2}$, we get $f(\varphi(t)) = \frac{1}{\sqrt{2}}$ with $\delta \to 0$. For the duration of population transfer, i.e. when $\Omega_0(\tilde{t})$ is considerably large, the $\tilde{t}$ dependence of the RHS of Eq. (2.39) varies from being singly peaked with maximum at $\tilde{t} = 0$ till $\tilde{\tau}$ is increased from 0 to about 1.4, to being doubly peaked as $\tilde{\tau}$ is increased further with a minimum at $\tilde{t} = 0$. It is thus sufficient to study the Eq. (2.39) at $\tilde{t} = 0$ for all values of $\tilde{\tau}$. Incorporating the above simplifications, the adiabaticity condition now is given as:

$$1 \ll \frac{\tilde{\Omega}^2}{\sqrt{N}\tilde{\tau}\tilde{\delta}} \exp\left(-\frac{\tilde{\tau}^2}{4}\right) \text{ when } \tilde{\delta} \gg \tilde{\Omega} \tag{2.40}$$

It is worthwhile to keep in mind that when $\delta \to 0$, this condition becomes:

$$1 \ll \frac{\tilde{\Omega}}{\sqrt{N}\tilde{\tau}} \exp\left(-\frac{\tilde{\tau}^2}{8}\right) \tag{2.41}$$

Note the dependence of the adiabaticity conditions in Eq. (2.40) and Eq. (2.41) on the number of atoms in the ensemble. The condition for adiabatic transfer along the $|O\rangle$ eigenstate becomes stricter by $\sqrt{\mathrm{N}}$ for an ensemble of N atoms. The optimum value of $\tau$ can be obtained numerically. When all other parameters are fixed, the condition $\tilde{\delta} \ll \tilde{\Omega}^2$ for the adiabatic transfer is similar to what was proved by Vitanov and Stenholm in 1997 [91] for a single atom case.

Let us now understand the condition required for the atomic population to remain in the state $|g^N\rangle$ when the added detuning due to Rydberg dipole-dipole interaction is introduced. For a single atom case, as long as $\tilde{\delta} \gg \tilde{\Omega}$, we can reduce the three level system to a two level system. In this case, the condition for adiabatic transfer from $|g\rangle$ to $|s\rangle$ is simply $\tilde{\delta} \ll \tilde{\Omega}^2$, ignoring the effects of $\tilde{\tau}$. On the other hand, the condition to remain in the $|g\rangle$ state is $\tilde{\Omega}^2 \ll \tilde{\delta}$ which is obtained by making the effective coupling between levels $|g\rangle$ and $|s\rangle$ small [91]. This situation changes a little in the presence of more than one atom. In this case, when we enforce that the effective couplings are kept small, the condition for the ensemble state to remain in the state $|g^N\rangle$ is modified to:

$$\sqrt{N}\tilde{\Omega}^2 \ll \tilde{\delta} \text{ when } \tilde{\Omega} \ll \tilde{\delta} \tag{2.42}$$

Thus, we can conclude that for the ensemble state to be transferred to $|s^N\rangle$ state from the initial state $|g^N\rangle$, assuming $\tilde{\tau}$ is fixed, we must have:

$$\tilde{\delta}_{|1\rangle} \ll \frac{\tilde{\Omega}^2}{\sqrt{N}} \text{ when } \tilde{\delta}_{|1\rangle} \gg \tilde{\Omega} \tag{2.43}$$

$$1 \ll \frac{\tilde{\Omega}}{\sqrt{N}} \text{ when } \tilde{\delta}_{|1\rangle} \to 0 \tag{2.44}$$

Also, for the ensemble state to remain in the $|g^N\rangle$ state, we must have:

$$\tilde{\delta}_{|0\rangle} \gg \sqrt{N}\tilde{\Omega}^2 \text{ when } \tilde{\delta}_{|0\rangle} \gg \tilde{\Omega} \tag{2.45}$$

In the above equations $\tilde{\delta}_{|0\rangle}$ and $\tilde{\delta}_{|1\rangle}$ are the detunings of ensemble atoms when the control atom is in state $|0\rangle$ and $|1\rangle$ respectively. For our protocol to work efficiently, our system should satisfy the conditions given in Eq. (2.43) or Eq. (2.44) along with Eq. (2.45). Thus, we can take $\tilde{\delta}_{|0\rangle} = \tilde{\delta}_{|1\rangle} + \tilde{\Delta}$.

To understand the implications of the adiabaticity conditions derived in this sec-

tion, we numerically evolve the Hamiltonian for the ensemble atoms given in Eq. (2.25) for different values of $\Omega T$ and $\delta T$. In Fig. 2.5 we plot the population of ensemble atoms in state $|s^N\rangle$ for $N = 1$ and 5 denoted by the co-efficient $|c_{s^N}(\infty)|^2$. To compare this with the population that remained in the initial state $|g^N\rangle$, we plot the total population in the states $|s^N\rangle$ and $|g^N\rangle$ after the completion of the protocol. This sum is denoted as $|c_{g^N}(\infty)|^2 + |c_{s^N}(\infty)|^2$. For $N = 1$, we see from Fig. 2.5a, the population gets completely transferred to $|s\rangle$ state for $\tilde{\Omega}^2 \gg \tilde{\delta}$. It is clear from Fig. 2.5b, there is only a small portion of the parameter space when $\frac{\tilde{\Omega}}{2} \approx \tilde{\delta} < 3$ where adiabatic transfer of population as described above does not take place for $N = 1$. This situation changes as the number of atoms in the target ensemble increases since more intermediate states now become available. For $N = 5$, as seen from Fig. 2.5c, the condition for adiabatic transfer from $|g^5\rangle$ to $|s^5\rangle$ becomes stricter compared to that for $N = 1$. Portions of the parameter space defined by $\tilde{\Omega}$ and $\tilde{\delta}$ open up where the adiabaticity conditions fail. This region clearly divides the parameter space into two sections, one which allows the adiabatic transfer of population from $|g^N\rangle$ to $|s^N\rangle$ with high fidelity marked out by the condition $\tilde{\Omega}^2 \gg \sqrt{N}\tilde{\delta}$ and the other where population remains in $|g^N\rangle$ with unit probability. The Rydberg-Rydberg interaction between the control and the ensemble atoms provides a tunable mechanism to increase or decrease the effective value of $\tilde{\delta}$ such that the target atoms are always in either of these two high fidelity transfer regions subject to the state of the control atom.

## 2.3 Introduction of spontaneous emissions

Before we start analyzing the numerical simulations for the control and target system together, let us introduce the effect of decoherence due to spontaneous emissions from the excited Rydberg states for the control atom and the target ensemble.

Assuming no collisions, the master equation for the density matrix, $\rho$, with $M$

number of spontaneous emission decay channels is given below:

$$\dot{\rho} = \frac{i}{\hbar}[\rho, H] + \hat{L}(\rho) \tag{2.46}$$

$$\hat{L}(\rho) = -\frac{1}{2}\sum_{m=1}^{M}(C_m^\dagger C_m \rho + \rho C_m^\dagger C_m) + \sum_{m=1}^{M} C_m \rho C_m^\dagger \tag{2.47}$$

For the control atom, we have only one decay channel with the decay rate $\Gamma_{0R}$, namely,

$$\hat{C}_{0R} = \sqrt{\Gamma_{0R}}|0\rangle\langle R| \tag{2.48}$$

For the target ensemble atoms, there are two decay channels with rates $\Gamma_{gr}$ and $\Gamma_{sr}$ defined as:

$$\hat{C}_{gr} = \sqrt{\Gamma_{gr}}|g\rangle\langle r| \tag{2.49}$$

$$\hat{C}_{sr} = \sqrt{\Gamma_{sr}}|s\rangle\langle r| \tag{2.50}$$

In the forth coming numerical calculations, we have chosen $\Gamma_{gr} = \Gamma_{sr} \equiv \Gamma_r$. It is straight-forward to extend the master equation calculations for a system with more than one target atom using the Fock number state basis.

We will first study the effect of decay due to spontaneous emissions on the target ensemble with different number of atoms. We choose the value of $T = 1\mu s$ and $\tilde{\tau} = 1.4$ for all the numerical results here after. From Fig. 2.6, we see that even for an ensemble of about ten atoms, the population transferred to the $|s^N\rangle$ state from the $|g^N\rangle$ state is greater than 99% for realistic values of Rydberg level spontaneous emission rates of about $\Gamma_r \approx 0.01 - 0.1$ MHz. As discussed above, we see that the spontaneous emissions from the Rydberg excited levels of the target ensemble atoms do not affect this protocol which makes it a very robust scheme.

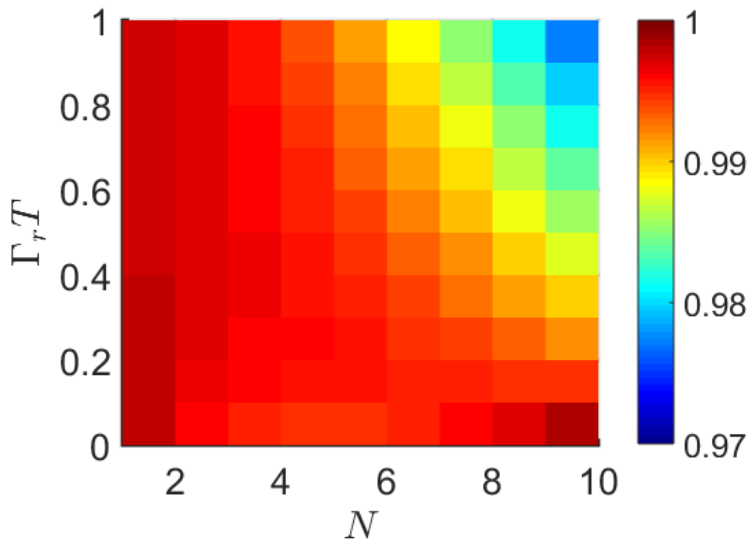


Figure 2.6: Effect of spontaneous emissions on ensemble atoms: The population in level $|s^N\rangle$ after the STIRAP pulses for different number of atoms in the target ensemble, N, and varying spontaneous emission rate $\Gamma_r T$. The value of detuning $\delta T = 0$, $\frac{\Omega T}{2} = 9.5$ and $\tau = 1.4T$. We see that the population transfer does not depend on the decay rate significantly and has values higher than 0.99 for typical range of $\Gamma_r T \approx 0.01 - 0.1$

## 2.4 Numerical results for GHZ state creation

Having laid the groundwork we will now look at the simulation of GHZ state creation. The total Hamiltonian for this system is:

$$H_{Tot}(t) \quad = \quad H_C(t) + H_T(t) + \hbar\Delta|R\rangle\langle R|\sigma_r^+\sigma_r^- \tag{2.51}$$

The expressions for $H_C(t)$ and $H_T(t)$ are given in the Eq. (2.10) and Eq. (2.25) respectively. The interaction between the target ensemble and the control atom is introduced via the last term in Eq. (2.51) with the interaction strength given by frequency $\Delta$. Ideally, $\Delta$ is a function of inter-atomic separation. In this case we can choose the value of $\Delta$ such that it defines the threshold for the blockade radius. All atoms in the ensemble will have a detuning greater than this value. The exact value of $\Delta$ is not important as long as it is large enough to avoid two Rydberg atom

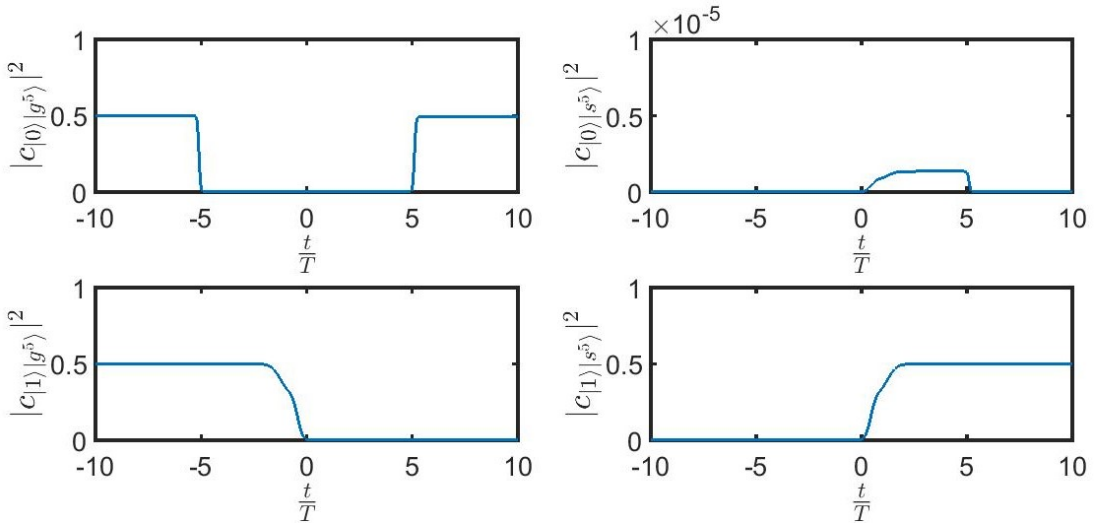


Figure 2.7: Implementation of the GHZ state generation protocol for N=5: Time evolution of the squared co-efficients of $|0\rangle|g^N\rangle$, $|0\rangle|s^N\rangle$, $|1\rangle|g^N\rangle$ and $|1\rangle|s^N\rangle$ under the influence of the Hamiltonian in Eq. (2.51) with the initial condition $\frac{1}{\sqrt{2}}(|0\rangle+|1\rangle)|g^N\rangle$. Chosen parameters: $\frac{\Omega_{c0}T}{2} = 6.2$, $\delta_R T = 0$, $T_c = 0.1T$, $\frac{\Omega T}{2} = 5$, $\delta T = 0$, $\tau = 1.4T$, $\Delta T = 500$, $\Gamma_r T = \Gamma_R T = 0$, $\tau_c = \tau + 4(T + T_c)$.

excitations.

We solve the Schrodinger equation numerically in the basis set $\{|0\rangle, |1\rangle, |R\rangle\} \otimes \{|g; s; r\rangle_N\}$ defined in Eq. (2.24) with the Hamiltonian defined by Eq. (2.51) for the control atom in the initial state, $\frac{1}{\sqrt{2}}(|0\rangle + |1\rangle)$ and the ensemble atoms initiated in the $|g^N\rangle$ state. In Fig. 2.7 we have plotted the modulus squared of the co-efficients corresponding to the components $|0\rangle|g^N\rangle$, $|0\rangle|s^N\rangle$, $|1\rangle|g^N\rangle$ and $|1\rangle|s^N\rangle$ of the wave-vector as it evolves with time in the absence of any decay from the excited levels of the control and the target atoms. The final state obtained after measuring the control atom in $\frac{1}{\sqrt{2}}(|0\rangle + |1\rangle)$ state has a fidelity of 0.97 with respect to the GHZ state $|\phi\rangle = \frac{1}{\sqrt{2}}(|g^N\rangle + |s^N\rangle)$ for a target ensemble with N = 5 atoms and having the interaction strength $\tilde{\Delta} = 500$. Note that for this simulation, $T = 1\mu s$, which means that the entire operation takes only about 15-20$\mu s$. Typical excited Rydberg level lifetimes for $n \gtrsim 60$ are of the order of 100 $\mu s$ [107]. Since the current time of gate operation is much less compared to the excited level lifetime, we can improve the fidelity by increasing the value of $\tilde{\Delta}$ without necessarily exciting the Rydberg atoms

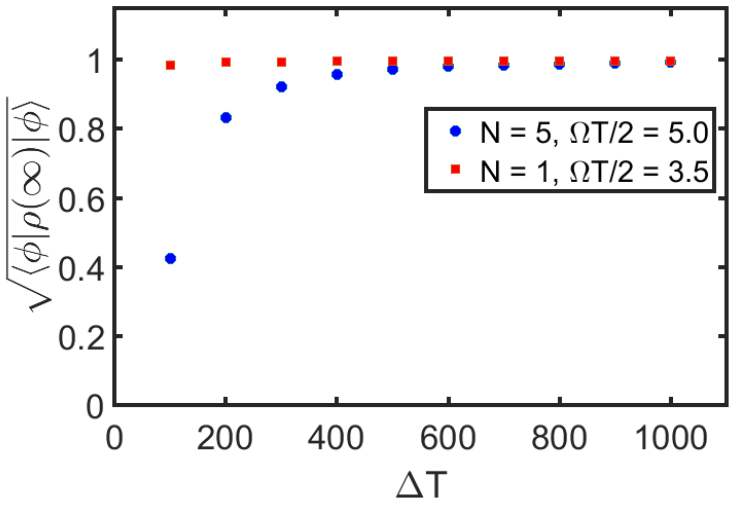


Figure 2.8: Fidelity of the final state with respect to the state $\frac{|g^N\rangle+|s^N\rangle}{\sqrt{2}}$: The fidelity of the final ensemble state with respect to $|\phi\rangle$ for N = 1 and 5 as a function of the interaction strength $\Delta T$ with the initial condition $\frac{1}{\sqrt{2}}(|0\rangle+|1\rangle)|g^N\rangle$. Parameters used in the simulation: $\frac{\Omega_{c0}T}{2} = 6.2$, $\delta_R T = 0$, $T_c = 0.1T$, $\delta T = 0$, $\tau = 1.4T$, $\Gamma_r T = \Gamma_R T = 0$, $\tau_c = \tau + 4(T + T_c)$

to much higher levels by simply increasing the width of the STIRAP pulses. In Fig. 2.8, we plot the fidelity of the obtained final ensemble state with respect to the GHZ state $|\phi\rangle$ as a function of the interaction strength $\tilde{\Delta}$ for a target ensemble having 1 and 5 atoms. The fidelity for a single target atom is above 98% for $\tilde{\Delta}$ of 100 or more. On the other hand the fidelity of the target ensemble with N = 5 is 98% and higher for values of $\tilde{\Delta} = 600$ and above.

As we have already seen, the spontaneous emission from the excited levels of the target atoms do not affect this protocol as long as the adiabaticity conditions are satisfied. What about the spontaneous emission from the excited level of the control atom? In Fig. 2.9 we show the decrease in the fidelity of the final density matrix with respect to the state $|\phi\rangle$ for the same initial conditions as above due to the decay from the $|R\rangle$ level. This plot shows the decay rate for the target ensemble having a single atom and 5 atoms with $\frac{\tilde{\Omega}}{2} = 3.5$, $\tilde{\Delta} = 200$ and $\frac{\tilde{\Omega}}{2} = 5$, $\tilde{\Delta} = 500$ respectively and $\tilde{\delta} = 0$. As expected the rate of the decay is same for both the cases since the number

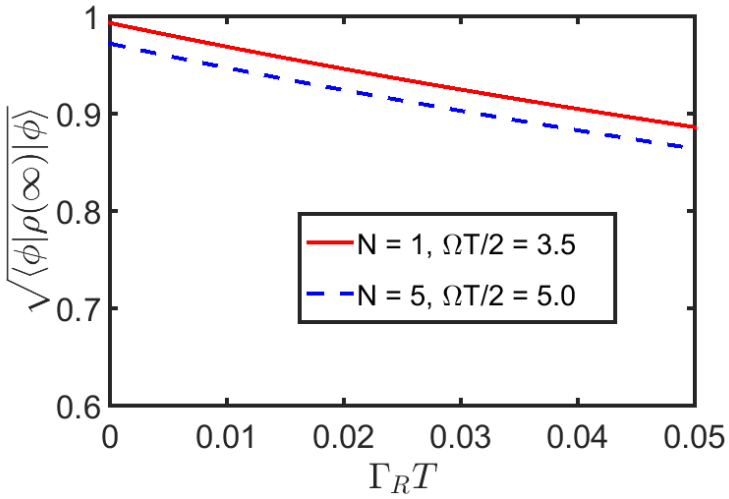


Figure 2.9: Fidelity of the final state with respect to $\frac{|g^N\rangle+|s^N\rangle}{\sqrt{2}}$ with spontaneous emissions: Fidelity of the target ensemble density matrix after measurement of the control atom in the superposition state measured with respect to the state $|\phi\rangle$ with N = 1 and 5 for different values of $\Gamma_R T = \Gamma_r T$ numerically evaluated with the initial condition $\frac{1}{\sqrt{2}}(|0\rangle + |1\rangle)|g^N\rangle$. Parameters: $\frac{\Omega_{c0}T}{2} = 6.2$, $\delta_R T = 0$, $T_c = 0.1T$, $\delta T = 0$, $\tau = 1.4T$, $\Delta T = 200$ for N = 1, $\Delta T = 500$ for N = 5, $\tau_c = \tau + 4(T + T_c)$

of target atoms does not influence it. The fidelity is seen to drop to a value of 97% from 99% for a single atom target ensemble when the value of $\Gamma_r T$ increases to 0.01, whereas for the target ensemble with 5 atoms, the fidelity drops from 97% to 95%.

It is possible to compensate for the losses due to spontaneous emission from the control atom by exciting it to higher Rydberg levels. This would serve the dual purpose of providing longer excited level lifetimes as well as stronger Rydberg dipole interaction strength [96], which would in turn improve the overall fidelity of the protocol.

## 2.5 Chapter Summary

In conclusion, we have presented here a protocol to create N particle GHZ state with a single control atom and an ensemble of N target atoms based on the principles of Rydberg dipole blockade and STIRAP. We have discussed the conditions under

which adiabatic transfer of the target ensemble population from one ground state to the other is facilitated subject to the state of the control atom. The biggest advantage of this scheme is that it is not affected by the decay from the excited Rydberg levels of the target ensemble atoms as long as the conditions for adiabatic transfer are satisfied. Spontaneous emission from the excited Rydberg level of the control atom leads to decrease in the fidelity of the protocol. This can be controlled for by exciting the control Rydberg atom to higher principal quantum number.

This chapter contains contents which were published elsewhere [108].

# CHAPTER III

# Analysis of Intrinsic Retrieval Efficiency for Atomic Quantum Interfaces

## 3.1 Introduction

With the gap between the vision and reality of establishing quantum communication via a quantum network of atomic ensembles and photons closing steadily ([109–111]), it becomes important to thoroughly understand every aspect of the individual units constituting this network. In this chapter we will elucidate the workings of a single quantum node comprising of atomic ensemble in Duan-Lukin-Cirac-Zoller (DLCZ) quantum repeater protocol and its variants by performing a full three dimensional analysis. These atomic nodes act as quantum interfaces as discussed in Sec. 1.2.3. We will be particularly interested in studying the intrinsic efficiency of these interfaces, i.e. how efficient is the process of coherently storing and retrieving a photonic signal from an atomic ensemble of three level atoms. Before we start building the atom-light interaction model to describe this process, let us discuss the quantum repeater protocol and understand the importance of atomic ensembles as quantum nodes in this context.

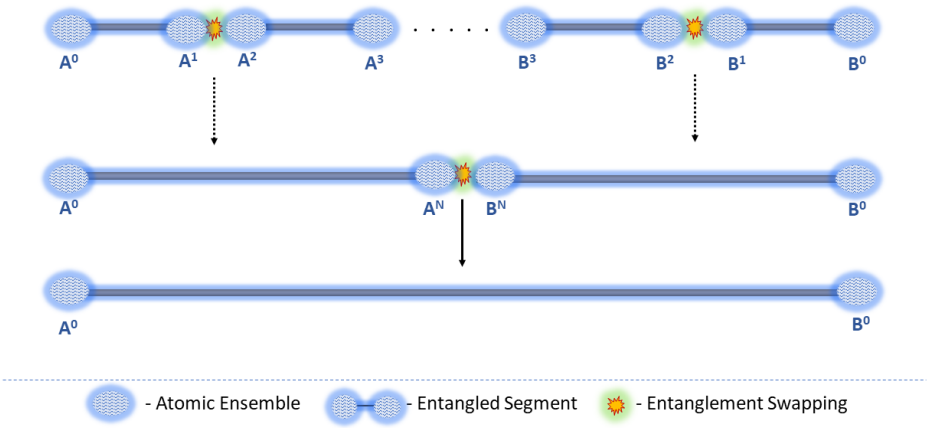


Figure 3.1: Working of quantum repeaters: To generate entanglement between two distant nodes $A^0$ and $B^0$, we start by dividing the total distance into smaller segments $A^0 - A^1$,$A^2 - A^3$,...,$B^3 - B^2$,$B^1 - B^0$ with their corresponding nodes. Entanglement is first generated in the smaller segments between each of these nodes independently. By entanglement swapping between two neighbouring nodes, e.g. $A^1$ and $A^2$, the entanglement can be extended over a longer segment $A^0 - A^3$. With every successful entanglement swapping step, the generated extended entanglement between two nodes on a segment must be purified. By successive swapping and purification in a hierarchical manner, entanglement can be generated over the original distance between $A^0$-$B^0$.

### 3.1.1 Quantum repeaters and quantum interfaces

Quantum communication relies on the ability of generating quantum entangled states over large distances. One way to accomplish this goal is to create entanglement between distant units with the help of appropriate communication channels between them. Typical carriers of quantum information, the photons, suffer from losses due to absorption and decoherence in the transfer channel. This leads to an exponential decay of communication fidelity with increasing distance of communication. The way out of this problem is to use quantum repeaters [112]. Quantum repeaters are modeled on the divide and conquer approach. The entire length over which entanglement is to be created is broken down into smaller segments. Physical systems at the ends of each smaller segment can be efficiently entangled because of smaller lengths between them [Fig. 3.1]. Entanglement can then be generated between two adjacent

segments by entanglement swapping using neighboring systems [21, 113]. This process is repeated until entanglement is generated over the full length. At each step though, the generated entanglement needs to be purified and doing so is a probabilistic process [36, 96]. Thus, to extend entanglement over two adjacent segments one has to wait till entanglement is generated and purified over each segment [36]. The upshot is that quantum repeater protocols require quantum memories [36, 114] that can store the entanglement for one segment till it is created in the neighboring segment.

In 2001, the DLCZ quantum repeater scheme was introduced as a way to generate heralded entanglement over a distance by using atomic ensembles as individual memory units in combination with linear optics and single-photon detectors [36]. Following the DLCZ scheme, many experiments have demonstrated remarkable advances towards quantum repeaters [110, 115, 116]. In these schemes the atomic ensembles act as the nodes at the end of each segment by storing de-localized atomic spin-wave states when entangled. These nodes are connected by fiber optic cables which serve as the communication channels between ensembles allowing efficient transfer of photons. Entanglement between two neighbouring nodes on adjacent segments can be generated by converting the stored spin-waves in the atomic ensembles into correlated photons and performing beam-splitter measurements on them. The generation and detection of a single photon from the atomic ensemble, in the absence of which way information, makes the two segments get entangled. Memory nodes based on atomic ensembles as opposed to single atoms make strong coupling between atoms and photons possible due to collective effects of a large number of atoms. A detailed description of the DLCZ scheme and the collective effects in atomic ensembles is provided in Sec. 3.1.2 for completeness.

### 3.1.2 The Duan-Lukin-Cirac-Zoller quantum repeater protocol

In this section, we will take a close look at the DLCZ scheme and define the associated atoms-light interaction configuration. As shown in Fig. 3.1, to generate entanglement over $A^0$ and $B^0$, we split the intermediate distance into multiple smaller segments and perform entanglement generation for each segment followed by entanglement swapping between neighbouring segments sequentially. A pictorial representation of the setup for entanglement generation between two atomic ensembles on a segment is shown in Fig. 3.2. The two ensembles $A^N$ and $A^{N+1}$ are simultaneously excited with weak Raman pulses (write pulse), such that there is a small but definite probability of one of the ensembles emitting a photon correlated with the coherent spin-wave mode in the atomic ensemble [36]. The photon generated from either of the samples is coupled to optical fibers and made to interfere at a 50-50 beam-splitter coupled to single photon detectors at the output arms. If either of the detectors clicks, that heralds entanglement between the two ensembles. This is how entanglement is generated within each segment of the quantum repeater scheme.

Once we have two such adjacent entangled segments eg. $A^0 - A^N$ and $B^N - B^0$ in Fig. 3.3, we implement entanglement swapping. The ensembles $A^N$ and $B^N$ are simultaneously excited with strong read-out pulses, such that there is a high probability of a stored spin-wave atomic excitation getting converted into a highly directional photon. These photons are collected and made to interfere at another 50-50 beam-splitter also connected to single photon detectors. If there is a click in either of the detector arms, it heralds entanglement between ensembles $A^0 - B^0$. The necessary requirement as discussed previously is that the entanglement in either segment needs to be stored until entanglement in the other segment can be generated and purified. The process of entanglement generation, purification and swapping can now be repeated to create entanglement sequentially between ensembles farther and farther apart. The details of read and write process for each atomic ensemble are

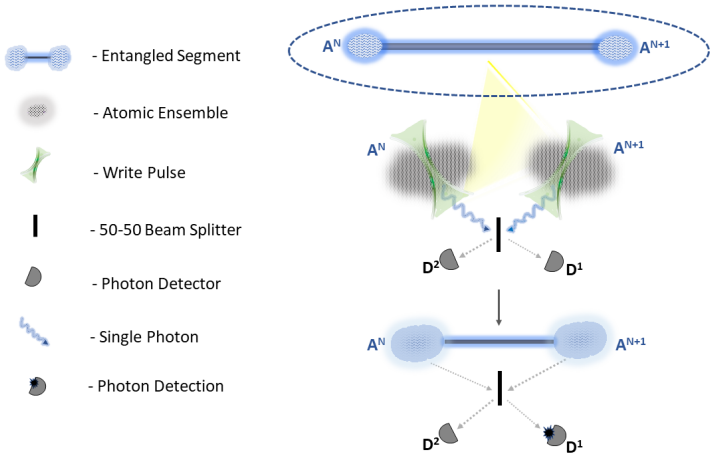


Figure 3.2: Entanglement generation between two neighboring atomic ensembles, $A^N$ and $A^{N+1}$: The atomic ensembles to be entangled are simultaneously excited with weak off-resonant Raman pulses, called the write pulse. A photon corresponding to the atomic spin wave mode emitted from any one of the ensembles is sent through the 50-50 beam-splitter. The output arms of the beam-splitter are in-turn coupled to single photon detectors. For ideal photon detectors, a click in any of the two detectors, e.g. $D^1$ in this case, heralds the generation of entanglement between the two atomic ensembles $A^N$ and $A^{N+1}$.

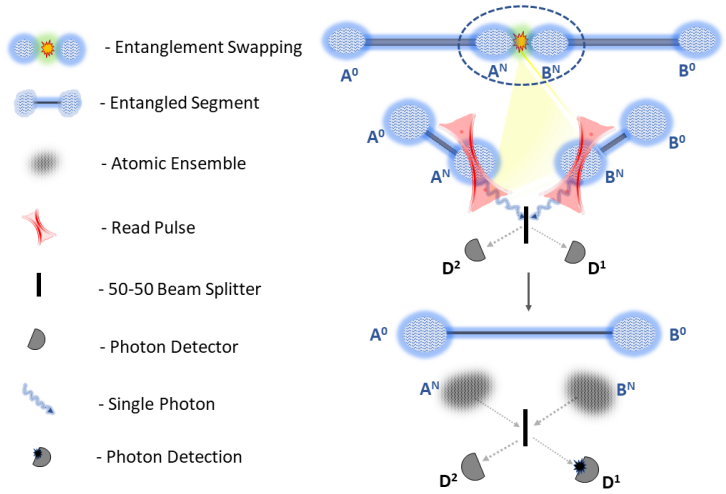


Figure 3.3: Entanglement swapping between two neighbouring entangled segments: Given two entangled segments $A^0 - A^N$ and $B^N - B^0$, entanglement is generated between atomic ensembles $A^0 - B^0$ by entanglement swapping between ensemble $A^N - B^N$. The atomic spin-wave modes in the neighbouring ensembles $A^N$ and $B^N$ are converted into photons using a strong and broad read-out pulse. Photons emitted by the atomic ensembles are coupled to a 50-50 beam-splitter. The output from the beam-splitter is coupled to single photon detectors. Whenever one of the detectors registers a photon, the atomic ensembles $A^0 - B^0$ get entangled due to entanglement swapping.

given in Sec. 3.2.

### 3.1.3 Intrinsic Retrieval Efficiency: An Introduction

The atomic ensembles that act as individual nodes to store de-localized quantum entangled spin-wave states must satisfy a few important properties. As described in [36], during the write process, storage of an atomic spin-wave state is heralded by the detection of a single photon which we will call the signal photon. After a certain time duration, this spin-wave is read out into another single photon, the idler photon. For efficient implementation of the quantum repeater protocol, each of these atomic memory units should satisfy the following key properties. They should have long storage lifetimes and high retrieval efficiency [114]. Storage lifetimes from about milliseconds to seconds have been achieved in quantum memories with atomic gases [72, 117–119]. Intrinsic Retrieval Efficiency (IRE) is defined as the probability of retrieving an idler photon in a particular spatio-temporal mode from the stored spin-wave excitation in the atomic ensemble conditioned on the successful detection of signal photon in the write process. Detailed theoretical description of IRE is given in Sec. 3.3. The spatio-temporal mode of the signal and the idler photon must have a high overlap with single mode optical fibers which are used in experiments to collect and propagate these photons for interference and detection. In our definition of the intrinsic retrieval efficiency, we include contributions from mode-overlap between emitted photon field and the optical fiber field as it is an integrated part of photon read-out process in experiments. Because of the collective effects of atoms involved in the light-matter interaction, the read-out photon is highly correlated with the spin-wave excitation stored in the atomic ensemble. High IRE values are extremely important for reasonable entanglement distribution rates [36, 114]. For example, as is stated in [114], 1% reduction in IRE, from 90% to 89%, increases the entanglement distribution time over a distance of 600 km by 10%-14% for the DLCZ protocol and its variants. Cal-

culations in [36] show that the scaling of the total time of entanglement generation between two distant atomic ensembles with the number of repeater nodes critically depends on the IRE. Free space IRE in experiments with cold atom ensembles is at best about 50% [120]. For atomic ensembles confined to cavities, IRE of more than 70% has been achieved [72, 121]. The IRE is sensitive to decoherence due to stray magnetic fields, atom loss as well as dephasing of the spin-wave caused by atomic motion. To understand the exact nature of the IRE, it is important to study the full three dimensional profile of the spin-wave excitation stored in the atomic ensemble and how it gets mapped into the transverse (angular) profile of the emitted photon following the read-out process. Our goal in this chapter is to understand the intrinsic memory retrieval efficiency by performing a thorough three-dimensional quantum mechanical calculation that also takes into account the mode matching between the emitted photons and single photon collection fibers.

We would like to note that previous efforts to theoretically describe the read-write process using the Maxwell-Bloch formalism use one dimensional description of the atomic density and electric field propagation [122]. Such a description works well only when we assume that the write beam waist is much broader than the beam waist of the emitted photon. Recent experiments [110] use beam parameters which are marginally close to not being described by this theoretical treatment. The transverse mode profile of the electric fields play an important role for understanding IRE. As we shall show in our results, IRE is sensitive to the ratio of the beam waists between the write and signal/idler photon beams. It is also important to note that the Maxwell-Bloch approach doesn't describe the electric field that gets scattered from the atoms. This scattered field is what we are interested in when calculating IRE as the desired spatio-temporal mode of the emitted photon continuously changes to the other scattered modes which contribute to noise. One of the ways of improving the IRE is by increasing the optical depth. This can be achieved by taking longer

atomic samples in the direction of light propagation without increasing the overall atomic density. For longer geometries of atomic samples it becomes essential to look at the variation of the transverse profile of the light beams due to diffraction.

A three-dimensional formalism for calculating the field modes of light scattered from an ensemble of hot atomic gas was presented in Ref. [47]. In this calculation, the atomic positions were averaged over the duration of interaction with light to get the emitted photon mode profile. This averaging significantly simplifies the calculations to get the mode profile of the photon correlated with the symmetric collective spin wave state. Since we are interested in describing cold atomic ensembles, such averaging over positions cannot be done. One of the interesting results from this calculation in Ref. [47] suggested that atomic density fluctuations give rise to intrinsic mode mismatching errors. We find that atomic density fluctuations have a significant role to play when determining IRE.

## 3.2 Read and write process of an atomic quantum memory

Consider an atomic ensemble with $N_a$ atoms each having a $\Lambda$ level structure as shown in Fig. 3.4. They have two meta-stable ground levels, $|g\rangle$ and $|s\rangle$ with long lifetimes and an excited level $|e\rangle$. All atoms are initially prepared in the ground state $|g\rangle$. The atoms in the ensemble are acted upon with a weak off-resonant laser pulse, the write-beam, on the $|g\rangle$-$|e\rangle$ transition. With some small probability a single photon, called the signal photon, corresponding to $|e\rangle$-$|s\rangle$ transition gets emitted spontaneously. The two-photon Raman scattering process thus results in the transition of one atom from $|g\rangle$ to $|s\rangle$ level. After interacting with the write beam, the quantum state of the atomic ensemble and the emitted signal photon is expressed as:

$$|\Psi\rangle^W = \int \frac{d^3\mathbf{k}}{(2\pi)^3} \sum_{j=1}^{N_a} C_j(\mathbf{k}) |s\rangle_j |\mathbf{k}\rangle_{ph} \tag{3.1}$$

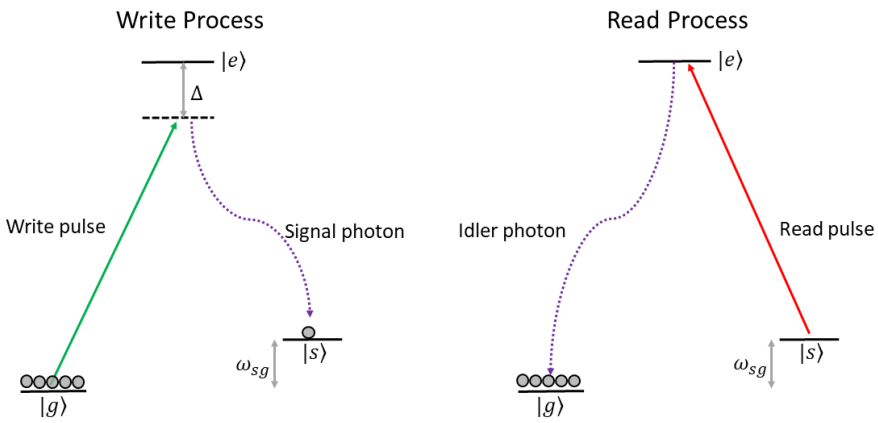


Figure 3.4: Atomic level diagram for the DLCZ protocol: Every atom in the atomic ensemble is considered to have a three level $\Lambda$ structure. Levels $|g\rangle$ and $|s\rangle$ are two metastable states separated by frequency equal to $\omega_{sg}$, with forbidden dipole transition between them. Level $|e\rangle$ is an excited state. At $t = 0$ all atoms are in the ground state $|g\rangle$. In the write process, the atomic ensemble is excited with a classical write-pulse that is detuned from the $|g\rangle$-$|e\rangle$ transition by a frequency $\Delta$. With the emission and detection of a signal photon on the $|e\rangle$-$|s\rangle$ transition the write process is complete with one atom excited to the $|s\rangle$ level. In the read process, the ensemble is excited with a strong on resonance read-pulse for $|s\rangle$-$|e\rangle$ transition. The emission and detection of a highly directed idler photon from $|e\rangle$-$|g\rangle$ concludes the read process.

where:

$$|s\rangle_j \leftarrow |g\rangle_1|g\rangle_2...|s\rangle_j...|g\rangle_{N_a} \tag{3.2}$$

and $C_j(\mathbf{k})$ is the photon wave function given an atomic excitation for atom $j$ . Sum over $j$ adds contribution of all the atoms of the sample and the integration over $\mathbf{k}$ for all the wave-vectors.

Information about which atom in the ensemble emitted the photon is lost for a far field detection of the photon. Detection of the signal photon can be expressed as the overlap of the above state in Eq. (3.1) with a transverse Gaussian electric field mode coupled to the single mode optical fiber. The resulting quantum state after this overlap is the obtained coherent collective spin-wave state of the form:

$$|\Psi_a\rangle^W = \sum_{j=1}^{N_a} \tilde{C}_j e^{i(\mathbf{k}_W - \mathbf{k}_S)\cdot\mathbf{r}_j} |s\rangle_j \tag{3.3}$$

where $\mathbf{k}_W$ and $\mathbf{k}_S$ are the wavevectors associated with the write-beam and the emitted signal photon respectively and $\mathbf{r}_j$ is the position vector for $j^{th}$ atom. The complex coefficients $\tilde{C}_j$ come from the overlap between $C_j(\mathbf{k})$ and the Gaussian profile, and they depend on the laser intensity at the $j^{th}$ atomic position. This state after appropriate normalization gives the initial condition of the atomic ensemble for the read process. With the detection of the signal photon, write process is complete and information is now stored in the coherent atomic spin-wave.

Now, the read-process. After a certain time $T_m$, the storage time, a strong classical laser pulse (read pulse) resonant with the $|e\rangle$-$|s\rangle$ transition is made to interact with the atomic ensemble such that any atom in the $|s\rangle$ state gets excited to the $|e\rangle$ state. The atom in $|e\rangle$ state emits an idler photon to relax back to the $|g\rangle$ state. After the interaction of the ensemble with the read pulse, the resulting atom-photon quantum state can be described as:

$$|\Psi\rangle^R = \int \frac{d^3\mathbf{k}}{(2\pi)^3} \sum_{j=1}^{N_a} D_j(\mathbf{k})|\mathbf{k}\rangle|g\rangle^{\otimes N_a} \tag{3.4}$$

where we define $|g\rangle^{\otimes N_a} = |g\rangle_1|g\rangle_2...|g\rangle_{N_a}$. We can again represent detection of the emitted idler photon as an overlap of the emitted photon state with a transverse Gaussian field. Squared norm of this overlap would correspond to the desired IRE. The atomic quantum state after taking this overlap is proportional to:

$$|\Psi_a\rangle^R \propto \sum_{j=1}^{N_a} \tilde{D}_j e^{i(\mathbf{k}_W - \mathbf{k}_S)\cdot\mathbf{r}_j} e^{i(\mathbf{k}_R - \mathbf{k}_I)\cdot\mathbf{r}'_j} |g\rangle^{\otimes N_a} \tag{3.5}$$

where $\mathbf{k}_R$ and $\mathbf{k}_I$ are the wave-vectors corresponding to the read beam and the emitted idler photon respectively. The position of the $j^{th}$ atom after the storage time $T_m$ is given by $\mathbf{r}'_j$. Because of finite temperatures of the atomic sample, $\mathbf{r}_j$ is generally different from $\mathbf{r}'_j$. For the calculations henceforth, we assume that the atomic ensemble is a cold-atom sample having a temperature of about $30\,\mu$K obtained by cooling

a MOT sample further via Polarization Gradient Cooling technique. The coefficients $\tilde{D}_j$ again arise from overlaping $D_j(\mathrm{k})$ with the Gaussian mode, depending on the atomic positions $\mathbf{r}_j$ as well as $\mathbf{r}'_j$ and properties specific to the atom-light interaction like polarization, dipole moment and beam parameters. Eq. (3.5) tells us that the amplitude of emission for the idler photon in the $\mathbf{k}_I$ direction is determined by interference between all the atoms of the ensemble scaled by factors $\tilde{D}_j$. Because of constructive interference between all atom contributions, the idler photon is emitted in a well specified direction based on the phase matching condition.

$$(\mathbf{k}_W - \mathbf{k}_S) \cdot \mathbf{r}_j + (\mathbf{k}_R - \mathbf{k}_I) \cdot \mathbf{r}'_j = 0 \tag{3.6}$$

As we shall see in the forth coming sections, the intrinsic retrieval efficiency is acutely affected by the interference condition. As discussed in Ref. [114], completely constructive interference is possible only when the atoms don't move within the storage time ($\mathbf{k}_W + \mathbf{k}_R = \mathbf{k}_S + \mathbf{k}_I$) or when the beams are co-linear ($\mathbf{k}_W = \mathbf{k}_S$, $\mathbf{k}_R = \mathbf{k}_I$). In experiments with cold atomic gases, both these conditions are seldom implementable. Because of position dependent weights associated with the angular profile of the light and atomic spin-wave and non-zero energy difference between the two ground levels, unit IRE cannot be achieved.

With the basic idea of the read-write protocol and importance of retrieval efficiency in mind, let us now look at the full derivation of the mathematical expression of retrieval efficiency with a complete 3-D analysis.

## 3.3 Theoretical formulation of the intrinsic retrieval efficiency

We will now formulate the interaction between light and the atomic ensemble which acts as a temporary storage for quantum entanglement and derive the expression for IRE.

### 3.3.1 The Write Process

For the atomic level structure given in Fig. 3.4, in the write process, the atomic ensemble is excited by a weak and short off-resonant Raman pulse (the write pulse) coupled to the $|g\rangle$-$|e\rangle$ transition. We treat this interaction semi-classically, by taking classical light pulse interacting with a quantum atomic system. The electric field associated with the write pulse is given as:

$$\mathbf{E}^w(\mathbf{r},t) = \frac{1}{2}\left[\hat{\epsilon}^w E^w(\mathbf{r},t) e^{i(\mathbf{k}^w\cdot\mathbf{r}-\omega^w t)} + \text{c.c.}\right] \tag{3.7}$$

where $\omega^w = k^w c$ is the carrier frequency of the write pulse and $|\mathbf{k}^w| = k^w$. Also $\hat{\epsilon}^w$ is the unit direction of the field. It is assumed to be a square pulse of width $T_w$ time units.

The spontaneously emitted photon corresponding to the $|e\rangle$-$|s\rangle$ transition is treated quantum mechanically. The electric field associated with the emitted signal photon is described by the sum of all the free field modes:

$$\hat{\mathbf{E}}(\mathbf{r}) = \sum_{\tau}\int \frac{d^3\mathbf{k}}{(2\pi)^3}\left[\hat{\epsilon}_{\mathbf{k},\tau} f(k) e^{i\mathbf{k}\cdot\mathbf{r}} a_{\mathbf{k},\tau} + \text{h.c.}\right] \tag{3.8}$$

In the above expression, $\mathbf{k}$ stands for the wavevector of the emitted photon and $\tau$ for one of the two independent polarization directions given a wavevector. The operators $a_{\mathbf{k},\tau}$ and its Hermitian conjugate $a^\dagger_{\mathbf{k},\tau}$ are the annihilation and creation operators for the given wavevector $\mathbf{k}$ and polarization $\tau$. The dispersion relation is given as $\omega_k = |\mathbf{k}|c$. Also for free space normal modes, the expression for the mode function $f(k)$ is:

$$f(k) = i\sqrt{\frac{\hbar\omega_k}{2\varepsilon_0}} \tag{3.9}$$

where $\varepsilon_0$ is the free space permittivity. Throughout this chapter we set $\hbar = 1$ for simplicity.

We assume that there is no atom-atom interaction in the system. The atom-field interaction Hamiltonian taken here is the dipole interaction with minimal coupling. Under the rotating wave approximation (RWA) we get the following Hamiltonian given in Eq. (3.10). Note that spontaneous emission from the state $|e\rangle$ to $|g\rangle$ is ignored as it is not important for our purpose. Taking the energy of the $|g\rangle$ state, $\omega_g$, to be our 0 reference, the write Hamiltonian is then:

$$\begin{aligned} H^w &= \sum_\tau \int \frac{d^3\mathbf{k}}{(2\pi)^3}\ \omega_k a^\dagger_{\mathbf{k},\tau} a_{\mathbf{k},\tau} + \sum_{j=1}^{N_a} (\omega_{eg}\sigma^j_{ee} + \omega_{sg}\sigma^j_{ss}) \\ &+ \sum_{j=1}^{N_a} \left[ \Omega^w_{eg,j} e^{i(\mathbf{k}^w\cdot\mathbf{r}_j - \omega^w t)}\sigma^j_{eg} + \sum_\tau \int \frac{d^3\mathbf{k}}{(2\pi)^3}\ g_{es,\tau}(\mathbf{k}) e^{i\mathbf{k}\cdot\mathbf{r}_j}\sigma^j_{es} a_{\mathbf{k},\tau} + \text{h.c.} \right] \end{aligned} \tag{3.10}$$

where:

$$\omega_{ab} = \omega_a - \omega_b \tag{3.11}$$

$$\sigma^j_{\mu\nu} = |\mu\rangle_j\langle\nu| \tag{3.12}$$

$$\Omega^w_{eg,j} = \frac{1}{2} e\langle e|\hat{\mathbf{r}}|g\rangle \cdot \hat{\epsilon}^w E^w(\mathbf{r}_j, t) \tag{3.13}$$

$$g_{es,\tau}(\mathbf{k}) = e\langle e|\hat{\mathbf{r}}|s\rangle \cdot \hat{\epsilon}_{\mathbf{k},\tau} f(k) \tag{3.14}$$

We can transform the Hamiltonian into the field interaction picture using the following unitary transformation:

$$U = \exp\left[ -i\sum_{j=1}^{N_a} (\omega^w \sigma^j_{ee} + \omega_{sg}\sigma^j_{ss})t - i\sum_\tau \int \frac{d^3\mathbf{k}}{(2\pi)^3}\ \omega_k a^\dagger_{\mathbf{k},\tau} a_{\mathbf{k},\tau} t \right] \tag{3.15}$$

With this unitary transformation the interaction Hamiltonian is given as:

$$H_{new} = U^\dagger H_{old} U + i(\partial_t U^\dagger)U \tag{3.16}$$

On solving the expression for $H_{new}$ we get:

$$\begin{aligned} H^w_{new} &= \sum_{j=1}^{N_a} \Delta^w \sigma^j_{ee} + \sum_{j=1}^{N_a} \Bigg[ \Omega^w_{eg,j} e^{i\mathbf{k}^w \cdot \mathbf{r}_j} \sigma^j_{eg} \\ &+ \sum_{\tau} \int \frac{d^3\mathbf{k}}{(2\pi)^3}\, g_{es,\tau}(\mathbf{k}) e^{i\mathbf{k}\cdot\mathbf{r}_j - i(\omega_k - \omega^w + \omega_{sg})t} \sigma^j_{es} a_{\mathbf{k},\tau} + \text{h.c.} \Bigg] \end{aligned} \tag{3.17}$$

where we have defined $\Delta^w = \omega_{eg} - \omega^w$ as the detuning of the write pulse from the $|e\rangle$-$|g\rangle$ transition. We can reduce the three level problem to a two level problem by adiabatic elimination of the excited level $|e\rangle$. This approximation is valid if the natural width $\Gamma$ of the excited level and frequency spread of the write pulse around $\omega^w$ are significantly smaller compared to the detuning $\Delta^w$. Adiabatic elimination of a highly detuned atomic level is a standard technique used in quantum optics and details can be found in these references [24–26].

The Hamiltonian after the adiabatic elimination thus obtained after ignoring the Stark shifts in level $|s\rangle$ due to spontaneous emission is given by:

$$\begin{aligned} H^w_{new} &= -\sum_{j=1}^{N_a} \frac{|\Omega^w_{eg,j}|^2}{\Delta^w} \sigma^j_{gg} - \sum_{j=1,\tau}^{N_a} \int \frac{d^3\mathbf{k}}{(2\pi)^3} \\ &\times \left[ \frac{\Omega^w_{eg,j} g^*_{es,\tau}(\mathbf{k})}{\Delta^w} e^{-i(\Delta\mathbf{k}\cdot\mathbf{r}_j - \Delta\omega t)} \sigma^j_{sg} a^\dagger_{\mathbf{k},\tau} + \text{h.c.} \right] \end{aligned} \tag{3.18}$$

where:

$$\Delta\mathbf{k} = \mathbf{k} - \mathbf{k}^w \tag{3.19}$$

$$\Delta\omega = \omega_k - (\omega^w - \omega_{sg}) \tag{3.20}$$

We can ignore the Stark shift in level $|s\rangle$ as it is much smaller than the other terms. The Stark energy shift is proportional to the intensity of the spontaneous emission field which is much weaker than the classical pumping field [47]. Let us perform another unitary transformation, rotating the vector $|g\rangle$ such that the resulting Hamilto-

nian depends only on the lowering and raising atomic operators. The corresponding unitary transformation is:

$$U = \exp\left[ i \int_0^{T_w} \sum_{j=1}^{N_a} \frac{|\Omega^w_{eg,j}|^2}{\Delta^w} \sigma^j_{gg} dt' \right] \tag{3.21}$$

The resulting transformed Hamiltonian is then:

$$\begin{aligned} H^w_{new} &= -\sum_{j=1,\tau}^{N_a} \int \frac{d^3\mathbf{k}}{(2\pi)^3} \left[ \frac{\Omega^w_{eg,j} g^*_{es,\tau}(\mathbf{k})}{\Delta^w} e^{-i(\Delta\mathbf{k}\cdot\mathbf{r}_j - \Delta\omega t)} \right. \\ &\quad \left. \times e^{i\int_0^{T_w} \frac{|\Omega^w_{eg,j}|^2}{\Delta^w} dt} \sigma^j_{sg} a^\dagger_{\mathbf{k},\tau} + \text{h.c.} \right] \end{aligned} \tag{3.22}$$

In the following calculations, we ignore the phase accumulated due to the Stark shift in $|g\rangle$ as it is small in comparison with the other phases accumulated in the duration $T_w$.

Let us start with the write Hamiltonian and derive the state of the system under the single photon excitation limit. We consider only single photon excitation as the write laser pulse is weak and off-resonant.

$$H^w_{new} = \sum_{j=1,\tau}^{N_a} \int \frac{d^3\mathbf{k}}{(2\pi)^3} \left[ C^w_{j,\tau}(\mathbf{k}, t) \sigma^j_{gs} a_{\mathbf{k},\tau} + \text{h.c.} \right] \tag{3.23}$$

We have defined:

$$C^w_{j,\tau}(\mathbf{k}, t) = -\frac{\Omega^{w*}_{eg,j} g_{es,\tau}(\mathbf{k})}{\Delta^w} e^{i(\Delta\mathbf{k}\cdot\mathbf{r}_j - \Delta\omega t)} \tag{3.24}$$

Consider the write pulse to be a square pulse with a Gaussian transverse profile travelling in the $+z$ direction whose electric field magnitude is given as:

$$E^w(\mathbf{r}, t) = Q^w(\mathbf{r}) V^w(t) \tag{3.25}$$

with:

$$Q^w(\mathbf{r}) = \frac{E_0^w}{\sqrt{1+\frac{z^2}{z_w^2}}} e^{-\frac{x^2+y^2}{W_w^2\left(1+\frac{z^2}{z_w^2}\right)}} e^{i\left[\frac{k^w(x^2+y^2)}{2R_w(z)}-\psi_w(z)\right]} \tag{3.26}$$

$$V^w(t) = \Theta(t)\Theta(T_w - t) \tag{3.27}$$

where:

$$z_w = \frac{k^w W_w^2}{2} \tag{3.28}$$

$$R_w(z) = z\left(1+\frac{z_w^2}{z^2}\right) \tag{3.29}$$

$$\psi_w(z) = \tan^{-1}\frac{z}{z_w} \tag{3.30}$$

In the above expression, $E_0^w$ is the peak value of electric field at the center of the Gaussian profile, $W_w$ is the beam waist. According to the usual convention of defining Gaussian beam we have, $z_w$ as the Rayleigh length, $R_w(z)$ as the radius of curvature of the beam wave-front at the position $z$ and $\psi_w(z)$ is the associated Gouy phase.

Also in Eq. (3.25), we have taken the liberty of expressing the electric field magnitude as a product of the spatial part and temporal part since the time taken for the propagation of a single wave-front from one end of the atomic sample to the other end is very small compared to the total time duration of the Gaussian square pulse and $T_w\omega^w \gg 1$. For a few recent experiments where the widths of the control pulses and the single photon optics is comparable, it becomes necessary to consider the phases introduced due to the transverse profile of these paraxial pulses [110].

A single photon excited state for the write Hamiltonian defined in Eq. (3.23) is given as:

$$|\phi\rangle^w = \left[1 - i\int_0^{T_w} dt\ H^w(t)\right]|vac\rangle \tag{3.31}$$

where:

$$|vac\rangle = |g\rangle^{\otimes N_a}|0\rangle_{ph} = |g\rangle_1|g\rangle_2...|g\rangle_N|0\rangle_{ph} \tag{3.32}$$

The state $|0\rangle_{ph}$ stands for the absence of any photons in the system.

On substituting the expression for the Hamiltonian we get:

$$\begin{aligned}
|\phi\rangle^w &= |vac\rangle + \frac{e^2\langle e|\mathbf{r}|g\rangle\cdot\hat{\epsilon}^w}{16\pi^3\Delta^w}\frac{1}{\sqrt{2\varepsilon_0}}\sum_{j=1,\tau}^{N_a} Q^w(\mathbf{r}_j) \\
&\quad\times\int d^3\mathbf{k}\ \langle s|\mathbf{r}|e\rangle\cdot\hat{\epsilon}^*_{\mathbf{k},\tau}\sqrt{\omega_k}e^{i(k^w\hat{\mathbf{z}}-\mathbf{k})\cdot\mathbf{r}_j} \\
&\quad\times\int_0^{T_w} dt\ e^{i(\omega_k-\omega^w+\omega_{sg})t}\ \Theta(T_w-t)\Theta(t)|s\rangle_j a^\dagger_{\mathbf{k},\tau}|0\rangle_{ph}
\end{aligned} \tag{3.33}$$

$$\begin{aligned}
&= |vac\rangle + \frac{e^2T_w\langle e|\mathbf{r}|g\rangle\cdot\hat{\epsilon}^w}{16\pi^3\Delta^w}\frac{1}{\sqrt{2\varepsilon_0}}\sum_{j=1,\tau}^{N_a} Q^w(\mathbf{r}_j) \\
&\quad\times\int d^3\mathbf{k}\langle s|\mathbf{r}|e\rangle\cdot\hat{\epsilon}^*_{\mathbf{k}\tau}\sqrt{\omega_k}e^{i(k^w\hat{\mathbf{z}}-\mathbf{k})\cdot\mathbf{r}_j}e^{i(\omega_k-\omega^w+\omega_{sg})\frac{T_w}{2}} \\
&\quad\times\mathrm{sinc}\left[(\omega_k-\omega^w+\omega_{sg})\frac{T_w}{2}\right]|s\rangle_j a^\dagger_{\mathbf{k},\tau}|0\rangle_{ph}
\end{aligned} \tag{3.34}$$

Under the assumption that the single photon detectors used for the detection of the emitted signal photon are ideal, we can ignore the vacuum component. In the Schrodinger picture, the above expression can then be understood as:

$$|\phi\rangle^w = \sum_\tau\int d^3\mathbf{k}\ \hat{f}^w(k,\theta_k,\phi_k,\tau)e^{-i\omega_k t}a^\dagger_{\mathbf{k},\tau}|0\rangle_{ph} \tag{3.35}$$

where:

$$\begin{aligned}\hat{f}^w(k,\theta_k,\phi_k,\tau) &= \frac{|e|^2 T_w \langle e|\mathbf{r}|g\rangle \cdot \hat{\epsilon}^w}{16\pi^3\Delta^w}\sqrt{\frac{\omega_k}{2\varepsilon_0}}\sum_{j=1}^{N_a} Q^w(\mathbf{r}_j) \\ &\times \langle s|\mathbf{r}|e\rangle \cdot \hat{\epsilon}^*_{\mathbf{k}\tau} e^{i(k^w\hat{\mathbf{z}}-\mathbf{k})\cdot\mathbf{r}_j} e^{i(\omega_k-\omega^w+\omega_{sg})\frac{T_w}{2}} \\ &\times \mathrm{sinc}\left[(\omega_k-\omega^w+\omega_{sg})\frac{T_w}{2}\right] e^{-i\omega_{sg}t}|s\rangle_j \end{aligned} \tag{3.36}$$

In the above equation, we do not consider the phase factors coming from unitary transformation in Eq. (3.21) as they do not influence the final expression for IRE . We can now trace over the $\omega_k$ component because the single photon detector is not sensitive to this value. The trace of $|\phi\rangle^{ww}\langle\phi|$ over $\omega_k$ diverges for the integration limits going from 0 to $\infty$, but we can restrict the integration from 0 to a finite value of frequency based on the validity of the dipole approximation. For such a situation the dominant contribution comes from a small window around $\omega_k = \omega^w - \omega_{sg}$. The remaining angular profile of Eq. (3.36) becomes:

$$\hat{f}^w(\theta_k,\phi_k,\tau) \propto \sum_j Q^w(\mathbf{r}_j)\langle s|\mathbf{r}|e\rangle \cdot \hat{\epsilon}^*_{\hat{\mathbf{k}},\tau} e^{i(k^w\hat{\mathbf{z}}-k^s\hat{\mathbf{k}})\cdot\mathbf{r}_j - i\omega_{sg}t}|s\rangle_j \tag{3.37}$$

where $\hat{\mathbf{k}}$ is the unit wave-vector and

$$ck^s = \omega^w - \omega_{sg} \tag{3.38}$$

Experimentally, we couple the emitted photon into a single mode optical fiber which in turn couples to the single photon detector. The polarization of the emitted photon is filtered before it is coupled to the optical fiber. The transverse mode associated with the optical fiber is considered to be a Gaussian mode propagating in the $+\hat{z}$ direction. The emitted signal photon mode function will be mostly confined in a

small angular region around the direction $+\hat{z}$, overlapping with the paraxial optical fiber mode profile. Thus, we can assume $\hat{\epsilon}^*_{\hat{\mathbf{k}},\tau} = \hat{\epsilon}^*_{\hat{\mathbf{z}},\tau}$ which can now be taken out of the integration. This approximation is valid since $\hat{\epsilon}^*_{\hat{\mathbf{k}},\tau}$ varies slowly over the solid angle around $\hat{\mathbf{z}}$ direction when compared to the rapidly varying phase factor $e^{-ik^s\hat{\mathbf{k}}\cdot\mathbf{r}_j}$ with changing $\hat{\mathbf{k}}$. Also, the polarization, $\tau$, is fixed by the polarization filters. Thus, we have:

$$\hat{f}^w(\theta_k,\phi_k) \propto \sum_j Q^w(\mathbf{r}_j) e^{i(k^w\hat{\mathbf{z}}-k^s\hat{\mathbf{k}})\cdot\mathbf{r}_j} e^{-i\omega_{sg}t}|s\rangle_j \tag{3.39}$$

$$= N_f \sum_{j=1}^{N_a} Q^w(\mathbf{r}_j) e^{i(k^w\hat{\mathbf{z}}-k^s\hat{\mathbf{k}})\cdot\mathbf{r}_j} e^{-i\omega_{sg}t}|s\rangle_j \tag{3.40}$$

where $N_f$ is the normalization constant for the angular mode function.

The angular mode function of the field associated with the optical fiber can be approximated by a Gaussian mode given below:

$$g^w(\theta_k,\phi_k) = N_g^w \; e^{-\frac{1}{4}(k^sW_s\sin\theta_k)^2} \tag{3.41}$$

with $N_g^w$ as the normalization factor.

On taking the overlap between Eq. (3.40) and Eq. (3.41) in the forward direction we get the spin-wave state $|\phi\rangle^{sw}$ as:

$$|\phi\rangle^{sw} = \int_0^{2\pi} d\phi_k \int_0^{\frac{\pi}{2}} d\theta_k \sin\theta_k \hat{f}^w(\theta_k,\phi_k) g^{w*}(\theta_k,\phi_k) \tag{3.42}$$

$$= N^{sw} \sum_{j=1}^{N_a} Q^w(\mathbf{r}_j) e^{ik^wz_j} \int_0^{\frac{\pi}{2}} d\theta_k \sin\theta_k e^{-ik^sz_j\cos\theta_k} J_0(k^s|\mathbf{r}_{j\perp}|\sin\theta_k) e^{-\frac{1}{4}(k^sW_s\sin\theta_k)^2} e^{-i\omega_{sg}t}|s\rangle_j \tag{3.43}$$

where $|\mathbf{r}_{j\perp}| = \sqrt{x_j^2+y_j^2}$ and $N^{sw} = N_f * N_g^w$.

For experimental parameters of interest, $k^s W_s \gg 1$. Thus, only a very small interval of values of $\theta_k$ above 0 contributes to the integration, suggesting that we can make the paraxial approximation. Taking the upper limit of integration to $\infty$, $\cos\theta_k \approx 1 - \theta_k^2/2$ and $\sin\theta_k \approx \theta_k$ we get:

$$\begin{aligned} |\phi\rangle^{sw} &= N^{sw} \sum_{j=1}^{N_a} Q^w(\mathbf{r}_j) e^{i(k^w - k^s)z_j} \int_0^\infty d\theta_k \theta_k \\ &\quad \times J_0(k^s |\mathbf{r}_{j\perp}| \theta_k) e^{-\theta_k^2 [\frac{1}{4}(W_s k^s)^2 - \frac{i}{2} k^s z_j]} e^{-i\omega_{sg} t} |s\rangle_j \end{aligned} \tag{3.44}$$

$$\begin{aligned} &= N^{sw} \sum_{j=1}^{N_a} Q^w(\mathbf{r}_j) \frac{e^{i(k^w - k^s)z_j}}{z_s k^s \sqrt{1 + \frac{z_j^2}{z_s^2}}} e^{-\frac{x_j^2 + y_j^2}{W_s^2 \left(1 + \frac{z_j^2}{z_s^2}\right)}} \\ &\quad \times e^{-i\left[\frac{k^s (x_j^2 + y_j^2)}{2R_s(z_j)} - \psi_s(z_j)\right]} e^{-i\omega_{sg} t} |s\rangle_j \end{aligned} \tag{3.45}$$

where:

$$z_s = \frac{k^s W_s^2}{2} \tag{3.46}$$

$$R_s(z_j) = z_j \left(1 + \frac{z_s^2}{z_j^2}\right) \tag{3.47}$$

$$\psi_s(z_j) = \tan^{-1} \frac{z_j}{z_s} \tag{3.48}$$

The normalization $N^{sw}$ need not be determined as it corresponds to the success rate of the write process and does not affect the desired IRE. We now proceed to the read process, where the spin-wave state is read out and a idler (read) photon is emitted after a memory storage time interval $T_m$.

### 3.3.2 The Read Process

Let us begin by formulating the read Hamiltonian in a way similar to the write Hamiltonian. In the read process, a short but strong classical laser pulse on resonance

with the $|s\rangle$-$|e\rangle$ transition is made to interact with the atomic ensemble. The photon emitted from the $|e\rangle$-$|g\rangle$ transition is collected after polarization filtering. Interaction for the $|s\rangle$-$|e\rangle$ transition is treated semi-classically and the spontaneous photon emission from $|e\rangle$-$|g\rangle$ transition is treated quantum mechanically. Assuming dipolar light-matter interactions and the RWA, we can write the read Hamiltonian as:

$$\begin{aligned} H^r &= \sum_{j=1}^{N_a}(\omega_{eg}\sigma_{ee}^j + \omega_{sg}\sigma_{ss}^j) + \sum_\tau \int \frac{d^3\mathbf{k}}{(2\pi)^3}\omega_k a_{\mathbf{k},\tau}^\dagger a_{\mathbf{k},\tau} \\ &+ \sum_{j=1}^{N_a}\left[\Omega_{es,j}^r e^{i(\mathbf{k}^r\cdot\mathbf{r}_j'-\omega^r t)}\sigma_{es}^j + \sum_\tau \int \frac{d^3\mathbf{k}}{(2\pi)^3} g_{eg,\tau}(\mathbf{k}) e^{i\mathbf{k}\cdot\mathbf{r}_j'}\sigma_{eg}^j a_{\mathbf{k}\tau} + \text{h.c.}\right] \end{aligned} \tag{3.49}$$

Definitions of $\Omega_{es,j}^r$ and $g_{eg,\tau}$ are analogous to the definitions in Eqs. (3.13-3.14). The atomic positions may have changed during $T_m$, and are denoted by $\mathbf{r}'$.

Using the resonance condition for the $|s\rangle$-$|e\rangle$ transition, the read Hamiltonian in the field interaction picture after the application of the unitary $U$

$$U = \exp\left[-i\sum_{j=1}^{N_a}(\omega^r\sigma_{ee}^j + \omega_{sg}\sigma_{ss}^j)t - i\sum_\tau \int \frac{d^3\mathbf{k}}{(2\pi)^3}\omega_k a_{\mathbf{k},\tau}^\dagger a_{\mathbf{k},\tau} t\right] \tag{3.50}$$

is given as:

$$\begin{aligned} H_{new}^r &= \sum_{j=1}^{N_a}\omega_{sg}\sigma_{ee}^j + \sum_{j=1}^{N_a}\left[\Omega_{es,j}^r e^{i(\mathbf{k}^r\cdot\mathbf{r}_j'-\omega_{sg}t)}\sigma_{es}^j\right. \\ &+ \left.\sum_\tau \int \frac{d^3\mathbf{k}}{(2\pi)^3} g_{eg,\tau}(\mathbf{k}) e^{i\mathbf{k}\cdot\mathbf{r}_j - i(\omega_k-\omega^r)t}\sigma_{eg}^j a_{\mathbf{k},\tau} + \text{h.c.}\right] \end{aligned} \tag{3.51}$$

We consider the classical read-out pulse to be a square pulse propagating in $-z$ direction with a Gaussian transverse profile and its magnitude given as:

$$E^r(\mathbf{r}) = Q^r(\mathbf{r})V^r(t) \tag{3.52}$$

With:

$$
\begin{aligned}
Q^r(\mathbf{r}) &= \frac{E_0^r}{\sqrt{1+\frac{z^2}{z_r^2}}} e^{-\frac{\mathbf{r}_\perp^2}{W_r^2\left(1+\frac{z^2}{z_r^2}\right)}} e^{-i\left[\frac{k^r\mathbf{r}_\perp^2}{2R_r(z)}-\psi_r(z)\right]} && (3.53)\\
z_r &= \frac{k^r W_r^2}{2} && (3.54)\\
R_r(z) &= z\left(1+\frac{z_r^2}{z^2}\right) && (3.55)\\
\psi_r(z) &= \tan^{-1}\frac{z}{z_r} && (3.56)\\
V^r(t) &= \Theta(t-T_p)\Theta(T_p+T_r-t) && (3.57)
\end{aligned}
$$

Here, $T_p = T_m + T_w$ is the duration after which the read pulse is sent measured from the beginning of the write pulse and $T_r$ is the duration of the read pulse.

Let us consider a general state which satisfies the Schrodinger's equation as follows:

$$
\begin{aligned}
|\phi(t)\rangle^r &= \sum_{j=1}^{N_a}\left[A_j(t)e^{-i\omega_{sg}t}|s\rangle_j|0\rangle_{ph} + B_j(t)e^{-i\omega^r t}|e\rangle_j|0\rangle_{ph}\right]\\
&\quad + \sum_\tau \int \frac{d^3\mathbf{k}}{(2\pi)^3} C_\tau(\mathbf{k},t)e^{-i\omega_k t}|g\rangle^{\otimes N} a^\dagger_{\mathbf{k},\tau}|0\rangle_{ph} \qquad (3.58)
\end{aligned}
$$

In the above equation, state $|e\rangle_j$ is defined similar to state $|s\rangle_j$ as Eq. (3.2). The initial condition for our system is given by Eq. (3.45).

Evaluating the Schrodinger's equation with the Hamiltonian defined in Eq. (3.51) and the state in Eq. (3.58) we get:

$$
\begin{aligned}
&i\frac{d|\phi(t)\rangle^r}{dt} = H^r|\phi(t)\rangle^r && (3.59)\\
&i\dot{A}_j(t) = \Omega^{*r}_{es,j}(t)e^{-i(\mathbf{k}^r\cdot\mathbf{r}'_j-\omega_{sg}t)}B_j(t) && (3.60)\\
&i\dot{B}_j(t) = \omega_{sg}B_j(t) + \Omega^r_{es,j}(t)e^{i(\mathbf{k}^r\cdot\mathbf{r}'_j-\omega_{sg}t)}A_j(t)\\
&\qquad + \sum_\tau \int \frac{d^3\mathbf{k}}{(2\pi)^3} g_{eg,\tau}(\mathbf{k})e^{i[\mathbf{k}\cdot\mathbf{r}'_j-(\omega_k-\omega^r)t]}C_\tau(\mathbf{k},t) && (3.61)\\
&i\dot{C}_\tau(\mathbf{k},t) = \sum_j g^*_{eg,\tau}(\mathbf{k})e^{-i[\mathbf{k}\cdot\mathbf{r}'_j-(\omega_k-\omega^r)t]}B_j(t) && (3.62)
\end{aligned}
$$

For simplicity, let us assume the dipole moment associated with the Rabi frequency $\Omega^r_{es,j}(t)$ to be real. This does not change the final result which only depends on the modulus of this Rabi frequency. With the definition

$$A_j(t) = e^{i\omega_{sg}t}e^{-i\mathbf{k}^r\cdot\mathbf{r}'_j}e^{i\left[\frac{k^r\mathbf{r}^2_{\perp j}}{2R_r(z_j)}-\psi_r(z_j)\right]}\alpha_j(t) \tag{3.63}$$

and the mathematical details provided in Appendix B we can simplify the Eqs. (3.60-3.62) to get:

$$\dot{\tilde{\alpha}}_j(t) = -i\Omega^r_{es,j}(t)\tilde{B}_j(t) \tag{3.64}$$

$$\dot{\tilde{B}}_j(t) = -i\Omega^r_{es,j}(t)\tilde{\alpha}_j(t) - \gamma_{eg}\tilde{B}_j(t) \tag{3.65}$$

where $\gamma_{eg} = \Gamma_{eg}/2$ and $\Gamma_{eg}$ is the spontaneous emission rate from $|e\rangle$ to $|g\rangle$.

For the electric field given in Eq. (3.52), $\Omega^r_{es,j}$ is non-zero only when $T_p \leq t \leq T_p + T_r$. For $t > T_p + T_r$:

$$\dot{\tilde{\alpha}}_j(t) = 0 \tag{3.66}$$

$$\dot{\tilde{B}}_j(t) = -\gamma_{eg}\tilde{B}_j(t) \tag{3.67}$$

Thus, for $t > T_p + T_r$:

$$\tilde{\alpha}_j(t) = \tilde{\alpha}_j(T_p + T_r) \tag{3.68}$$

$$\tilde{B}_j(t) = \tilde{B}_j(T_p + T_r)\, e^{-\gamma_{eg}(t-T_p-T_r)} \tag{3.69}$$

Now let us evaluate the solution to Eqs. (3.64, 3.65) for $T_p \leq t \leq T_p + T_r$. This set of two first order differential equations can be combined into a single second order

differential equation given as:

$$\ddot{\tilde{B}}_j(t) = -(\Omega^r_{es,j})^2 \tilde{B}_j(t) - \gamma_{eg}\dot{\tilde{B}}_j(t) \tag{3.70}$$

Define $\tilde{\Omega}_{es,j} \equiv \sqrt{(\Omega^r_{es,j})^2 - \frac{\gamma^2_{eg}}{4}}$. The solution to the Eq. (3.70) is:

$$\tilde{B}_j(t) = C_1 e^{(-\frac{\gamma_{eg}}{2} - i\tilde{\Omega}_{es,j})t} + C_2 e^{(-\frac{\gamma_{eg}}{2} + i\tilde{\Omega}_{es,j})t} \tag{3.71}$$

Using the initial conditions at $t = T_p$ we get:

$$C_1 = \frac{\Omega^r_{es,j}}{2\tilde{\Omega}_{es,j}} \alpha_j(T_P) e^{(\frac{\gamma_{eg}}{2} + i\tilde{\Omega}_{es,j} + i\omega_{sg})T_p} \tag{3.72}$$

$$C_2 = -\frac{\Omega^r_{es,j}}{2\tilde{\Omega}_{es,j}} \alpha_j(T_P) e^{(\frac{\gamma_{eg}}{2} - i\tilde{\Omega}_{es,j} + i\omega_{sg})T_p} \tag{3.73}$$

Evaluating $C_\tau(\mathbf{k}, t)$ using Eqs. (3.72, 3.73, B.4 and B.7) with the definition $\Delta^r_k \equiv (\omega_k - \omega^r - \omega_{sg})$ we get:

$$\begin{aligned} C_\tau(\mathbf{k}, t) &= -\sum_j g^*_{eg,\tau}(\mathbf{k}) \frac{\Omega^r_{es,j}}{\tilde{\Omega}_{es,j}} \alpha_j(T_p) e^{(\frac{\gamma_{eg}}{2} + i\omega_{sg})T_p} e^{-i\mathbf{k}\cdot\mathbf{r}'_j} \int_{T_p}^{t} dt' e^{i(\omega_k - \omega^r - \omega_{sg})t' - \frac{\gamma_{eg}}{2}t'} \\ &\quad \times \sin[\tilde{\Omega}_{es,j}(t' - T_p)] \qquad (3.74) \\ &= -\sum_j g^*_{eg,\tau}(\mathbf{k}) \Omega^r_{es,j} \alpha_j(T_p) e^{i(\omega_k - \omega^r)T_p} e^{-i\mathbf{k}\cdot\mathbf{r}'_j} \\ &\quad \times \frac{e^{(-\frac{\gamma_{eg}}{2} + i\Delta^r_k)(t - T_p)} \left\{ \cos[\tilde{\Omega}_{es,j}(t - T_p)] - \frac{i\Delta^r_k - \gamma_{eg}/2}{\tilde{\Omega}_{es,j}} \sin[\tilde{\Omega}_{es,j}(t - T_p)] \right\} - 1}{(\Delta^r_k - \tilde{\Omega}_{es,j} + i\frac{\gamma_{eg}}{2})(\Delta^r_k + \tilde{\Omega}_{es,j} + i\frac{\gamma_{eg}}{2})} \qquad (3.75) \end{aligned}$$

At $t = T_p + T_r$ we get:

$$\begin{aligned} C_\tau(\mathbf{k}, T_p + T_r) &= -\sum_j g^*_{eg,\tau}(\mathbf{k})\Omega^r_{es,j}\alpha_j(T_p)e^{i(\omega_k-\omega^r)T_p}e^{-i\mathbf{k}\cdot\mathbf{r}'_j} \\ &\quad \times \frac{e^{(-\frac{\gamma_{eg}}{2}+i\Delta^r_k)T_r}\left[\cos(\tilde{\Omega}_{es,j}T_r) - \frac{i\Delta^r_k-\gamma_{eg}/2}{\tilde{\Omega}_{es,j}}\sin(\tilde{\Omega}_{es,j}T_r)\right] - 1}{(\Delta^r_k - \tilde{\Omega}_{es,j} + i\frac{\gamma_{eg}}{2})(\Delta^r_k + \tilde{\Omega}_{es,j} + i\frac{\gamma_{eg}}{2})} \end{aligned} \tag{3.76}$$

We can now find the explicit expression for $C_\tau(\mathbf{k}, t)$ when $t > T_p + T_r$:

$$C_\tau(\mathbf{k}, t) = C_\tau(\mathbf{k}, T_p + T_r) - i\sum_j \int_{T_p+T_r}^{t} dt' g^*_{eg,\tau}(\mathbf{k})e^{-i[\mathbf{k}\cdot\mathbf{r}'_j-(\omega_k-\omega^r)t']}B_j(t') \tag{3.77}$$

After evaluating the integral we get:

$$\begin{aligned} C_\tau(\mathbf{k}, t) &= C_\tau(\mathbf{k}, T_p + T_r) - \sum_j g^*_{eg,\tau}(\mathbf{k})\frac{\Omega^r_{es,j}}{\tilde{\Omega}_{es,j}}\alpha_j(T_p)e^{-(\frac{\gamma_{eg}}{2}+i\omega_{sg})T_r}\sin(\tilde{\Omega}_{es,j}T_r)e^{-i\mathbf{k}\cdot\mathbf{r}'_j} \\ &\quad \times e^{i\omega_{sg}(T_p+T_r)}e^{\gamma_{eg}(T_p+T_r)}\frac{e^{(i\Delta^r_k-\gamma_{eg})t} - e^{(i\Delta^r_k-\gamma_{eg})(T_p+T_r)}}{i\Delta^r_k - \gamma_{eg}} \end{aligned} \tag{3.78}$$

We then substitute the value of $C_\tau(\mathbf{k}, T_p + T_r)$ and simplify the equation.

$$\begin{aligned} C_\tau(\mathbf{k}, t) &= -\sum_j g^*_{eg,\tau}(\mathbf{k})\Omega^r_{es,j}\alpha_j(T_p)e^{-i\mathbf{k}\cdot\mathbf{r}'_j}\Bigg\{ e^{i\Delta^r_k(T_p+T_r)}e^{i\omega_{sg}T_p}e^{-\frac{\gamma_{eg}}{2}T_r} \\ &\quad \times\Bigg[\frac{\cos(\tilde{\Omega}_{es,j}T_r) - \frac{i\Delta^r_k-\gamma_{eg}/2}{\tilde{\Omega}_{es,j}}\sin(\tilde{\Omega}_{es,j}T_r)}{(\Delta^r_k - \tilde{\Omega}_{es,j} + i\frac{\gamma_{eg}}{2})(\Delta^r_k + \tilde{\Omega}_{es,j} + i\frac{\gamma_{eg}}{2})} \\ &\quad + \frac{\sin(\tilde{\Omega}_{es,j}T_r)}{\tilde{\Omega}_{es,j}}\frac{e^{(i\Delta^r_k-\gamma_{eg})(t-T_p-T_r)} - 1}{i\Delta^r_k - \gamma_{eg}}\Bigg] \\ &\quad - \frac{e^{i(\Delta^r_k+\omega_{sg})T_p}}{(\Delta^r_k + i\frac{\gamma_{eg}}{2} - \tilde{\Omega}_{es,j})(\Delta^r_k + i\frac{\gamma_{eg}}{2} + \tilde{\Omega}_{es,j})}\Bigg\} \end{aligned} \tag{3.79}$$

Substituting $\alpha_j(T_p)$ back using Eq. (3.63) and defining:

$$\phi^r(\mathbf{r}'_j) = \frac{k^r \mathbf{r}'^2_{\perp j}}{2R_r(z'_j)} - \psi_r(z'_j) \tag{3.80}$$

we get:

$$C_\tau(\mathbf{k},t) = -\sum_j g^*_{eg,\tau}(\mathbf{k})\Omega^r_{es,j}A_j(T_p)e^{i\mathbf{k}^r\cdot\mathbf{r}'_j}e^{-i\phi^r(\mathbf{r}'_j)}e^{-i\mathbf{k}\cdot\mathbf{r}'_j}\zeta(\omega_k,\mathbf{r}'_j,t) \tag{3.81}$$

where:

$$\begin{aligned}\zeta(\omega_k,\mathbf{r}'_j,t) &= e^{i\Delta^r_k(T_p+T_r)}e^{-\frac{\gamma_{eg}}{2}T_r} \\ &\times\Bigg[\frac{\cos(\tilde{\Omega}_{es,j}T_r) - \frac{i\Delta^r_k-\frac{\gamma_{eg}}{2}}{\tilde{\Omega}_{es,j}}\sin(\tilde{\Omega}_{es,j}T_r)}{(\Delta^r_k)^2-(\Omega^r_{es,j})^2+i\gamma_{eg}\Delta^r_k} \\ &\quad+\frac{\sin(\tilde{\Omega}_{es,j}T_r)}{\tilde{\Omega}_{es,j}}\frac{e^{(i\Delta^r_k-\gamma_{eg})(t-T_p-T_r)}-1}{i\Delta^r_k-\gamma_{eg}}\Bigg] \\ &- \frac{e^{i\Delta^r_k T_p}}{(\Delta^r_k)^2-(\Omega^r_{es,j})^2+i\gamma_{eg}\Delta^r_k}\end{aligned} \tag{3.82}$$

At this point another simplification can be made by taking the experimental conditions into consideration. The read-out pulse generally has a very broad waist size compared to the write pulse i.e. $W_r \gg W_w$, so that the stored spin-wave can be fully read out. In this case, we can assume that the Gaussian read-out pulse is spatially broad enough to neglect the dependence of $\Omega^r_{es,j}$ on atomic positions. Similarly, we can neglect the phase contributions $\phi^r(\mathbf{r}'_j)$. Also, we assume that $\Omega^r_{es} > \frac{\gamma_{eg}}{2}$.

The last term of Eq. (3.82) is the only term that doesn't have the decay contributions from the excited level. From the experimental perspective, we can choose

$\gamma_{eg}T_r \gg 1$, thus we can neglect the first two terms:

$$\zeta(\omega_k, \mathbf{r}'_j, t) \approx -\frac{e^{i\Delta_k^r T_p}}{(\Delta_k^r)^2 - (\Omega_{es}^r)^2 + i\gamma_{eg}\Delta_k^r} \tag{3.83}$$

Incorporating these approximations we have:

$$\begin{aligned} C_\tau(\mathbf{k}, t) &= \Omega_{es}^r \sum_j g^*_{eg,\tau}(\mathbf{k}) A_j(T_p) e^{i\mathbf{k}^r \cdot \mathbf{r}'_j} e^{-i\mathbf{k}\cdot\mathbf{r}'_j} \\ &\quad \times \frac{e^{i\Delta_k^r T_p}}{(\Delta_k^r)^2 - (\Omega_{es}^r)^2 + i\gamma_{eg}\Delta_k^r} \end{aligned} \tag{3.84}$$

After sufficiently long time interval only the $C_\tau(\mathbf{k}, t)$ co-efficient survives. Thus, the final state after the action of the read Hamiltonian can be written as:

$$|\Phi\rangle^r = \sum_\tau \frac{1}{8\pi^3} \int d^3\mathbf{k} C_\tau(\mathbf{k}, t) e^{-i\omega_k t} |g\rangle^{\otimes N_a} a^\dagger_{\mathbf{k}\tau} |0\rangle_{ph} \tag{3.85}$$

We see that the mode function in Eq. (3.85) peaks for a small range of values of $\omega_k$. We can take the frequency at which the photon gets emitted by setting $\Delta_k^r \pm \Omega_{es}^r = 0$. Since $\omega^r \gg \Omega_{es}^r$, taking $\Delta_k^r = 0$ is a good approximation. Then by tracing over the frequency part we can now write the angular part of the emitted photon as:

$$\hat{f}^r(\theta_k, \phi_k, \tau) = \sum_j g^*_{eg,\tau}(\theta_k, \phi_k) A_j(T_p) e^{i\mathbf{k}^r \cdot \mathbf{r}'_j} e^{-ik^i \hat{\mathbf{k}}\cdot\mathbf{r}'_j} \frac{\omega^r + \omega_{sg}}{\sqrt{8\pi^2 \gamma_{eg} c^3}} |g\rangle^{\otimes N_a} \tag{3.86}$$

where:

$$ck^i = \omega^r + \omega_{sg} \tag{3.87}$$

Using arguments similar to those used in the write part we assume $g^*_{ge,\tau}(\theta_k, \phi_k)$ varies slowly for the relevant values of $\theta_k, \phi_k$ around $\theta_k = \pi$. Thus, fixing the wave-vector

direction to be $-\hat{\mathbf{z}}$, as was done for the write process, we can find the overlap between the angular profile of the emitted photon and the optical fiber used to collect it. The polarization also gets fixed by the polarization filter before coupling into the optical fiber. We can also ignore the phase factors associated with time evolution as the final IRE expression is independent of it. Note that Eq. (3.86) has the same normalization as $A_j(T_p)$:

$$\int d\Omega_k |\hat{f}^r(\theta_k, \phi_k)|^2 \;=\; \sum_j |A_j(T_p)|^2 \tag{3.88}$$

Here we calculate the normalization factor only for the completeness of the formula. In the numerical simulation it is much easier to directly sample the angular dependence and then normalize the function, because $g_{eg,\tau}$ is taken as constant. See Sec. 3.4 for more details. Let the angular profile of the electric field associated with the optical fiber be given as:

$$g^r(\theta_k, \phi_k) = N_g^r e^{-\frac{1}{4}(k^i W_i \sin\theta_k)^2} \tag{3.89}$$

In the calculation of the overlap we again use the paraxial approximation due to the fact that $k^i W_i \gg 1$. The normalization factor $N_g^R$ under this approximation is given as $N_g^r = k^i W_i/\sqrt{2}$. Taking the overlap of the emitted photon profile with the Gaussian collection mode then gives the final atomic state:

$$|\phi\rangle^{fs} \;=\; \int_0^{2\pi} d\phi_k \int_{\frac{\pi}{2}}^{\pi} d\theta_k \sin\theta_k \hat{f}^r(\theta_k, \phi_k) g^{r*}(\theta_k, \phi_k) \tag{3.90}$$

$$\begin{aligned} &= \frac{\omega^r + \omega_{sg}}{\sqrt{8\pi^2 \gamma_{eg} c^3}} \frac{W_i k^i}{\sqrt{2}} \sum_{j=1}^{N_a} A_j(T_p) e^{-ik^r z'_j} \int_0^{\frac{\pi}{2}} d\theta_k \sin\theta_k \\ &\quad \times e^{ik^i z'_j \cos\theta_k} J_0(k^i |\mathbf{r}'_{j\perp}| \sin\theta_k) e^{-\frac{1}{4}(k^i W_i \sin\theta_k)^2} |g\rangle^{\otimes N_a} \end{aligned} \tag{3.91}$$

$$
\begin{aligned}
|\phi\rangle^{fs} &= \frac{(\omega^r+\omega_{sg})}{\sqrt{8\pi^2\gamma_{eg}c^3}}\frac{W_i k^i}{\sqrt{2}}\sum_{j=1}^{N_a} A_j(T_p)e^{-ik^r z'_j}\frac{e^{ik^i z'_j}}{\sqrt{1+\frac{z'^2_j}{z_i^2}}} \\
&\quad \times e^{-\frac{x'^2_j+y'^2_j}{W_i^2\left(1+\frac{z'^2_j}{z_i^2}\right)}} e^{i\left[\frac{k^i(x'^2_j+y'^2_j)}{2R_i(z'_j)}-\psi_i(z'_j)\right]}|g\rangle^{\otimes N_a} \qquad (3.92)\\
&\equiv \sum_j \Lambda(\mathbf{r}_j,\mathbf{r}'_j)|g\rangle^{\otimes N_a} \qquad (3.93)
\end{aligned}
$$

where:

$$
\begin{aligned}
z_i &= \frac{k^i W_i^2}{2} \qquad (3.94)\\
R_i(z'_j) &= z'_j\left(1+\frac{z_i^2}{z'^2_j}\right) \qquad (3.95)\\
\psi_i(z'_j) &= \tan^{-1}\frac{z'_j}{z_i} \qquad (3.96)
\end{aligned}
$$

Any subscript or superscript 'i' in the above equations stands for the idler photon.

### 3.3.3 Intrinsic Retrieval Efficiency: The Expression

In this section, we will describe and discuss the final expression obtained for the Intrinsic Retrieval Efficiency $\eta$. The IRE, $\eta$, is given by the modulus squared of the above overlap defined in Eq. (3.93).

$$
\eta = \frac{\left|\sum_j \Lambda(\mathbf{r}_j,\mathbf{r}'_j)\right|^2}{\sum_j |A_j(T_p)|^2} \qquad (3.97)
$$

In the above equation, we make sure that the initial state of the atomic ensemble at the beginning of the read process is normalized. As stated before, we evaluate this normalization factor numerically for our calculations. For an explicit expression

of $\Lambda(\mathbf{r}_j, \mathbf{r}'_j)$, we substitute $A_j(T_p)$ from Eq. (3.45), with its normalization factors neglected:

$$\begin{aligned}\Lambda(\mathbf{r}_j, \mathbf{r}'_j) &= \frac{\omega^r + \omega_{sg}}{\sqrt{8\pi^2\gamma_{eg}c^3}}\frac{W_i k^i}{\sqrt{2}} e^{-ik^r z'_j} \frac{e^{ik^i z'_j}}{\sqrt{1+\frac{z'^2_j}{z_i^2}}} \frac{e^{-ik^s z_j}}{\sqrt{1+\frac{z_j^2}{z_s^2}}} \frac{e^{ik^w z_j}}{\sqrt{1+\frac{z_j^2}{z_w^2}}} e^{-\frac{x_j^2+y_j^2}{W_w^2\left(1+\frac{z_j^2}{z_w^2}\right)}} e^{-\frac{x_j^2+y_j^2}{W_s^2\left(1+\frac{z_j^2}{z_s^2}\right)}} \\ &\times e^{-\frac{x'^2_j+y'^2_j}{W_I^2\left(1+\frac{z'^2_j}{z_i^2}\right)}} e^{i\left[\frac{k^w(x_j^2+y_j^2)}{2R_w(z_j)}-\psi_w(z_j)\right]} e^{-i\left[\frac{k^s(x_j^2+y_j^2)}{2R_s(z_j)}-\psi_s(z_j)\right]} e^{i\left[\frac{k^i(x'^2_j+y'^2_j)}{2R_i(z'_j)}-\psi_i(z'_j)\right]}\end{aligned} \tag{3.98}$$

As seen from Eq. (3.98), the coefficient of the the ground state is a result of weighted interference effects between all the atoms in the ensemble. The overall effect is equivalent to the overlap of three Gaussian beams with different beam parameters along with the phase contribution of the read beam in the $z$ direction. Note that the Gaussian structure of the read beam does not show up in Eq. (3.98) because of the assumption that the read beam waist is much larger than that of the write beam made below Eq. (3.82). Incidentally, the phase-matching condition cannot be perfectly satisfied even if atoms are stationary as well as for colinear beams. Substituting the values of $k_s$ and $k_i$ from Eq. (3.38) and Eq. (3.87) respectively into Eq. (3.98), we see that there is always a non-zero phase contribution along the $z$ axis due to $\omega_{sg}$. More precisely, the coherent atomic spin wave has a wavelength of about $2\pi c/(2\omega_{sg})$ in the $z$ direction. For $^{87}$Rb the hyper-fine splitting $|\omega_{sg}| = 2\pi \times 6.8\,\mathrm{GHz}$, which means $2\pi c/(2\omega_{sg}) \approx 22\mathrm{mm}$. Nevertheless, most experiments never use atomic samples having sizes lager than a few mm, so this effect will be small. The Gaussian transverse structure is another contributor that prevents the IRE from being unity.

## 3.4 Numerical Analysis of intrinsic retrieval efficiency

Let us now use the above framework to look at IRE calculated from a numerical simulation of an atomic sample that mimics the write-read process for realistic experimental setup to gain further insight.

### 3.4.1 Incorporating Experimental Setup

To avoid the noise associated with detection of the classical write and read pulses instead of emitted signal and idler photons, a skewed beam configuration of the write and read beams is implemented experimentally as is shown in Fig. 3.5 [72, 110, 114, 118, 121]. The write and read laser pulses aligned along the same axis are rotated by a small angle $\Theta$ with respect to the alignment axis of the signal and idler collection ports. This can be easily incorporated into our expression of $\eta$. Assume that the expressions for the write and read pulse electric field in Eq. (3.26) and Eq. (3.53) is evaluated in a frame of reference rotated along the x-axis by a skew angle $\Theta$ such that the beams propagate along the $\tilde{z}$-direction of this new frame. The signal and idler photon beams propagate along the $z$-axis in the original frame of reference. We can express the write and read beams in the un-rotated frame of reference by making the following transformations:

$$\tilde{x} = x \tag{3.99}$$

$$\tilde{y} = y\cos\Theta - z\sin\Theta \tag{3.100}$$

$$\tilde{z} = y\sin\Theta + z\cos\Theta \tag{3.101}$$

Here the coordinates with tilde denote those in the rotated frame expressed in terms of the coordinates in the original frame of reference. With this given transformation, we get the expression for IRE as:

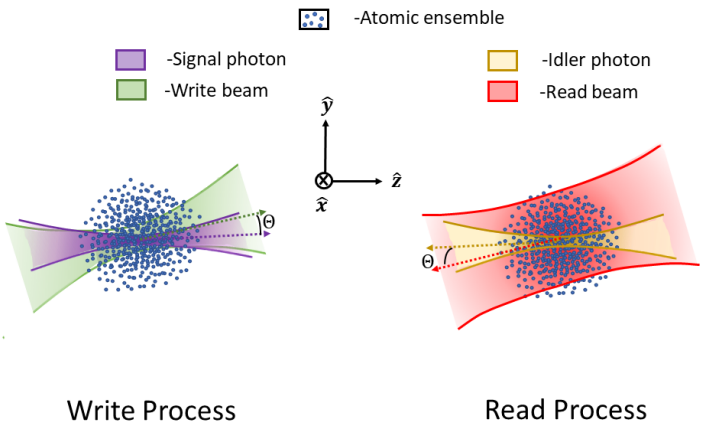


Figure 3.5: Experimental configuration of the write-read process: (1)The write process: The atomic ensemble is first excited with a classical write pulse, and the emitted signal photon is collected by an optical fiber rotated by an angle $\Theta$ with respect to write pulse axis. The centers of the atomic ensemble and both the beams are aligned. The write beam is generally broader than the signal photon collection beam. (2) The read process: After the write process the ensemble is excited with a very broad read beam which is rotated by an angle $\Theta$ with respect to the idler photon collection beam.

$$\Lambda(\mathbf{r}_j,\mathbf{r}'_j) = \frac{(\omega^r+\omega_{sg})}{\sqrt{8\pi^2\gamma_{eg}c^3}}\frac{W_i k^i}{\sqrt{2}}\frac{e^{ik^i z'_j}e^{-ik^s z_j}e^{ik^w(y_j\sin\Theta+z_j\cos\Theta)}e^{-ik^r(y'_j\sin\Theta+z'_j\cos\Theta)}}{\sqrt{1+\frac{z'^2_j}{z_i^2}}\sqrt{1+\frac{z_j^2}{z_s^2}}\sqrt{1+\frac{(y_j\sin\Theta+z_j\cos\Theta)^2}{z_w^2}}}$$
$$\times e^{i(\psi_s(z_j)-\psi_i(z'_j)-\psi_w(y_j\sin\Theta+z_j\cos\Theta)]}e^{-\frac{x'^2_j+y'^2_j}{W_i^2\left(1+\frac{z'^2_j}{z_i^2}\right)}}e^{-\frac{x_j^2+y_j^2}{W_s^2\left(1+\frac{z_j^2}{z_s^2}\right)}}$$
$$\times e^{-\frac{x_j^2+(y_j\cos\Theta-z_j\sin\Theta)^2}{W_w^2\left[1+\frac{(y_j\sin\Theta+z_j\cos\Theta)^2}{z_w^2}\right]}}e^{i\left\{\frac{k^w[x_j^2+(y_j\sin\Theta+z_j\cos\Theta)^2]}{2R_w(y_j\sin\Theta+z_j\cos\Theta)}-\frac{k^s(x_j^2+y_j^2)}{2R_s(z_j)}+\frac{k^i(x'^2_j+y'^2_j)}{2R_i(z'_j)}\right\}} \tag{3.102}$$

Throughout the numerical analysis we will assume a Gaussian distribution of atoms inside a MOT. After the atoms have been cooled by using cyclic cooling and optical gradient cooling, the atomic sample has a standard deviation of 0.75 mm and the temperature of the atomic sample is about tens of $\mu$K. We get a most probable speed $\sqrt{\frac{2k_BT}{M}}$ which is about a few cm/s. For Rb atoms with mass $M = 87\,a.u.$ at the

temperature of $30\,\mu K$, this value is about 7.5 cm/s. For the time duration when the spin wave is stored in the atomic ensemble, atomic motion causes degradation of coherence. We introduce this effect in our calculations by assuming ballistic motion of atoms:

$$\mathbf{r}'_j = \mathbf{r}_j + \mathbf{v}_j T_m \tag{3.103}$$

where $\mathbf{v}_j$ are drawn from a Maxwell-Boltzmann distribution of velocities. Since the atomic density is not very high, we can ignore collisions.

We have neglected the motion of atoms when the write and read pulses interact with the atomic ensemble, since they are short enough to assume that the atoms are stationary for $T_p$ and $T_r$. The expression for $\eta$ with the velocities included can be derived by substituting Eq. (3.103) into Eq. (3.102). From this equation it becomes clear that the decoherence effect for a non-zero storage time is a direct result of the atomic motion.

### 3.4.2 Optical Depth

Let us look at the behaviour of the IRE as a function of the different experimental parameters obtained from a Monte-Carlo sampling of a Gaussian atomic ensemble with spherical symmetry. The range of parameters chosen for all the numerical simulation henceforth have been inspired by experiments reported in Ref. [110]. The atomic samples generated for the numerical simulations have a peak density of the order of $10^{17}$ atoms/m$^3$. An important quantity that captures the strength of interaction between the atomic ensemble and the light is the Optical Depth (OD) of the ensemble. For a given Gaussian density profile the optical depth for a sample of

atoms interacting with Gaussian beams is given by the following expression:

$$OD = \frac{2}{\pi}\int_{-\infty}^{\infty} dz \frac{2\pi c_{CG}^2 \sigma_0}{w_0^2(1+\frac{z^2}{z_w^2})} \int_0^{\infty} r dr n_0 e^{-\frac{r^2+z^2}{2r_0^2}} e^{-\frac{2r^2}{w_0^2(1+\frac{z^2}{z_w^2})}} \tag{3.104}$$

where $w_0$ is the Gaussian beam waist at $z = 0$, $\sigma_0$ the atomic cross-section, $n_0$ the peak atomic density and $r_0$ as the standard deviation of the atomic distribution. $z_w$ is the Rayleigh length for the Gaussian beam given as $k_0 w_0^2/2$ for wave-number $k_0$. $c_{CG}^2$ is the square of the Clebsch-Gordon coefficient associated with the particular atomic transition of interest. We will calculate the optical depth for the interaction with a resonant write-pulse corresponding to the 795nm D1 line in $^{87}$Rb. The cross-section for this transition is $\sigma_0 = 1.082 * 10^{-9}\text{cm}^{-2}$ [40]. For convenience, we set $c_{CG} = 1$. The OD can be scaled with the appropriate value of $c_{CG}$ if necessary.

For all the numerical results presented in Sec. 3.4, we use $\Delta = 2\pi \times 10\text{MHz}$ and $\omega_{sg} = -2\pi \times 6.8\text{GHz}$ for $|g\rangle = |5S_{1/2}, F = 2\rangle$, $|s\rangle = |5S_{1/2}, F = 1\rangle$ and $|e\rangle = |5P_{1/2}, F' = 2\rangle$ as reported in Ref. [110]. The angular wave-function of the idler photon is calculated by sampling the $\theta_k, \phi_k$ dependent part of Eq. (3.86) (without the $g_{eg,\tau}$ term, which is taken to be a constant according to the argument below Eq. (3.87)) and is normalized numerically. Then we calculate its overlap with the normalized Gaussian mode of Eq. (3.89) to get the IRE $\eta$.

### 3.4.3 Intrinsic Retrieval Efficiency: Numerical Results

First, we will look at the ideal case of stationary atoms, implying a storage time $T_m = 0$. The IRE thus evaluated is independent of storage time. In Fig. 3.6, we observe that $\eta$ always remains smaller than unity for the given optical depth OD = 24.7, and different values of skew angle, $\Theta$, as a function of the Width Ratio (WR) between the write-pulse and the optical fiber mode waists:

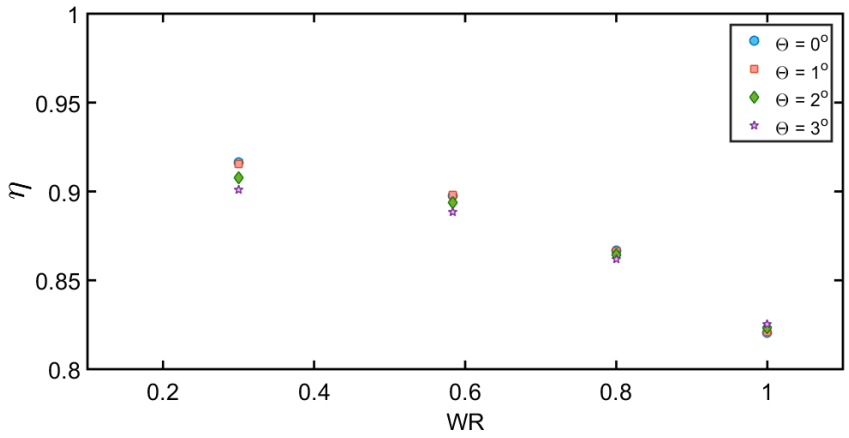


Figure 3.6: Intrinsic retrieval efficiency $\eta$ as a function of the width ratio WR between the waist width of the signal (idler) optical fiber mode over that of the write beam for different values of skew angle.

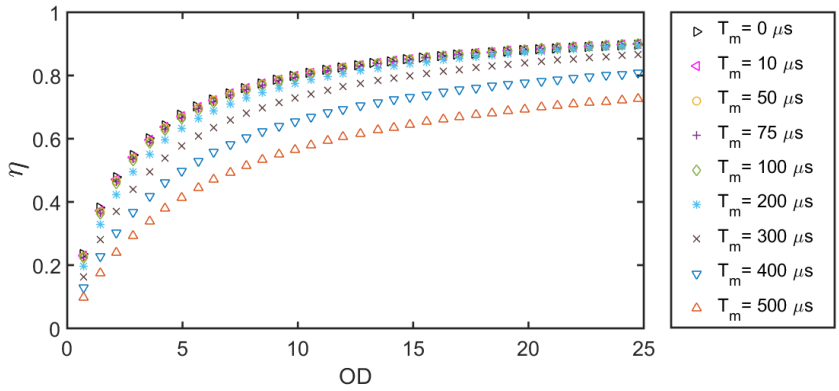


Figure 3.7: The intrinsic retrieval efficiency as a function of the optical depth for increasing memory storage times $T_m$ with skew angle fixed to be 0.

$$WR = \frac{W_i}{W_w} = \frac{W_s}{W_w} \tag{3.105}$$

As we can see, $\eta$ increases with decreasing WR. The reason $\eta$ cannot reach 1 is that there is a mismatch between the photon profile and the optical fiber mode. Fig. 3.7 captures the variation of the IRE as a function of the optical depth of the system for different values of $T_m$ with $\Theta = 0^o$ and WR $= 35\mu$m$/60\mu$m fixed. The OD is adjusted by changing the atomic density while keeping the beam parameters constant.

Now let us look at the effect of non-zero $T_m$ values for skew angle $\Theta = 2^o$ and WR $= 35\mu$m$/60\mu$m which correspond to the experimental value of parameters from

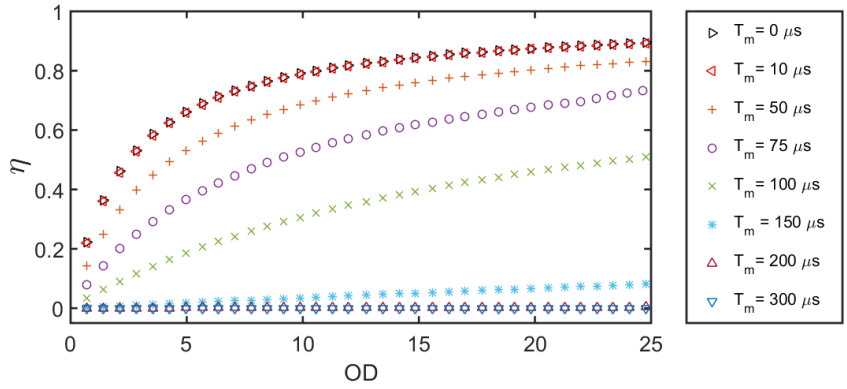


Figure 3.8: The intrinsic retrieval efficiency as a function of optical depth for increasing storage times $T_m$ with skew angle $\Theta = 2^o$

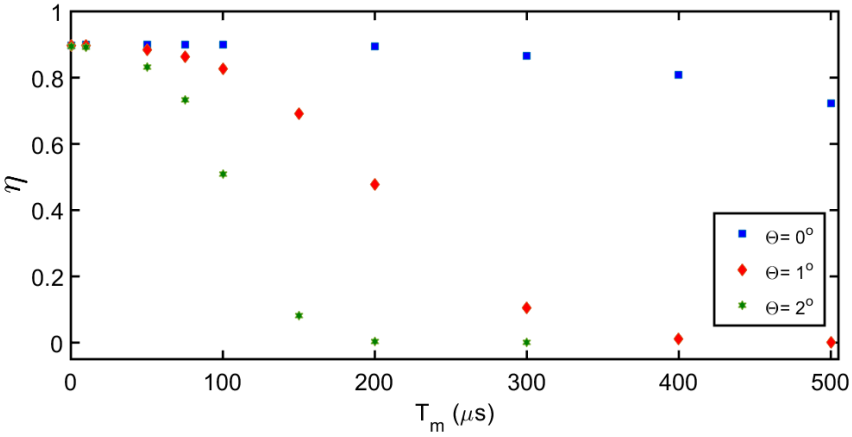


Figure 3.9: Intrinsic retrieval efficiency as a function of memory storage time: At optical depth = 24.7, intrinsic retrieval efficiency varies as a function of the memory storage time $T_m$ for skew angle values $\Theta = (0^o, 1^o, 2^o)$

the Tsinghua setup [110]. Fig. 3.8 shows the variation of the IRE as a function of OD for different values of $T_m$ at $\Theta = 2^o$. Comparing Fig. 3.7 for $\Theta = 0^o$ and Fig. 3.8 for $\Theta = 2^o$, we see the effect of decoherence due to misalignment between the write-read and the signal-idler electric fields. The IRE falls from 80% for $T_m = 0\,\mu s$ to 50 % for $T_m = 100\,\mu s$ when skew angle is $2^o$ for OD of 24.7 compared to no noticeable change in the $\eta$ value (90%) for $T_m$ increasing from 0 to $100\,\mu s$ when skew angle is set to $0^o$. The variation in the IRE for different skew angles and memory storage times at a fixed OD = 24.7 are shown in Fig. 3.9. We see a rapid decrease in the IRE for non-zero skew angles as the memory storage time is increased. For a

retrieval efficiency larger than 80% we can store the atomic spin wave for a maximum of 50 $\mu s$ with $\Theta = 2^o$ which is not sufficient for implementation of DLCZ quantum repeater protocol efficiently. An important point that must be mentioned here is that the IRE can be increased by using optical traps for the atomic ensemble which restrict the atomic motion and hence help reduce atomic motion induced decoherence, though even after the implementation of such traps, it is still not possible to reach unit retrieval efficiency. Our current theoretical model can be extended to include the effects of optical traps by changing the expression for the atomic positions in Eq. (3.103) appropriately.

### 3.4.4 The mode profile of the emitted read photon

Let us now focus on the angular mode profile of the emitted idler photon. As was briefly described in Sec. 1.2.2, because of the collective enhancement due to the atoms in the ensemble, the idler photon that is emitted is highly directional. We see the signature of collective enhancement as has been proved in [47] in our numerical results. The output photon mode that is correlated with the atomic spin wave has higher fractional contribution along the $\theta_k = \pi$ direction which increases as the number of atoms goes up. The normalized angular mode $\hat{f}^r(\theta_k, \phi_k)$ for the idler photon obtained for a dense atomic ensemble is shown in Fig. 3.10 for $T_m = 0$ and $\Theta = 0^o$. This angular profile for an atomic sample with OD = 24.7 and for WR = 35/60 gives about 90% IRE.

The real part of the angular mode profile, in the absence of decoherence effects due to non-zero $T_m$ and $\Theta$, is plotted in Fig. 3.10a. It clearly shows a pronounced emission peak near angle $\theta_k = \pi$ (shown in the inset) for all azimuthal angles. Apart from the emission around the $\theta_k = \pi$ direction, there are noisy contributions present along all other directions as well. The idler photon mode profile has contributions that are prominently from the real part as expected. Without any atomic density

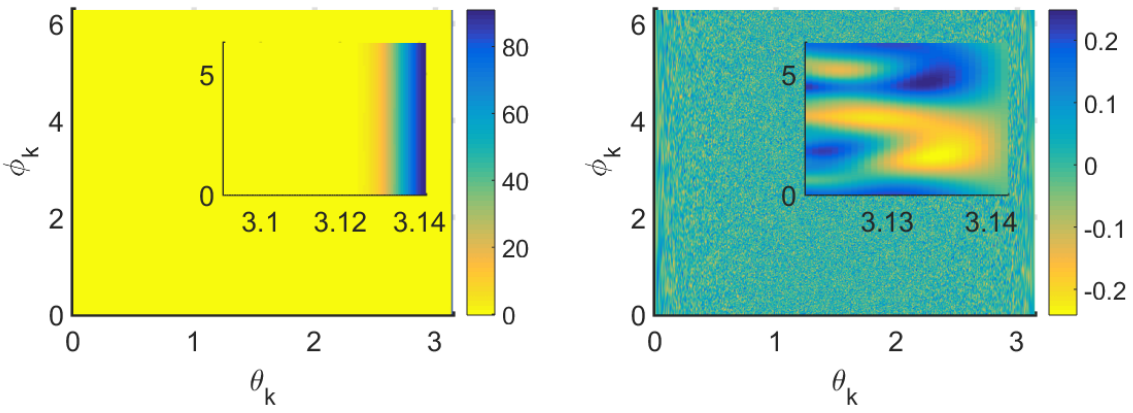


(a) Re[ $f^r(\theta_k, \phi_k)$] (b) Im[$f^r(\theta_k, \phi_k)$]

Figure 3.10: The normalized angular mode function, $f^r(\theta_k, \phi_k)$, at OD = 24.7, $\Theta = 0^o$, WR = 35/60 and $T_m = 0\,\mu$s.

fluctuations, that is, replacing the summation over atoms in Eq. (3.86) with a continuous integration, the imaginary part of the mode function would be identically zero. Thus, imaginary part of the angular profile gives us a scale of fluctuations in all the directions. These fluctuations are related to the density fluctuations of the atomic sample. Important feature to note is that the scale of these fluctuations is very small compared to the scale of the enhanced photon emission to be collected. It is a function of OD and $\Theta$; with decreasing OD and increasing skew angle, we see the relative contributions of the fluctuations in all directions go up. There is a limit to increasing the optical depth by raising the atomic density because the low atomic density assumption would then breakdown and effects of atom-atom interactions mediated by light will have to be considered [46].

Let us also look at the angular profile for non-zero skew angles and memory storage times. Specifically, we choose a configuration of parameters that gives around $\eta = 80\%$, particularly, $\Theta = 1^o$ and $T_m = 100\,\mu s$ [Fig. 3.11] and compare it with a value of $\eta = 0.3\%$ for $\Theta = 2^o$ and $T_m = 200\,\mu s$ [Fig. 3.12].

We see that Fig. 3.11a shows a prominent contribution around $\theta_k = \pi$. On close observation, as shown in the inset, we can detect slight variation in the transverse

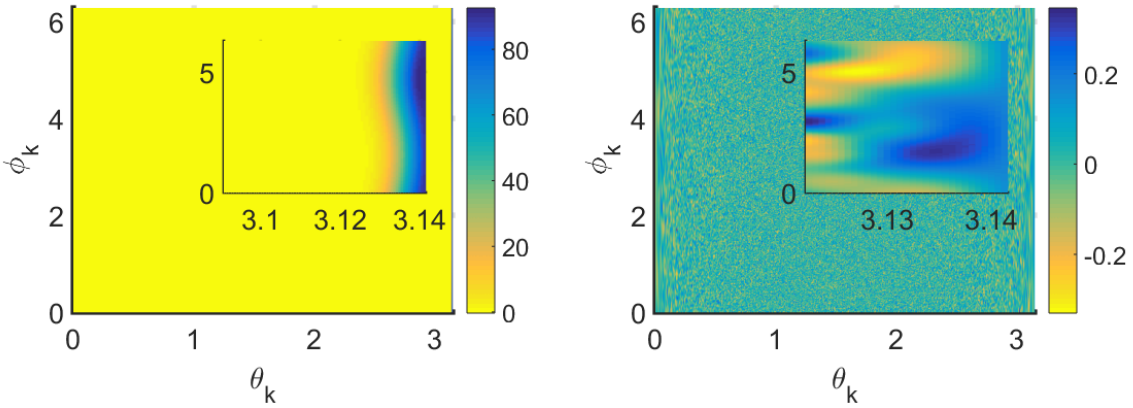


(a) Re$[f^r(\theta_k, \phi_k)]$ (b) Im$[f^r(\theta_k, \phi_k)]$

Figure 3.11: The normalized angular mode function, $f^r(\theta_k, \phi_k)$, at OD $= 24.7$, $\Theta = 1^o$, WR $= 35/60$ and $T_m = 100\,\mu s$.

profile along the $\phi_k$ direction for $\theta_k \approx \pi$, which becomes more pronounced with larger skew angle and longer storage time in Fig. 3.12a. The $\theta_k$ and $\phi_k$ dependence of the observed mode profiles can be attributed to the disruption of symmetry in the z-direction due to non-zero skew angle. As already mentioned, the imaginary part of the mode profile gives an insight about the fluctuations present in all the directions that do not have overlap with the optical fiber electric field. These fluctuations are present in the real part as well, but get washed out by the dominant contribution of the idler photon. Fluctuations in the mode profile are also caused by the atomic density fluctuations in the sample. The fluctuations observed in Fig. 3.11b are of the same order as those observed in Fig. 3.10b. In Fig. 3.12a we see higher contribution to the mode profile from all values of $\theta_k$ and $\phi_k$ when compared to Fig. 3.10a and Fig. 3.11a, and the fluctuations are significantly higher as seen from Fig. 3.12b. With this we conclude the discussion of the numerical results.

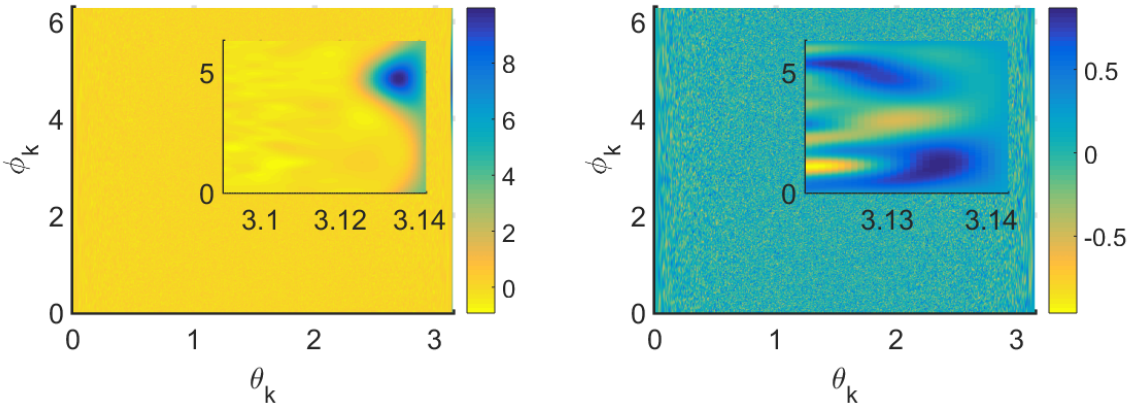


(a) Re$[f^r(\theta_k, \phi_k)]$ (b) Im$[f^r(\theta_k, \phi_k)]$

Figure 3.12: The normalized angular mode function, $f^r(\theta_k, \phi_k)$, at OD $= 24.7$, $\Theta = 2^o$, WR $= 35/60$ and $T_m = 200\,\mu s$.

## 3.5 Chapter Summary

We have formulated a three-dimensional theory to study the intrinsic retrieval efficiency (IRE) during the write-read process for quantum repeater protocols. The focus of this calculation was to describe the quantum mechanical process involved in the interaction of the atomic ensemble with the control light pulses in a three-level $\Lambda$ system. The motivation for this work was primarily to understand the factors that influence the IRE which plays a crucial role in the success of quantum repeater protocols like DLCZ method and its variants [114].

Different interaction strengths involved in the write process and read process were looked at separately. The quantum state obtained by perturbative analysis in the write process provides us with the initial condition for the quantum evolution during the read process. An important result obtained from this calculation is the expression of the IRE as a function of the parameters of the atomic ensemble and control pulses. We show that unit retrieval efficiency is not possible for realistic experimental parameters. We also show the effects of decoherence introduced due to atomic motion in the sample, which drastically reduce $\eta$ for the skewed configuration of atomic beams.

Neglecting the atomic motion for the duration of write and read pulses, within which the accumulated phase is small, only the change in atomic positions during the storage period contributes to the decoherence. In general, for ballistic motion of atoms in the absence of collisions, the average separation between atoms increases with time and the IRE decreases. This can be corrected by using atomic traps which limit the atomic motion. On average the atomic separations with increasing storage times are constant in atomic traps thus improving the atomic retrieval efficiency [72, 117].

Some parts of the contents of this chapter have overlap with previously published material [123].

# CHAPTER IV

# Conclusion and Future Directions

## 4.1 Summary

In this dissertation we have explored many concepts centered around the central idea of light-matter interactions for applications of quantum communication and quantum information science. This dissertation was an attempt to add a drop in the vast ocean of applications that have been made possible because of decades of research into the quantum nature of collective matter interacting with optical fields. We have looked at two applications of these systems: for creation of highly entangled quantum states and as a means for entanglement distribution.

To summarize, in the first chapter of this dissertation, we introduced a few basic but important concepts that lay the foundation for the rest of the chapters. In particular we discussed the two different ways of modelling light interacting with an atom. In both cases the atom is treated quantum mechanically, where as light could be treated classically or quantum mechanically. In situations where the number of relevant photons is of the order or less compared to the number of atoms, we must use a quantum mechanical description of light. We also studied the importance of collective properties in an ensemble of atoms as opposed to a single atom system. From an applications point of view, we discussed the idea of a quantum network and the different ways in which neutral atom ensembles play a pivotal role in many of the

protocols for quantum communication.

In Chapter II, we focused on the first of the two applications of ensembles of neutral atoms interacting with optical fields for the creation of highly entangled multi-particle Greenberger-Horne-Zeilinger (GHZ) states. Rydberg blockade mechanism in conjugation with Stimulated Raman Adiabatic Passage was used to enable one step generation of GHZ states in a target ensemble with the help of a control atom. A thorough analysis of the adiabatic conditions required to facilitate the STIRAP process in an ensemble of target atoms was presented. The novel feature of this scheme is that it is robust to spontaneous emission losses from the excited Rydberg levels of the target ensemble. We numerically showed that it is possible to generate multi-particle GHZ states with high fidelity using this scheme.

In Chapter III, the second part of the dissertation, the properties of quantum interfaces made from neutral atom ensembles were studied. Neutral atom ensembles form important quantum nodes in quantum repeater protocols to facilitate long distance entanglement distribution. We provided a detailed derivation of the write and read process that facilities storage of information carrying photon as an atomic spin wave and its release back to a photon. In particular, we derived the expression of the intrinsic retrieval efficiency (IRE) which is a measure of the efficiency of the write and read process in three dimensions. High values of IRE are crucial for the success of quantum repeaters and we numerically showed that unit efficiency for IRE cannot be achieved for realistic experimental parameters.

## 4.2 Outlook

Based on the discussion of the topics in this dissertation and the existing literature, we can find several directions for expansion of the current work in the future.

In this dissertation, we have assumed that the density of atomic ensembles is such that any two ground state atoms have negligible interactions between them. This

assumption gets violated when the optical depth of the ensemble is kept on increasing by increasing the atomic density [46, 124, 125]. This is the regime where phenomena like super-radiance can be realized. The three dimensional theory of atomic quantum interfaces can be extended with addition of atom-atom interactions, to study the effect of extremely dense atomic samples on the intrinsic retrieval efficiency. The dynamics of Rydberg blockade are also expected to change when the Rydberg atoms are excited to higher Rydberg levels as the size of the atom gets larger. Electrons excited to high lying Rydberg levels can get scattered by neighbouring ground state atoms because of the enormous size of the Rydberg atoms.

A lot of experimental progress has been made in the field of Rydberg atom physics in terms of storage and manipulation of Rydberg atoms [126–129]. Similarly, Stimulated Adiabatic Raman Transition in a single atom is extremely well studied and one of the most robust ways of population transfer [89]. Testing the experimental feasibility of the proposed GHZ state generation scheme could be made possible by combining the techniques from these two approaches. Experimental validation of the theoretical scheme for GHZ state generation presented here would be an important next step. To assist in the experimental realization of this scheme, the impact of atomic motion generated in the experimental systems could be incorporated.

As already discussed in this dissertation, neutral atom ensembles provide a versatile platform for the development of quantum networks. There are many aspects of these systems that need to be studied further. Proposals for storage of multiple spin-wave modes in the same atomic ensemble have been implemented [110]. A complete theoretical analysis of how many such modes can be simultaneously stored can be performed and the sources of decoherence and mixing between nodes can be explored. Novel ways of constructing optical lattices can be studied where in atomic positions are engineered to optimize the multi-atom interference effects to give higher values of intrinsic retrieval efficiency.

In this dissertation we have described atoms with two levels and three levels, especially the lambda three level configuration. Atomic ensembles modelled as four level systems or more show many interesting properties and are at the same time more complex to handle [89, 130, 131]. The collective properties of ensembles with such a structure may offer surprising and subtle ways of fabricating quantum optical systems for myriad applications. Many exciting experiments are already in progress in the fields of quantum optics, quantum simulation, chemistry which exploit the novel properties of Rydberg-Rydberg interactions. Recent progress made in the studies of many-body physics using Rydberg atoms to study phase transitions is particularly exciting [132–134]. For the field of quantum computation and communication, there are many exciting proposals that suggest the use of integrated architecture employing multiple quantum systems for example co-planar waveguides and atomic ensembles with Rydberg interactions could potentially lead to optical storage devices with long memories and hence efficient optical interfaces [135–137].

# APPENDICES

# APPENDIX A

# Derivation of the Eigenvalue Structure

The Hamiltonian of the target ensemble atoms is given in Eq. A.1.

$$\frac{H_T(t)}{\hbar} = \delta\sigma_r^+\sigma_r^- + \big[\frac{\Omega_g^*(t)}{2}a_g^\dagger\sigma_r^- + \frac{\Omega_s^*(t)}{2}a_s^\dagger\sigma_r^- + \text{h.c.}\big] \tag{A.1}$$

By using the substitutions given below:

$$\Omega_0(t) = \sqrt{\Omega_g^2(t) + \Omega_s^2(t)} \tag{A.2}$$

$$\tan\theta(t) = \frac{\Omega_g(t)}{\Omega_s(t)} \tag{A.3}$$

$$\tan\phi(t) = \frac{\Omega_0(t)}{\delta} \tag{A.4}$$

We can write the Hamiltonian as a block matrix in the basis given in Eq. (2.24) for N atoms

$$H_T(t) = \frac{\hbar\Omega_0(t)}{2}\begin{bmatrix} A & B \\ C & D \end{bmatrix} \tag{A.5}$$

Where $A$ is a zero square matrix of dimensions $N+1$, $D$ is an $N$ dimensional identity

matrix with co-efficient $2\cot\phi(t)$ and $C = B^\dagger$ where:

$$B = \begin{bmatrix} \sqrt{N}\sin\theta(t) & 0 & \dots & 0 \\ \cos\theta(t) & \sqrt{N-1}\sin\theta(t) & \dots & 0 \\ 0 & \sqrt{2}\cos\theta(t) & \dots & 0 \\ \vdots & \vdots & \dots & \vdots \\ 0 & 0 & \dots & \sqrt{N}\cos\theta(t) \end{bmatrix} \tag{A.6}$$

Let $\lambda$ be the eigenvalues of the Hamiltonian which can be obtained by solving the equation below:

$$\det(H_T - \lambda\mathbb{I}_{2N+1}) = 0 \tag{A.7}$$

For a matrix that has structure given in Eq. (A.5), the solution of Eq. (A.7) is (ref):

$$\det(H_T - \lambda\mathbb{I}_{2N+1}) = 0 \tag{A.8}$$

$$\implies \det(\frac{\hbar\Omega_0}{2}D - \lambda\mathbb{I}_N)\det\big[(\frac{\hbar\Omega_0}{2}A - \lambda\mathbb{I}_{N+1}) - \frac{\hbar^2\Omega_0^2}{4}B(\frac{\hbar\Omega_0}{2}D - \lambda\mathbb{I}_N)^{-1}B^\dagger\big] = 0 \tag{A.9}$$

To make sure that we do not have a singular matrix, $\lambda \neq \hbar\Omega_0\cot\phi$. Using the fact that $A$ is a zero matrix, we can thus rewrite Eq. (A.9) as:

$$\det(-\lambda\mathbb{I}_{N+1} - \frac{\hbar^2\Omega_0^2}{4}\frac{1}{(\hbar\Omega_0\cot\phi - \lambda)}BB^\dagger) = 0 \tag{A.10}$$

Notice that the characteristic equation given above remains invariant under the transformation of $\lambda \to -\lambda$ and $\delta \to -\delta$. Let us redefine:

$$\alpha = \frac{-4\lambda(\hbar\Omega_0\cot\phi - \lambda)}{\hbar^2\Omega_0^2} \tag{A.11}$$

Thus, from Eqs. (A.10)-(A.11), we get:

$$\det(BB^\dagger - \alpha \mathbb{I}_{N+1}) = 0 \tag{A.12}$$

The matrix $BB^\dagger$ is a tridiagonal matrix given below:

$$BB^\dagger = \begin{bmatrix} N\sin^2\theta & \sqrt{N}\sin\theta\cos\theta & 0 & \dots & 0 \\ \sqrt{N}\sin\theta\cos\theta & (N-1)\sin^2\theta+\cos^2\theta & \sqrt{N-1}\sin\theta\sqrt{2}\cos\theta & \dots & 0 \\ 0 & \sqrt{N-1}\sin\theta\sqrt{2}\cos\theta & (N-1)\sin^2\theta+\cos^2\theta & \dots & 0 \\ \vdots & \vdots & \ddots & \dots & \vdots \\ 0 & 0 & 0 & \dots & N\cos^2\theta \end{bmatrix} \tag{A.13}$$

Eq. (A.12) is the eigenvalue equation for matrix $BB^\dagger$. On solving for eigenvalues of $BB^\dagger$ we get:

$$\alpha = 0, 1, 2, ..., N \tag{A.14}$$

Substituting $\alpha$ in Eq. (A.11), we see that one of the eigenvalues of the Hamiltonian is always zero independent of the number of atoms. Rest of the $2N$ eigenvalues are given by solving Eq. (A.15)

$$\lambda^2 - \hbar\Omega_0 \cot\phi\lambda - \frac{\hbar^2\Omega_0^2}{4}\alpha = 0,\ \alpha = 1, 2, .., N \tag{A.15}$$

On solving the quadratic equation above, we get:

$$\lambda_{\pm\alpha} = \frac{\hbar\Omega_0}{2}\left[\cot\phi \pm \sqrt{\cot^2\phi + \alpha}\right] \tag{A.16}$$

For, $\delta = 0$ i.e. $\cot\phi = 0$, we get a ladder of symmetrically placed eigenvalues around

the eigenvalue 0.

# APPENDIX B

# Simplification of System of Rate Equations

Here we present a derivation from Eqs. (3.60-3.62) to Eqs. (3.64, 3.65) in the main text.

First we substitute $A_j(t)$ as given in Eq. (3.63) into the rate Eqs. (3.60-3.62) and get

$$i\dot{\alpha}_j(t) = \omega_{sg}\alpha_j(t) + \Omega^r_{es,j}(t)B_j(t) \tag{B.1}$$

$$\begin{aligned} i\dot{B}_j(t) &= \omega_{sg}B_j(t) + \Omega^r_{es,j}(t)\alpha_j(t) \\ &+ \sum_\tau \int \frac{d^3\mathbf{k}}{(2\pi)^3} g_{eg,\tau}(\mathbf{k}) e^{i[\mathbf{k}\cdot\mathbf{r}'_j - (\omega_k - \omega^r)t]} C_\tau(\mathbf{k},t) \end{aligned} \tag{B.2}$$

$$i\dot{C}_\tau(\mathbf{k},t) = \sum_j g^*_{eg,\tau}(\mathbf{k}) e^{-i[\mathbf{k}\cdot\mathbf{r}'_j - (\omega_k - \omega^r)t]} B_j(t) \tag{B.3}$$

Formally integrating Eq. (B.3) with $C_\tau(\mathbf{k}, T_p) = 0$ we get:

$$C_\tau(\mathbf{k},t) \;=\; -i\sum_j \int_{T_p}^{t} dt' g^*_{eg,\tau}(\mathbf{k}) e^{-i[\mathbf{k}\cdot\mathbf{r}'_j - (\omega_k - \omega^r)t']} B_j(t') \tag{B.4}$$

Plugging the above equation into Eq. (B.2), we get:

$$
\begin{aligned}
i\dot{\alpha}_j(t) &= \omega_{sg}\alpha_j(t) + \Omega^r_{es,j}(t)B_j(t) && \text{(B.5)}\\
i\dot{B}_j(t) &= \omega_{sg}B_j(t) + \Omega^r_{es,j}(t)\alpha_j(t) \\
&- i\sum_{l,\tau}\int \frac{d^3\mathbf{k}}{(2\pi)^3}|g_{eg,\tau}(\mathbf{k})|^2 e^{i\mathbf{k}\cdot(\mathbf{r}'_j-\mathbf{r}'_l)} \\
&\times \int_{T_p}^{t} dt' e^{-i(\omega_k-\omega^r)(t-t')}B_l(t') && \text{(B.6)}
\end{aligned}
$$

Then by making a further substitution

$$
\begin{aligned}
\tilde{B}_j(t) &= B_j(t)e^{i\omega_{sg}t} && \text{(B.7)}\\
\tilde{\alpha}_j(t) &= \alpha_j(t)e^{i\omega_{sg}t} && \text{(B.8)}
\end{aligned}
$$

we get

$$
\begin{aligned}
\dot{\tilde{\alpha}}_j &= -i\Omega^r_{es,j}(t)\tilde{B}_j(t) && \text{(B.9)}\\
\dot{\tilde{B}}_j(t) &= -i\Omega^r_{es,j}(t)\tilde{\alpha}_j(t) - \int_{T_p}^{t} dt' I_j(t,t') && \text{(B.10)}
\end{aligned}
$$

where

$$
I_j(t,t') = I^{(1)}_j(t,t') + I^{(2)}_j(t,t') \qquad \text{(B.11)}
$$

with:

$$
I^{(1)}_j(t,t') = \sum_{\tau}\int \frac{d^3\mathbf{k}}{(2\pi)^3}|g_{eg,\tau}(\mathbf{k})|^2 e^{-i(\omega_k-\omega^r-\omega_{sg})(t-t')}\tilde{B}_j(t') \qquad \text{(B.12)}
$$

$$
\begin{aligned}
I_j^{(2)}(t,t') &= \sum_{\tau}\sum_{l=1,l\neq j}^{N_a}\int \frac{d^3\mathbf{k}}{(2\pi)^3}|g_{eg,\tau}(\mathbf{k})|^2 e^{i\mathbf{k}\cdot(\mathbf{r}'_j-\mathbf{r}'_l)} \\
&\quad e^{-i(\omega_k-\omega^r-\omega_{sg})(t-t')}\tilde{B}_l(t') \qquad \text{(B.13)} \\
&= \sum_{\tau}\sum_{l=1,l\neq j}^{N_a}\int \frac{d^3\mathbf{k}}{(2\pi)^3}\frac{\omega_k}{2\varepsilon_0}|\mathbf{d}_{eg}\cdot\hat{\epsilon}_{\mathbf{k},\tau}|^2 e^{i\mathbf{k}\cdot(\mathbf{r}'_j-\mathbf{r}'_l)} \\
&\quad e^{-i(\omega_k-\omega^r-\omega_{sg})(t-t')}\tilde{B}_l(t') \qquad \text{(B.14)} \\
&= \sum_{l=1,l\neq j}^{N_a}\int \frac{d^3\mathbf{k}}{(2\pi)^3}\frac{\omega_k}{2\varepsilon_0}\mathbf{d}_{eg}\cdot[I-\hat{\mathbf{k}}\hat{\mathbf{k}}]\cdot\mathbf{d}^*_{eg} \\
&\quad e^{i\mathbf{k}\cdot(\mathbf{r}'_j-\mathbf{r}'_l)}e^{-i(\omega_k-\omega^r-\omega_{sg})(t-t')}\tilde{B}_l(t') \qquad \text{(B.15)} \\
&= \sum_{l=1,l\neq j}^{N_a}\int_0^{\infty}\frac{dkk^3c}{16\pi^3\varepsilon_0}\int d\Omega_k\mathbf{d}_{eg}\cdot[I-\hat{\mathbf{k}}\hat{\mathbf{k}}]\cdot\mathbf{d}^*_{eg} \\
&\quad e^{i\mathbf{k}\cdot(\mathbf{r}'_j-\mathbf{r}'_l)}e^{-i(kc-\omega^r-\omega_{sg})(t-t')}\tilde{B}_l(t') \qquad \text{(B.16)} \\
&= \sum_{l=1,l\neq j}^{N_a}\int_0^{\infty}\frac{dkk^3c}{4\pi^2\varepsilon_0}e^{-i(kc-\omega^r-\omega_{sg})(t-t')}\tilde{B}_l(t') \\
&\quad \left\{\mathbf{d}_{eg}\cdot\left[I-\frac{\mathbf{r}_{jl}\mathbf{r}_{jl}}{|\mathbf{r}_{jl}|^2}\right]\cdot\mathbf{d}^*_{eg}\ j_0(k|\mathbf{r}_{jl}|)\right. \\
&\quad \left.-\mathbf{d}_{eg}\cdot\left[I-3\frac{\mathbf{r}_{jl}\mathbf{r}_{jl}}{|\mathbf{r}_{jl}|^2}\right]\cdot\mathbf{d}^*_{eg}\frac{j_1(k|\mathbf{r}_{jl}|)}{k|\mathbf{r}_{jl}|}\right\} \qquad \text{(B.17)}
\end{aligned}
$$

where we have defined:

$$
\mathbf{r}_{jl} = \mathbf{r}'_j - \mathbf{r}'_l \qquad \text{(B.18)}
$$

In Eq. (B.17), $j_0(x)$ and $j_1(x)$ are spherical Bessel functions of the first kind. As we can see, $I_j^{(2)}(t,t')$ consists of terms with $l \neq j$, which corresponds to atom-atom interactions induced by the quantized electric field. In other words, such terms describe one atom absorbing the emitted photon field from another atom. For ex-

perimental atomic densities of interest, the average number of atoms separated by a distance of about a $\lambda = 2\pi c/\omega^r$ is less than 1. For such low densities we can ignore the re-absorption terms from our calculations, keeping only the terms where $j = l$ in Eq. (B.11). Then

$$
\begin{aligned}
I_j(t,t') &= I_j^{(1)}(t,t') && \text{(B.19)}\\
&= \int_0^\infty d\omega \frac{\omega^3}{6\pi^2\varepsilon_0 c^3}|\mathbf{d}_{eg}|^2 e^{-i(\omega-\omega^r-\omega_{sg})(t-t')}\tilde{B}_j(t') && \text{(B.20)}\\
&= \frac{(\omega^r+\omega_{sg})^3|\mathbf{d}_{eg}|^2}{6\pi^2\varepsilon_0 c^3} 2\pi\delta(t-t')\tilde{B}_j(t') && \text{(B.21)}\\
&\equiv \Gamma_{eg}\delta(t-t')\tilde{B}_j(t') && \text{(B.22)}
\end{aligned}
$$

In the above derivation we used the Wigner-Weisskopf approximation [24], and $\Gamma_{eg}$ is the rate of spontaneous emission from $|e\rangle$ to $|g\rangle$. Substituting Eq. (B.22) into Eq. (B.10) we get

$$
\begin{aligned}
\dot{\tilde{\alpha}}_j(t) &= -i\Omega^r_{es,j}(t)\tilde{B}_j(t) && \text{(B.23)}\\
\dot{\tilde{B}}_j(t) &= -i\Omega^r_{es,j}(t)\tilde{\alpha}_j(t) - \gamma_{eg}\tilde{B}_j(t) && \text{(B.24)}
\end{aligned}
$$

where $\gamma_{eg} = \Gamma_{eg}/2$. They are just Eqs. (3.64) and (3.65) in the main text.

# BIBLIOGRAPHY

# BIBLIOGRAPHY


[1] J. N. Tinsley, M. I. Molodtsov, R. Prevedel, D. Wartmann, J. Espigule-Pons, M. Lauwers, and A. Vaziri. Direct detection of a single photon by humans. *Nat. Commun.*, 7(12172), 2016.

[2] N. Bohr. The spectra of helium and hydrogen. *Nature*, 92:231232, 1913.

[3] N. Bohr. On the constitution of atoms and molecules. *Philosophical Magazine*, 26(6), 1913.

[4] W. E. Lamb Jr. and R. C. Retherford. Fine structure of the hydrogen atom by a microwave method. *Phys. Rev.*, 72, 1947.

[5] M. O. Scully and M. S. Zubairy. *Quantum Optics*. Cambridge University Press, 1997.

[6] M. Planck. über das gesetz der energieverteilung im normalspektrum (on the law of distribution of energy in the normal spectrum). *Ann. Phys.*, 4(3), 1901.

[7] A. Einstein. über einen die erzeugung und verwandlung des lichtes betreffenden heuristischen gesichtspunkt (concerning an heuristic point of view toward the emission and transformation of light). *Ann. Phys.*, 17(32), 1905.

[8] N. Bohr. Rydberg's discovery of the spectral laws. In J. Kalckar, editor, *N. Bohr: Collected Works*, chapter 10, pages 373–379. North-Holland Publ., Amsterdam, 1954.

[9] A. Einstein. Zur quantentheorie der strahlung. *Phys Z.*, 18(121), 1917.

[10] M. Bertolotti. *Masers and Lasers: An Historical Approach, Second Edition*. CRC Press, 2015.

[11] T. H. Maiman. Stimulated optical radiation in ruby. *Nature*, 187, 1960.

[12] D. F. Walls. Squeezed states of light. *Nature*, 206, 1983.

[13] U. L. Andersen, T. Gehring, C. Marquardt, and G. Leuchs. 30 years of squeezed light generation. *Phys. Scr.*, 91(5), 2016.

[14] Edo Waks, Eleni Diamanti, and Yoshihisa Yamamoto. Generation of photon number states. *New J. Phys.*, 8(4), 2006.

[15] M. H. Anderson, J. R. Ensher, M. R. Matthews, C. E. Wieman, and E. A. Cornell. Observation of bose-einstein condensation in a dilute atomic vapor. *Science*, 269(5221), 1995.

[16] C. E. Wieman, D. E. Pritchard, and D. J. Wineland. Atom cooling, trapping, and quantum manipulation. *Rev. Mod. Phys.*, 71(s253), 1999.

[17] A. M. Kaufman, B. J. Lester, and C. A. Regal. Cooling a single atom in an optical tweezer to its quantum ground state. *Phys. Rev. X*, 2(041014), 2012.

[18] V. Bendkowsky, B. Butscher, J. Nipper, J. P. Shaffer, R. Löw, and T. Pfau. Observation of ultralong-range rydberg molecules. *Nature*, 458, 2009.

[19] J. G. Ren, P. Xu, H. L. Yong, L. Zhang, S. K. Liao, J. Yin, W. Y. Liu, W. Q. Cai, M. Yang, L. Li, K. X. Yang, X. Han, Y. Q. Yao, J. Li, H. Y. Wu, S. Wan, L. Liu, D. Q. Liu, Y. W. Kuang, Z. P. He, P. Shang, C. Guo, R. H. Zheng, K. Tian, Z. C. Zhu, N. L. Liu, C. Y. Lu, R. Shu, Y. A. Chen, C. Z. Peng, J. Y. Wang, and J. W. Pan. Ground-to-satellite quantum teleportation. *Nature*, 549, 2017.

[20] D. Bouwmeester, J.-W. Pan, K. Mattle, M. Eibl, H. Weinfurter, and A. Zeilinger. Experimental quantum teleportation. *Nature*, 390:575–579, 1997.

[21] C. H. Bennett, G. Brassard, C. Crepeau, R. Jozsa, A. Peres, and W. K. Wootters. Teleporting an unknown quantum state via dual classical and einstein-podolsky-rosen channels. *Phys. Rev. Lett.*, 70(1895), 1993.

[22] *Quantum cryptography: Public key distribution and coin tossing*, volume 175. New York, 1984.

[23] U. Vazirani and T. Vidick. Fully device-independent quantum key distribution. *Phys. Rev. Lett.*, 113(140501), 2012.

[24] P. R. Berman and V. S. Malinovsky. *Principles of Laser Spectroscopy and Quantum Optics*. Princeton University Press, Princeton, NJ, 2010.

[25] D. A. Steck. Quantum and atom optics. `http://steck.us/teaching`, 2015.

[26] L. Mandel and E. Wolf. *Optical Coherence and Quantum Optics*. Cambridge University Press, 1995.

[27] C. Cohen-Tannoudji, J. Dupont-Roc, and G. Grynberg. *Photons and Atoms Introduction to Quantum Electrodynamics*. Wiley-Interscience, New York, 1989.

[28] P. A. M. Dirac. *Lectures on Quantum Mechanics*. Yeshiva University Belfer Graduate School of Science, 1964.

[29] M. Peskin and D. Schroeder. *An introduction to quantum field theory*. Avalon Publishing, 1995.

[30] W. R. Hindmarsh, editor. *Calculation of the natural line width on the basis of Diracs theory of light*, London, 1967. Pergamon Press.

[31] P. Farrera, G. Heinze, B. Albrecht, M. Ho, M. Chavez, C. Teo, N. Sangouard, and H. de Riedmatten. Generation of single photons with highly tunable wave shape from a cold atomic ensemble. *Nat. Commun.*, 7(13556), 2016.

[32] M. Saffman and T. G. Walker. Creating single-atom and single-photon sources from entangled atomic ensembles. *Phys. Rev. A*, 66(065403), 2002.

[33] I. I. Beterov, M. Saffman, E. A. Yakshina, V. P. Zhukov, D. B. Tretyakov, V. M. Entin, I. I. Ryabtsev, C. W. Mansell, C. MacCormick, S. Bergamini, and M. P. Fedoruk. Quantum gates in mesoscopic atomic ensembles based on adiabatic passage and rydberg blockade. *Phys. Rev. A*, 88(010303(R)), 2013.

[34] C. Monroe. Quantum information processing with atoms and photons. *Nature*, 416:238246, 2002.

[35] H. Yan, G. Yang, T. Shi, J. Wang, and M. Zhan. Quantum gates with atomic ensembles on an atom chip. *Phys. Rev. A*, 78(034304), 2008.

[36] L.M. Duan, M.D. Lukin, J.I. Cirac, and P. Zoller. Long-distance quantum communication with atomic ensembles and linear optics. *Nature*, (414), 2001.

[37] J. Nunn, K. Reim, K. C. Lee, V. O. Lorenz, B. J. Sussman, I. A. Walmsle, and D. Jaksch. Multimode memories in atomic ensembles. *Phys. Rev. Lett.*, 101(260502), 2008.

[38] Markus K. Oberthaler Roman Schmied Luca Pezz, Augusto Smerzi and Philipp Treutlein. Quantum metrology with nonclassical states of atomic ensembles. *Rev. Mod. Phys.*, 90(035005), 2018.

[39] A. Kuzmich, N. P. Bigelow, and L. Mandel. Atomic quantum non-demolition measurements and squeezing. *EPL*, 42(5), 1998.

[40] D.A.Steck. Rubidium 87 d line data. `http://steck.us/alkalidata/`, 2009.

[41] M. D. Lukin. Colloquium: Trapping and manipulating photon states in atomic ensembles. *Rev. Mod. Phys.*, 75(457), 2003.

[42] T. F. Gallagher. *Rydberg Atoms*. Cambridge University Press, UK, 1994.

[43] D. Jaksch, J. I. Cirac, P. Zoller, S. L. Rolston, R. Cote, and M. D. Lukin. Fast quantum gates for neutral atoms. *Phys. Rev. Lett.*, 85(2208), 2000.

[44] Y. O. Dudin, L. Li, F. Bariani, and A. Kuzmich. Observation of coherent many-body rabi oscillations. *Nature Phys.*, 8, 2012.

[45] F. W. Cummings and A. Dorri. Exact solution for spontaneous emission in the presence of n atoms. *Phys. Rev. A*, 28(2282), 1983.

[46] R. H. Dicke. Coherence in spontaneous radiation processes. *Phys. Rev.*, 93(99), 1954.

[47] L.M.Duan, J.I. Cirac, and P.Zoller. Three-dimensional theory for interaction between atomic ensembles and free space light. *Phys. Rev. A*, 66(023818), 2002.

[48] A. Ashkin, J. M. Dziedzic, J. E. Bjorkholm, and S. Chu. Observation of a single-beam gradient force optical trap for dielectric particles. *Opt. Lett.*, 11, 1986.

[49] T. Grünzweig, A. Hilliard, M. McGovern, and M. F. Andersen. Near-deterministic preparation of a single atom in an optical microtrap. *Nature Phys.*, 6, 2010.

[50] N. Schlosser, G. Reymond, I. Protsenko, and P. Grangier. Sub-poissonian loading of single atoms in a microscopic dipole trap. *Nature*, 411, 2001.

[51] F. Nogrette, H. Labuhn, S. Ravets, D. Barredo, L. Beguin, A. Vernier, T. Lahaye, and A. Browaeys. Single-atom trapping in holographic 2d arrays of microtraps with arbitrary geometries. *Phys. Rev. X*, 4(021034), 2014.

[52] H. Tamura, T. Unakami, J. He, Y. Miyamoto, and K. Nakagawa. Highly uniform holographic microtrap arrays for single atom trapping using a feedback optimization of in-trap fluorescence measurements. *Opt. Express*, 24, 2016.

[53] S. P. Yu, J. D. Hood, J. A. Muniz, M. J. Martin, R. Norte, C. L. Hung, S. M. Meenehan, J. D. Cohen, O. Painter, and H. J. Kimble. Nanowire photonic crystal waveguides for single-atom trapping and strong light-matter interactions. *Appl. Phys. Lett.*, 104(111103), 2014.

[54] D. W. Vernooy J. Ye and H. J. Kimble. Trapping of single atoms in cavity qed. *Phys. Rev. Lett.*, 83(4987), 1999.

[55] J. McKeever, J. R. Buck, A. D. Boozer, A. Kuzmich, H.-C. Nägerl, D. M. Stamper-Kurn, and H. J. Kimble. State-insensitive cooling and trapping of single atoms in an optical cavity. *Phys. Rev. Lett.*, 90(133602), 2003.

[56] Immanuel Bloch and Peter Zoller. Focus on cold atoms in optical lattices. *New J. Phys.*, 8, 2006.

[57] B. Bederson and H. Walther, editors. *Optical lattices*, volume 37, New York, 1996. Academic Press.

[58] H. Robinson C. Wieman C. Monroe, W. Swann. Very cold trapped atoms in a vapor cell. *Phys. Rev. Lett.*, 65(13), 1990.

[59] H. J. Metcalf and P. van der Straten. *Laser Cooling and Trapping*. Springer-Verlag New York, 1999.

[60] P. Zoller, T. Beth, and D. Binosi et al. Quantum information processing and communication. *Eur. Phys. J. D*, 36(203), 2005.

[61] M. A. Nielsen and I. L. Chuang. *Quantum Computation and Quantum Information*. Cambridge University Press, UK, 10th anniversary edition edition, 2010.

[62] H. J. Kimble. The quantum internet. *Nature*, 453:10231030, 2008.

[63] K. Hammerer, A. S. Srensen, and E. S. Polzik. Quantum interface between light and atomic ensembles. *Rev. Mod. Phys.*, 82(1041), 2010.

[64] L.-M. Duan and C. Monroe. Colloquium: Quantum networks with trapped ions. *Rev. Mod. Phys.*, 82(1209), 2010.

[65] M. Afzelius, H. de Riedmatten C. Simon, and N. Gisin. Multimode quantum memory based on atomic frequency combs. *Phys. Rev. A*, 79(052329), 2009.

[66] P. Lodahl. Quantum-dot based photonic quantum networks. *Quantum Sci. Technol.*, 3(1), 2017.

[67] B. J. M. Hausmann, B. Shields, Q. Quan, P. Maletinsky, M. McCutcheon, J. T. Choy, T. M. Babinec, A. Kubanek, A. Yacoby, M. D. Lukin, and M. Lonca. Integrated diamond networks for quantum nanophotonics. *Nano Lett.*, 12(3), 2012.

[68] J. S. Bell. On the einstein podolsky rosen paradox. *Physics*, 1(195), 1964.

[69] A. Einstein, B. Podolsky, and N. Rosen. Can quantum-mechanical description of physical reality be considered complete? *Phys. Rev.*, 47(10), 1935.

[70] A. Ekert. Quantum cryptography based on bell's theorem. *Phys. Rev. Lett.*, 67:661–663, 1991.

[71] Y. Li, K. Zhang, and K. Peng. Multiparty secret sharing of quantum information based on entanglement swapping. *Phys. Lett. A*, 324, 2004.

[72] S.J. Yang, X.J. Wang, X.H. Bao, and J. W. Pan. An efficient quantum light-matter interface with sub-second lifetime. *Nat. Photonics.*, 10:381–384, 2016.

[73] K.-C. Nguyen, V. A. Gilles, N. J. Cerf, H. Weier, T. Scheidl, M. Lindenthal, B. Blauensteiner, T. Jennewein, J. Perdigues, P. Trojek, B. Ömer, M. Fürst, M. Meyenburg, J. Rarity, Z. Sodnik, C. Barbieri, H. Weinfurter, and A. Zeilinger. Free-space distribution of entanglement and single photons over 144 km. *Nature Phys.*, 3(7), 2006.

[74] D. M. Greenberger, M. A. Horne, and A. Zeilinger. Going beyond bell's theorem. In M. Kafatos, editor, *Bells Theorem, Quantum Theory and Conceptions of the Universe*, pages 69–72. Kluwer Academic Publishers, Dordrecht, The Netherlands, 1989.

[75] M. A. Horne D. M. Greenberger, A. Shimony, and A. Zeilinger. Bells theorem without inequalities. *Am. J. Phys.*, 58(1131), 1990.

[76] C. Ren, H.-Y. Su, Z.-P. Xu, C. Wu, and J.-L. Chen. Optimal ghz paradox for three qubits. *Sci. Rep.*, 5(13080), 2015.

[77] N. D. Mermin. What's wrong with these elements of reality? *Phys. Today*, 43(9), 1990.

[78] G. Carvacho, F. Graffittiand, V. DAmbrosio, Hiesmayr, C. Beatrix, and F. Sciarrino. Experimental investigation on the geometry of ghz states. *Scientific Reports*, 7(13265), 2017.

[79] C. H. Bennett, S. Popescu, D. Rohrlich, J. A. Smolin, and A. V. Thapliyal. Exact and asymptotic measures of multipartite pure-state entanglement. *Phys. Rev. A*, 63(012307), 2000.

[80] N. Friis, O. Marty, C. Maier, C. Hempel, M. Holzäpfel, P. Jurcevic, M. B. Plenio, M. Huber, C. Roos, R. Blatt, and B. Lanyon. Observation of entangled states of a fully controlled 20-qubit system. *Phys. Rev. X*, 8(021012), 2018.

[81] F. Fröwis, P. Sekatski, W. Dür, N. Gisin, and N. Sangouard. Macroscopic quantum states: Measures, fragility, and implementations. *Rev. Mod. Phys.*, 90(025004), 2018.

[82] Z. Zhao, Y.-A. Chen, A.-N. Zhang, T. Yang, H. J. Briegel, and J.-W. Pan. Experimental demonstration of five-photon entanglement and open-destination teleportation. *Nature*, 430:54–58, 2004.

[83] J. Kempe. Multiparticle entanglement and its applications to cryptography. *PRA*, 60(2), 1999.

[84] T. Gao, F. L. Yan, and Z. X. Wang. Deterministic secure direct communication using ghz states and swapping quantum entanglement. *J. Phys. A: Math. Gen.*, 38(5761), 2005.

[85] D. Gottesman and I. L. Chuang. Demonstrating the viability of universal quantum computation using teleportation and single-qubit operations. *Nature*, 402:390–393, 1999.

[86] R. Barends, J. Kelly, A. Megrant, A. Veitia, D. Sank, E. Jeffrey, T. C. White, J. Mutus, A. G. Fowler, B. Campbell, Y. Chen, Z. Chen, B. Chiaro, A. Dunsworth, C. Neill, P. OMalley, P. Roushan, A. Vainsencher, J. Wenner, A. N. Korotkov, A. N. Cleland, and J. M. Martinis. Superconducting quantum circuits at the surface code threshold for fault tolerance. *Nature*, 508:500–503, 2014.

[87] M. Hillery, V. Buzek, and A. Berthiaume. Quantum secret sharing. *Phys. Rev. A*, 59(1829), 1999.

[88] G. Toth. Multipartite entanglement and high-precision metrology. *Phys. Rev. A*, 85(022322), 2012.

[89] N. V. Vitanov, A. A. Rangelov, B. W. Shore, and K. Bergmann. Stimulated raman adiabatic passage in physics, chemistry, and beyond. *Rev. Mod. Phys.*, 89(015006), 2017.

[90] J. R. Kuklinski, U. Gaubatz, F. T. Hioe, and K. Bergmann. Adiabatic population transfer in a three-level system driven by delayed laser pulses. *Phys. Rev. A*, 40(6741(R)), 1989.

[91] N. V. Vitanov and S. Stenholm. Properties of stimulated raman adiabatic passage with intermediate-level detuning. *Opt. Commun.*, 135, 1997.

[92] T. A. Laine and S. Stenholm. Adiabatic processes in three-level systems. *Phys. Rev. A*, 53(2501), 1996.

[93] H. Theuer Bergmann, K. and B. W. Shore. Coherent population transfer among quantum states of atoms and molecules. *Rev. Mod. Phys.*, 70(1003), 1998.

[94] J. Klein, F. Beil, and T. Halfmann. Robust population transfer by stimulated raman adiabatic passage in a $pr^{3+}$:$y_2sio_5$ crystal. *Phys. Rev. Lett.*, 99(113003), 2007.

[95] Y.-X. Du, Z.-T. Liang, W. Huang, H. Yan, and S.-L. Zhu. Experimental observation of double coherent stimulated raman adiabatic passages in three-level $\lambda$ systems in a cold atomic ensemble. *Phys. Rev. A*, 90(023821), 2014.

[96] M. Saffman, T. G. Walker, and K. Mølmer. Quantum information with rydberg atoms. *Rev. Mod. Phys.*, 82(3), 2010.

[97] Ditte Møller, L. B Madsen, and Klaus Mølmer. Quantum gates and multiparticle entanglement by rydberg excitation blockade and adiabatic passage. *Phys. Rev. Lett.*, 100(170504), 2008.

[98] R. G. Unanyan and M. Fleischhauer. Efficient and robust entanglement generation in a many-particle system with resonant dipole-dipole interactions. *Phys. Rev. A*, 66(032109), 2002.

[99] M. D. Lukin, M. Fleischhauer, R. Cote, L. M. Duan, D. Jaksch, J. I. Cirac, and P. Zoller. Dipole blockade and quantum information processing in mesoscopic atomic ensembles. *Phys. Rev. Lett.*, 87(3), 2001.

[100] M. Müller, I. Lesanovsky, H. Weimer, H. P. Büchler, and P. Zoller. Mesoscopic rydberg gate based on electromagnetically induced transparency. *Phys. Rev. Lett.*, 102(170502), 2009.

[101] M. Ostmann, J. Minář, M. Marcuzzi, E. Levi, and I. Lesanovsky. Non-adiabatic quantum state preparation and quantum state transport in chains of rydberg atoms. *New J. Phys.*, 19(123015), 2017.

[102] K. Bergmann, H. Theuer, and B. W. Shore. Coherent population transfer among quantum states of atoms and molecules. *Rev. Mod. Phys.*, 70(1003), 1998.

[103] F. Schwabl. *Advanced quantum mechanics*. Springer-Verlag, India, second edition edition, 2004.

[104] J. R. Silvester. Determinants of block matrices. *The Mathematical Gazette*, 84(501):460–467, 2000.

[105] M. E. A. El-Mikkawy. On the inverse of a general tridiagonal matrix. *Appl. Math. Comput.*, 150:669–679, 2004.

[106] D. Comparat. General conditions for quantum adiabatic evolution. *Phys. Rev. A*, 80(012106), 2009.

[107] M. Saffman and T. G. Walker. Analysis of a quantum logic device based on dipole-dipole interactions of optically trapped rydberg atoms. *Phys. Rev. A*, 72(022347), 2005.

[108] T. P. Gujarati. Rydberg-atom-based creation of a n-particle greenberger-horne-zeilinger state using stimulated raman adiabatic passage. *Phys. Rev. A*, 98(062326), 2018.

[109] T. Chaneliere, D. N. Matsukevich, S. D. Jenkins, S.-Y. Lan, T. A. B. Kennedy, and A. Kuzmich. Storage and retrieval of single photons transmitted between remote quantum memories. *Nature*, 438:833–836, 2005.

[110] Y.F. Pu, N. Jiang, W. Chang, H.X. Yang, C. Li, and L.M.Duan. Experimental realization of a multiplexed quantum memory with 225 individually accessible memory cells. *Nat. Commun.*, 8(15359), 2017.

[111] K. S. Choi, A. Goban, S. B. Papp, S. J. van Enk, and H. J. Kimble. Entanglement of spin waves among four quantum memories. *Nature*, 468:412–416, 2010.

[112] H.J. Briegel, W.Dür, J.I.Cirac, and P.Zoller. Quantum repeaters: The role of imperfect local operations in quantum communication. *Phys. Rev. Lett.*, 81(5932), 1998.

[113] M. Zukowski, A. Zeilinger, M.A. Horne, and A. Ekert. "event-ready-detectors" bell experiment via entanglement swapping. *Phys. Rev. Lett.*, 71(4287-4290), 1993.

[114] N. Sangouard, C. Simon, H. de Riedmatten, and N. Gisin. Quantum repeaters based on atomic ensembles and linear optics. *Rev. Mod. Phys*, 83:33–80, 2011.

[115] C. W. Chou, H. de Riedmatten, D. Felinto, S. V. Polyakov, S. J. van Enk, and H. J. Kimble. Measurement-induced entanglement for excitation stored in remote atomic ensembles. *Nature*, (438), 2005.

[116] C. W. Chou, J. Laurat, Deng, K. S. Choi, H. de Riedmatten, D. Felinto, and H. J. Kimble. Functional quantum nodes for entanglement distribution over scalable quantum networks. *Science*, 316, 2007.

[117] R. Zhao, Y.O.Dudin, S.D.Jenkins, C.J. Campbell, D.N.Matsukevich, T.A.B. Kennedy, and A. Kuzmich. Long-lived quantum memory. *Nat. Phys.*, 5:100–104, 2009.

[118] B. Zhao, Y.A. Chen, X.H. Bao, T. Strassel, C.S. Chuu, X.M. Jin, J. Schmiedmayer, Z.S. Yuan, S. Chen, and J.W. Pan. A millisecond quantum memory for scalable quantum networks. *Nat. Phys.*, 5:95–99, 2009.

[119] Y. O. Dudin, L. Li, and A. Kuzmich. Light storage on the time scale of a minute. *Phys. Rev. A*, 87(031801(R)), 2013.

[120] J. Laurat, H. de Riedmatten, D. Felinto, C.-W. Chou, E. W. Schomburg, and H. J. Kimble. Efficient retrieval of a single excitation stored in an atomic ensemble. *Opt. Express*, 14(6912), 2006.

[121] J. Simon, H. Tanji, J. K. Thompson, and V. Vuletić. Interfacing collective atomic excitations and single photons. *Phys. Rev. Lett.*, 98(183601), 2007.

[122] A. V. Gorshkov, A. Andrè, M. D. Lukin, and A. S. Srensen. Photon storage in $\lambda$-type optically dense atomic media. ii. free-space model. *Phys. Rev. A*, 76(033805), 2007.

[123] Y. Wu T. P. Gujarati and L. M. Duan. Intrinsic retrieval efficiency for quantum memories: A three-dimensional theory of light interaction with an atomic ensemble. *Phys. Rev. A*, 97(033826), 2018.

[124] M. Gross and S.Haroche. Superradiance: An essay on the theory of collective spontaneous emission. *Phys. Rep.*, 93, 1982.

[125] S. Inouye, A. P. Chikkatur, D. M. Stamper-Kurn, J. Stenger, D. E. Pritchard, and W. Ketterle. Superradiant rayleigh scattering from a bose-einstein condensate. *Science*, 285, 1999.

[126] H. Bernien, S. Schwartz, A. Keesling, H. Levine, A. Omran, H. Pichler, S. Choi, A. S. Zibrov, M. Endres, M. Greiner, V. Vuletic, and M. D. Lukin. Probing many-body dynamics on a 51-atom quantum simulator. *Nature*, 551:579–584, 2017.

[127] H. Levine, A. Keesling, A. Omran, H. Bernien, S. Schwartz, A. S. Zibrov, M. Endres, M. Greiner, V. Vuletic, and M. D. Lukin. High-fidelity control and entanglement of rydberg-atom qubits. *Phys. Rev. Lett.*, 121(123603), 2018.

[128] D. Barredo, V. Lienhard, S. de Leseleuc, T. Lahaye, and A. Browaeys. Synthetic three-dimensional atomic structures assembled atom by atom. *Nature*, 561:79–82, 2018.

[129] V. Lienhard, S. de Leseleuc, D. Barredo, T. Lahaye, A. Browaeys, M. Schuler, L.-P. Henry, and A. M. Lauchli. Observing the space- and time-dependent growth of correlations in dynamically tuned synthetic ising models with antiferromagnetic interactions. *Phys. Rev. X*, 8(8, 021070), 2018.

[130] R. G. Unanyan and M. Fleischhauer. Geometric phase gate without dynamical phases. *Phys. Rev. A*, 69(050302), 2004.

[131] S. Nakamura, H. Goto, and K. Ichimura. Quantum phase gate via stimulated raman adiabatic passage with time-dependent two-photon detuning. *Opt. Commun.*, 293(160), 2013.

[132] I. Lesanovsky, K. Macieszczak, and J. P. Garrahan. Non-equilibrium absorbing state phase transitions in discrete-time quantum dynamics. *arXiv:1804.09794*, 2018.

[133] C. Perez-Espigares, I. Lesanovsky, J. P. Garrahan, and R. Gutierrez. Glassy dynamics due to a trajectory phase transition in dissipative rydberg gases. *Phys. Rev. A*, 98(021804(R)), 2018.

[134] S. de Leseleuc, S. Weber, V. Lienhard, D. Barredo, H. P. Büchler, T. Lahaye, and A. Browaeys. Accurate mapping of multilevel rydberg atoms on interacting spin-$\frac{1}{2}$ particles for the quantum simulation of ising models. *Phys. Rev. Lett.*, 120(113602), 2018.

[135] G. Kurizki, P. Bertet, Y. Kubo, K. Molmer, D. Petrosyan, P. Rabl, and J. Schmiedmayer. Quantum technologies with hybrid systems. *PNAS*, 112(13):3866–3873, 2015.

[136] S. D. Hogan, J. A. Agner, F. Merkt, T. Thiele, S. Filipp, and A. Wallraff. Driving rydberg-rydberg transitions from a coplanar microwave waveguide. *Phys. Rev. Lett.*, 108(6), 2012.

[137] D. Petrosyan, G. Bensky, G. Kurizki, I. Mazets, J. Majer, and J. Schmiedmayer. Reversible state transfer between superconducting qubits and atomic ensembles. *Phys. Rev. A*, 79(4), 2009.